∂ 29 ν

JOURNAL OF
ELECTROANALYTICAL
CHEMISTRY
AND INTERFACIAL ELECTROCHEMISTRY

International Journal devoted to all Aspects
of Electroanalytical Chemistry, Double Layer
Studies, Electrokinetics, Colloid Stability, and
Electrode Kinetics.

ELSEVIER

GENERAL INFORMATION

See also Suggestions and Instructions to Authors which will be sent free, on request to the Publishers.

Types of contributions

    (a) Original research work not previously published in other periodicals.
    (b) Reviews on recent developments in various fields.
    (c) Short communications.
    (d) Bibliographical notes and book reviews.

Languages

    Papers will be published in English, French or German.

Submission of papers

    Papers should be sent to one of the following Editors:
        Professor J. O'M. BOCKRIS, John Harrison Laboratory of Chemistry,
            University of Pennsylvania, Philadelphia 4, Pa. 19104, U.S.A.
        Dr. R. H. OTTEWILL, Department of Chemistry, The University, Bristol 8, England.
        Dr. R. PARSONS, Department of Chemistry, The University, Bristol 8, England.
            Until June 1967: Gates and Crellin Laboratories of Chemistry, California Institute of Technology, Pasadena, Calif. 91109, U.S.A.
        Professor C. N. REILLEY, Department of Chemistry,
            University of North Carolina, Chapel Hill, N.C. 27515, U.S.A.

Authors should preferably submit two copies in double-spaced typing on pages of uniform size. Legends for figures should be typed on a separate page. The figures should be in a form suitable for reproduction, drawn in Indian ink on drawing paper or tracing paper, with lettering etc. in thin pencil. The sheets of drawing or tracing paper should preferably be of the same dimensions as those on which the article is typed. Photographs should be submitted as clear black and white prints on glossy paper. Standard symbols should be used in line drawings, the following are available to the printers:

    ▼ ▽ ■ ◻ ● ◎ ▪ ◻ ⬦ ▣ ▪ + ×

All references should be given at the end of the paper. They should be numbered and the numbers should appear in the text at the appropriate places.
A summary of 50 to 200 words should be included.

Reprints

    Fifty reprints will be supplied free of charge. Additional reprints can be ordered at quoted prices. They must be ordered on order forms which are sent together with the proofs.

Publication

    The *Journal of Electroanalytical Chemistry and Interfacial Electrochemistry* appears monthly and has four issues per volume and three volumes per year.

    Subscription price: £ 18.18.0 or $ 52.50 or Dfl. 189.00 per year; £ 6.6.0 or $ 17.50 or Dfl. 63.00 per volume; plus postage. Additional cost for copies by air mail available on request. For advertising rates apply to the publishers.

Subscriptions

    Subscriptions should be sent to:

ELSEVIER PUBLISHING COMPANY, P.O. Box 211, Amsterdam, The Netherlands.

ADVANCES
IN COLLOID
AND INTERFACE
SCIENCE

AN INTERNATIONAL JOURNAL DEVOTED TO EXPERIMENTAL AND THEOR ETICAL DEVELOPMENTS IN INTERFACIAL AND COLLOIDAL PHENOMEN, AND THEIR IMPLICATIONS IN CHEMISTRY, TECHNOLOGY AND BIOLOG)

TO BE INCLUDED IN EARLY ISSUES:

The nature of the association equilibria and hydrophobic bonding in aqueous solutions
of association colloids (P. Mukerjee)

The physical adsorption of gases on solids (W. A. Steele)

Particle adhesion: theory and experiment (H. Krupp)

La structure des solutions aqueuses concentrees de savon (A. Skoulios)

Semiconductor surfaces and the electrical double layer (M. J. Sparnaay)

The amount of work published on the various aspects of colloid and interface science makes it increasingly difficult for the scientist to keep abreast of the latest developments. Reviews on specialized topics can do a great deal to help, but these often appear in annual volumes with the result that great delays in publication can occur. In an effort to eliminate the difficulties associated with projects involving many authors, it has been decided to publish ADVANCES IN COLLOID AND INTERFACE SCIENCE as a journal.

The whole range of colloidal and interfacial phenomena (chemical, physical, biological, technological) will be covered and a multidisciplinary approach encouraged.

Reviews are accepted in English, German and French. Authors intending to prepare reviews are invited to contact the editors for a preliminary discussion of scope.

The first issue is scheduled for publication in the spring of 1967; four issues will appear per volume. Subscription price is £7.10.0, Dfl. 75.00 or US$21.00 per volume plus postage 8s., US$1.10 or Dfl. 4.00. Subscription orders and requests for specimen copies may be sent to your usual supplier or directly to the publisher.

JOURNAL

of

ELECTROANALYTICAL CHEMISTRY

and

INTERFACIAL ELECTROCHEMISTRY

AN INTERNATIONAL JOURNAL DEVOTED TO ALL
ASPECTS OF ELECTROANALYTICAL CHEMISTRY,
DOUBLE LAYER STUDIES, ELECTROKINETICS,
COLLOID STABILITY AND ELECTRODE KINETICS

VOL. 14   1967

INTERMETALLIC COMPOUND FORMATION BETWEEN COBALT AND ZINC IN MERCURY

B. K. HOVSEPIAN AND IRVING SHAIN

Chemistry Department, University of Wisconsin, Madison, Wis. (U.S.A.)

(Received May 16th, 1966)

Mixed amalgams and intermetallic compounds in mercury have been studied using many classical techniques[1,2], but recently, modern electroanalytical methods have been used in studying such systems, including polarography with dropping amalgam electrodes[3], stationary electrode polarography with hanging mercury drop electrodes[4–6], and controlled-potential coulometry with an amalgam pool electrode[7]. In general, the results of the more recent studies have been less ambiguous and more easily interpreted than the early work, because controlled pre-electrolysis procedures can be used to prepare known amalgam concentrations. In recent papers on the stripping analysis of mixtures using the hanging mercury drop electrode, KEMULA and co-workers reported many cases in which intermetallic coumpounds form in the amalgam[5,6]. The effect of the formation of such compounds is to reduce the height of the dissolution wave of one of the electroactive species, and in a number of cases, a new peak for the dissolution of the intermetallic compound is observed.

Thus, one of the most convenient ways of studying mixed amalgams involves techniques that are direct extensions of stripping analysis procedures[8]. These methods were applied to the study of the intermetallic compound formed when cobalt and zinc are present together in a hanging mercury drop electrode. The particular selection of these species was made on the basis of previous reports that zinc forms intermetallic compounds with many metals[6], and because two of these previous reports actually concerned the Co–Zn system[3,7], thus providing data for comparison of some of the results of the investigation.

The work reported here consisted of two parts. First, the composition of the Co–Zn compound in mercury was determined from anodic stationary electrode polarograms. Then, the rate of formation of this intermetallic compound was determined using a step-functional controlled-potential method[9].

EXPERIMENTAL

Instrumentation

For the electroanalytical experiments carried out in this work, the instrument used was the multipurpose operational amplifier device previously described[10]; the basic circuit was the potentiostat configuration shown previously in Fig. 4 of ref. 10. Along with this basic circuit, the signal generator section (SG) and the readout device (M) were selected as required for the particular experiments in progress, from those described in ref. 10. For polarography, stationary electrode polarography, and poten-

tiostatic experiments (1–20 sec time scale) these components have been described previously[11].

The electrolysis cell in all cases involved a three electrode configuration.

Step-functional potentiostatic experiments. The kinetic measurements involved a two-step potentiostatic method, in which a single square-wave pulse (amplitude 0.8 V in these experiments) was applied to the cell. For this, the signal generator section (SG) involved a low voltage power supply to set the initial potential, and a manually-triggered function generator (which provided the single pulse) identical to that described in Fig. 7 of ref. 10. The readout device (M) was a Tektronix 536 oscilloscope, provided with a Type D plug-in preamplifier in the vertical channel, and a Type T plug-in time base unit in the horizontal channel. The time base, which was triggered by the square-wave signal generator, was calibrated against a frequency counter (Beckman Model 7360 R). The data were recorded on a Dumont type 302 Polaroid oscilloscope camera, using Polaroid Type 42 film.

Chemicals, cells and electrodes

The chemicals, cells and electrodes have been described previously[11]. The separate cobalt plating bath used in the study of intermetallic compound formation had the same type of cell, Teflon lid, and electrodes except that it was not maintained at constant temperature. Reproducible stirring was provided by a synchronous magnetic stirrer, made by mounting a small horse-shoe magnet on a Sargent synchronous rotator. A Teflon-covered stirring bar was used to stir the solution.

COMPOSITION OF THE Co–Zn INTERMETALLIC COMPOUND IN MERCURY

Although the stoichiometry of only a few intermetallic compounds in mercury has been studied carefully, in each case the intermetallic compound appears to be exceptionally stable. Thus it is possible to prepare mixed amalgams containing known amounts of each species, and then the composition of the intermetallic compound is determined by measuring the amount of free excess of one of the components. This assumes that only a single intermetallic compound is formed, and that its rate of dissociation is very low, since the analysis for the free excess of one component usually involves removal of at least a portion of that species from the amalgam. Thus, the free amalgam concentrations of the component species are assumed not to be replenished by significant further dissociation of the intermetallic compound during the time required for the analysis.

The methods that have been developed all involve similar concepts. The simplest approach was reported by KEMULA AND GALUS[5], who studied the Ni–Sn system with hanging mercury drop electrodes. The calculations were based on measuring the free excess of tin in the mixed amalgam from stripping analysis data when the concentration of nickel was varied. The method can be applied to any system in which the dissociation constant of the intermetallic compound is extremely low.

A second approach was used by STROMBERG AND GORODOVYKH[4], who studied the Cu–Zn system, in which the intermetallic compound apparently is insoluble, and the solubility product is not exceeded until significant amounts of both species are present. The stoichiometry of the system was evaluated from solubility product expressions. These were taken in pairs with different concentration conditions, and

were solved simultaneously to determine the combining ratio Cu/Zn, and also the solubility product.

When the intermetallic compound is soluble in the mercury, and its dissociation constant is not extremely low, the calculations must be based on other equilibrium expressions. These were first formulated for the Co–Zn system by BABKIN AND KOSLOVSKII[3]

$$Co_nZn \rightleftharpoons n\,Co + Zn \qquad\qquad\qquad\qquad\qquad (I)$$

$$K = \frac{[Co]^n[Zn]}{[Co_nZn]} \qquad\qquad\qquad\qquad\qquad (1)$$

who studied the Co–Zn intermetallic compound using dropping amalgam electrodes. The anodic zinc current was diminished in the presence of cobalt, and the amount of intermetallic compound formed was taken as proportional to this decrease in the current. The various concentrations in the equilibrium expression can be stated in terms of the known initial concentrations and the observed stripping current for the zinc. If this is done for two sets of concentration conditions, two equations are obtained which can be solved simultaneously to determine n and K. The results of these dropping amalgam electrode experiments gave a value of n close to 1, and a value of K equal to 1.3×10^{-2}, although there was considerable scatter in the data.

The only other previous study of the Co–Zn system was carried out by FICKER AND MEITES[7] who made rather large amounts of the mixed amalgams by electrolysis with mercury pool electrodes, which were then coulometrically stripped. These experiments lasted much longer times than the voltammetric studies. The results indicated that several intermetallic compounds were present in the aged amalgams, and that the decomposition of these various species was very slow, with half-lives of the order of hundreds of hours. In addition, the data indicated that, in the simplest intermetallic compound present the Co–Zn ratio was unity, both the free cobalt and zinc species were present in the amalgam as dimers (Co_2 and Zn_2), and for the equilibrium

$$2\,CoZn \rightleftharpoons Co_2 + Zn_2 \qquad\qquad\qquad\qquad\qquad (II)$$

the dissociation constant

$$K_2 = \frac{[Co_2][Zn_2]}{[CoZn]^2} \qquad\qquad\qquad\qquad\qquad (2)$$

is of the order of 25 ± 8.

These previous studies had fairly well established that the cobalt and zinc are present in equal amounts in the intermetallic compound, but the exact nature of the species involved had not been established. Thus, this work was designed to determine if the stripping analysis approach to these studies could provide a rapid way to evaluate the gross stoichiometry of the intermetallic compound, and also provide sufficiently precise data to permit an unambiguous choice between the various possible equilibria.

Basis of the calculation

To carry out the calculations, the concentrations of the intermetallic compound

and each component were determined from the stripping analysis results. These data were taken in sets of two concentrations, substituted into eqn. (1) for each, and since K is assumed constant, the two equilibrium expressions can be equated to obtain

$$\frac{[\text{Co}]_1{}^n[\text{Zn}]_1}{[\text{Co}_n\text{Zn}]_1} = \frac{[\text{Co}]_2{}^n[\text{Zn}]_2}{[\text{Co}_n\text{Zn}]_2} \tag{3}$$

Here, [Co] and [Zn] are the free cobalt and free zinc concentrations in the amalgam, and $[\text{Co}_n\text{Zn}]$ is the intermetallic compound concentration. If the concentrations of all these species are known, the value of n is readily obtained.

The concentrations can be evaluated from the stripping analysis data by first determining the "accumulation coefficients"[4], γ_{Co} and γ_{Zn}, from calibration experiments using the cobalt and zinc separately. These coefficients take into account the combined mass transfer effects, stirring efficiency, diffusion coefficients, time of electrolysis, etc., and as long as the pre-electrolysis conditions are maintained constant, these are simply proportionality constants relating the amalgam concentration to the original solution concentration. Thus, the total amount of cobalt or zinc in the amalgam phase is given by

$$[\text{Co}]_t = \gamma_{\text{Co}}[\text{Co}^{2+}] \tag{4}$$

$$[\text{Zn}]_t = \gamma_{\text{Zn}}[\text{Zn}^{2+}] \tag{5}$$

where $[\text{Co}^{2+}]$ and $[\text{Zn}^{2+}]$ are the bulk solution concentrations. The free zinc concentration is obtained from the stripping peak current of the zinc that still remains in the presence of cobalt

$$[\text{Zn}] = (i/i_t)[\text{Zn}]_t = (i/i_t)\gamma_{\text{Zn}}[\text{Zn}^{2+}] \tag{6}$$

Here, i_t is the stripping peak current obtained when only zinc is present, and i is the stripping peak current obtained in the presence of the cobalt. The concentration of the intermetallic compound is assumed to be proportional to the amount of zinc not available for stripping, *i.e.*, the amount by which the zinc stripping current has been diminished

$$\begin{aligned}[\text{Co}_n\text{Zn}] &= [(i_t - i)/i_t][\text{Zn}]_t \\ &= [1 - (i/i_t)]\gamma_{\text{Zn}}[\text{Zn}^{2+}] \end{aligned} \tag{7}$$

Then the concentration of free cobalt is taken as the difference between that originally electrolyzed into the amalgam and that tied up in the intermetallic compound

$$\begin{aligned}[\text{Co}] &= [\text{Co}]_t - n[\text{Co}_n\text{Zn}] \\ &= \gamma_{\text{Co}}[\text{Co}^{2+}] - n[1 - (i/i_t)]\gamma_{\text{Zn}}[\text{Zn}^{2+}] \end{aligned} \tag{8}$$

These expressions can be substituted into eqn. (3) to obtain the actual working equation

$$\frac{\{\gamma_{\text{Co}}[\text{Co}^{2+}] - n[1 - (i/i_t)]\gamma_{\text{Zn}}[\text{Zn}^{2+}]\}_1{}^n\{(i/i_t)\gamma_{\text{Zn}}[\text{Zn}^{2+}]\}_1}{\{[1 - (i/i_t)]\gamma_{\text{Zn}}[\text{Zn}^{2+}]\}_1} =$$

$$\frac{\{\gamma_{\text{Co}}[\text{Co}^{2+}] - n[1 - (i/i_t)]\gamma_{\text{Zn}}[\text{Zn}^{2+}]\}_2{}^n\{(i/i_t)\gamma_{\text{Zn}}[\text{Zn}^{2+}]\}_2}{\{[1 - (i/i_t)]\gamma_{\text{Zn}}[\text{Zn}^{2+}]\}_2} \tag{9}$$

This equation can be simplified greatly if equal zinc concentrations are selected for

the two experiments. Under these conditions, the terms i_t and $[Zn^{2+}]$ can in part be cancelled, to obtain

$$\frac{\gamma_{Co}[Co^{2+}]_1 - n[1-(i_1/i_t)]\gamma_{Zn}[Zn^{2+}]}{\gamma_{Co}[Co^{2+}]_2 - n[1-(i_2/i_t)]\gamma_{Zn}[Zn^{2+}]} = \left[\frac{[1-(i_1/i_t)]}{[1-(i_2/i_t)]} \cdot \frac{i_2}{i_1}\right]^{1/n} \qquad (10)$$

Equation (10) can be solved graphically by plotting each side of the equation as a function of n on the same graph. The intersection of the two lines provides the value of n. Alternatively a method of successive approximations can be used, since the left side of eqn. (10) generally is not very sensitive to changes in n.

These relations enabled the applicability of stripping analysis methods in studying the stoichiometry of the Co–Zn system to be determined. Then, values of K were obtained by substituting the concentration values, along with the calculated value of n (taken as the nearest integer), back into the three most reasonable of the various possible equilibrium expressions that can be written to describe the system. These calculations were used to determine if the dissociation constants were actually independent of concentration, and in this way, an attempt was made to differentiate between the various possibilities.

Evaluation of experimental conditions

Stripping analysis conditions. The solution conditions selected for these experiments were based on the previous work on the stripping analysis of cobalt[11]. The complexing buffer was 0.1 M pyridine–pyridinium chloride, pH 6.0, containing either 0.1 M sodium nitrate or 0.2 M potassium chloride, and $10^{-4}\%$ gelatin.

Although zinc forms a well-behaved amalgam, and stripping analysis procedures for this system were expected to be straightforward, the actual use of an indifferent electrolyte containing pyridine–pyridinium chloride had not been reported previously for the stripping analysis of zinc. Therefore, the characteristics of the system were checked. Standard stripping analysis experiments were carried out using three zinc concentrations (2.5, 5.0 and 10.0 $\times$ 10^{-5} M) and a pre-electrolysis time of 5 min. The pre-electrolysis potential was -1.20 V *vs.* S.C.E., a value previously found to be suitable for the cobalt system. The experimental results, which are summarized in Table 1, indicate that the function i_p/tC (where i_p is the anodic peak current, t is the pre-electrolysis time, and C is the original concentration of zinc in the bulk of the solution) is constant over the entire range studied.

TABLE 1

STRIPPING ANALYSIS OF ZINC

Solution: 0.1 M pyridine–pyridinium chloride, 0.1 M NaNO₃, $10^{-4}\%$ gelatin, pH 6.0. Pre-electrolysis for 5 min at -1.20 V *vs.* S.C.E. Rate of voltage scan, 50 mV/sec.

Zinc concn., $C(m/l \cdot 10^5)$	Peak current,[a] $i_p(\mu A)$	$i_p/Ct \cdot 10^{-6}$	Rel. Sd. Dv. (%)
2.5	20.4	0.163	0.50
5.0	40.1	0.160	0.80
10.0	80.6	0.161	0.75

[a] Av. of six replicate determinations on the same solution, using a fresh hanging mercury drop electrode for each.

Pre-electrolysis efficiencies. To make valid correlations between the solution concentrations of cobalt(II) and zinc(II), and the corresponding amalgam concentrations, it was necessary to measure the accumulation coefficients, γ_{Co} and γ_{Zn}.

The accumulation coefficient for cobalt was determined by the procedure described previously[11,12]. Cathodic plating currents were measured as a function of concentration, using cobalt(II) solutions without zinc present. From the quantity of electricity involved and the electrode volume, amalgam concentrations were calculated directly. For the particular cell–electrode-stirring combination used in these experiments (5-min pre-electrolysis time), γ_{Co} was found to be equal to 200, with a relative standard deviation of about 5% on replicate determinations.

The accumulation coefficient for zinc, γ_{Zn}, was determined in the same manner, and the value obtained was 190, with a relative standard deviation of about 5%. Because of the fairly large uncertainty in these measurements, corroborative estimates of the ratio γ_{Zn}/γ_{Co} were obtained by comparing the relative rates of deposition of the two species under other conditions. From conventional polarographic experiments using the dropping mercury electrode, the ratio of the diffusion current constants I_{Zn}/I_{Co} was 0.97. The ratio of the peak currents $(i_p)_{Zn}/(i_p)_{Co}$, measured in stationary electrode polarography experiments with the hanging drop electrode, was 0.96. From potentiostatic experiments, the diffusion coefficient for cobalt, measured from the slopes of the i vs. $1/\sqrt{t}$ curves was 6.40×10^{-6} cm^2/sec, while that for zinc was 6.24×10^{-6} cm^2/sec. The ratio D_{Zn}/D_{Co} was 0.97.

These results all indicated that the ratio of γ_{Zn}/γ_{Co} should be close to unity, within about 5%. Because an uncertainty of about the same magnitude was present in the stripping-analysis data used for stoichiometry and equilibrium constant calculations, the ratio γ_{Zn}/γ_{Co} was simply taken as unity. This permitted further minor simplification of eqn. (10).

Experimental procedure. The experimental method followed standard stripping-analysis procedure[8]. Fifty millilitres of solution, containing the desired amount of zinc and cobalt, 0.1 M pyridine–pyridinium chloride (pH 6.0), 0.1 M NaNO$_3$ (or 0.2 M KCl) and 10^{-4}% gelatin were pipetted into the electrolysis cell and deaerated for 10 min. Then two drops of mercury were caught from the capillary on the Teflon scoop and transferred to the HMDE. Stirring was started, and after a 30-sec interval, the pre-electrolysis potential of -1.2 V vs. S.C.E. was applied. The electrolysis time was 5 min, and at the end of this time, stirring was stopped. A 30-sec interval was allowed for the solution to come to rest, and then the potential was scanned anodically at a rate of 0.050 V/sec. The anodic peak current at -0.94 V vs. S.C.E. was measured, corresponding to the dissolution of the uncombined zinc.

Using this analytical procedure, experiments were carried out with three different solution concentrations of zinc (2.5×10^{-5} M, 5.00×10^{-5} M, 1.00×10^{-4} M), and for each zinc solution the concentration of cobalt ion was systematically varied from 0 to at least 2.0 times the zinc. Typical experimental results are shown in Fig. 1.

Mixed amalgam stability. In discussing the results of their coulometric experiments, FICKER AND MEITES[7] questioned KEMULA's results[5] on the basis that a relatively short pre-electrolysis time, followed by an immediate anodic scan, did not provide enough time for the mixed amalgam to come to equilibrium. To determine if significant time-dependent differences in the stripping characteristics of a mixed amalgam could be influencing these experiments, stripping experiments were carried
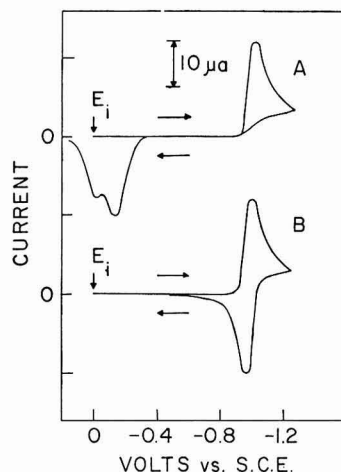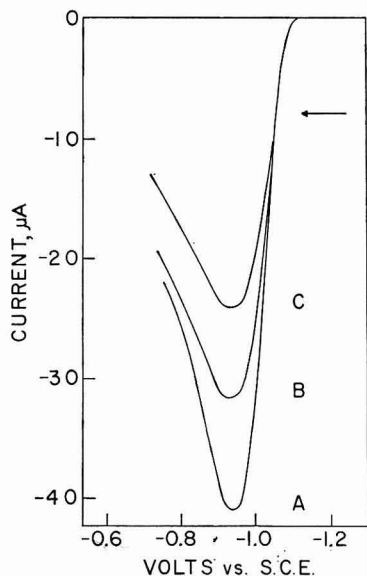
Fig. 1. Stationary electrode polarograms for the dissolution of zinc from mixed Co–Zn amalgams. Soln.: $5.0 \cdot 10^{-5}$ M Zn; 0.1 M pyridine–pyridinium chloride, pH 6.0; 0.1 M NaNO$_3$; $10^{-4}\%$ gelatin. Pre-electrolysis for 5 min, at -1.20 V $vs.$ S.C.E. Rate of anodic voltage scan, 0.050 V/sec. Co(II) concn.: (A), none; (B), $1.00 \cdot 10^{-4}$ M; (C), $1.5 \cdot 10^{-4}$ M.

Fig. 2. Typical cyclic triangular wave polarograms for Co and Zn solns. at a hanging mercury drop electrode. Scan rate, 0.050 V/sec. Both solns. contained 0.1 M pyridine–pyridinium chloride, pH 6.0; 0.1 M NaNO$_3$; $10^{-4}\%$ gelatin. (A), $1.00 \cdot 10^{-3}$ M Co(II); (B), $1.00 \cdot 10^{-3}$ M Zn(II).

TABLE 2

PEAK CURRENTS OBSERVED FOR THE STRIPPING OF FREE ZINC FROM MIXED Co–Zn AMALGAMS

$[Zn^{2+}]$ $(m/l \cdot 10^5)$	$[Co^{2+}]_1$ $(m/l \cdot 10^5)$	$[Co^{2+}]_2$ $(m/l \cdot 10^5)$	$i_t(\mu A)$	$i_1(\mu A)$	$i_2(\mu A)$
10.0	1.0	2.0	80.6	77.5	74.5
10.0	2.0	7.0	80.6	74.5	60.6
10.0	2.0	13.0	80.6	74.5	54.0
5.0	2.5	7.5	40.1	37.9	33.5
5.0	2.5	10.0	40.1	37.9	30.6
5.0	2.5	12.5	40.1	37.9	27.2
5.0	2.5	15.0	40.1	37.9	24.3
2.5	2.0	3.0	24.2	19.2	17.3
2.5	2.0	3.5	24.2	19.2	16.5
2.5	3.0	3.5	24.2	17.3	16.5
10.0	12.0	20.0	80.6	58.7	49.5
2.5	4.0	4.5	24.2	16.1	15.3

In each case, the pre-electrolysis was carried out for 5 min at -1.20 V $vs.$ S.C.E.; the anodic rate of voltage scan was 0.050 V/sec. All solns. contained 0.1 M pyridine–pyridinium chloride, pH 6.0; and $10^{-4}\%$ gelatin. Those containing $5.0 \cdot 10^{-5}$ and $1.0 \cdot 10^{-4}$ M zinc were 0.1 M in NaNO$_3$; those containing $2.5 \cdot 10^{-5}$ M zinc were 0.2 M in KCl. Each result is the average of six replicate determinations on the same soln. using a fresh hanging mercury drop electrode for each expt.

out with solutions containing equal amounts of cobalt and zinc $(2.5 \times 10^{-5} M)$. After a 5-min pre-electrolysis interval at -1.2 V, the potential was switched to -1.00 V *vs.* S.C.E. (a potential at which the cell current was zero) for a timed quiescent period. Then the potential was scanned anodically to record the zinc dissolution current. The results indicated that over the time intervals used in this work, the amalgams are stable, and that the composition of the intermetallic compound does not change during the stripping experiments.

Results and discussion

Stoichiometry of the Co–Zn system. The experimental results are summarized in Table 2, where the peak currents observed for the stripping of zinc in the presence of cobalt are listed. These data were used first to study the applicability of the stripping analysis procedures in determining the stoichiometry of the system. Typical calculations of n-values obtained for each set of concentrations, using eqn. (10), are listed in Table 3. Based on these calculations, the ratio of Co/Zn in the intermetallic compound was taken as unity, in accord with previously reported results.

TABLE 3

STOICHIOMETRIC RATIOS FOR THE Co–Zn INTERMETALLIC COMPOUND IN MERCURY

$[Co]_1/[Zn]_t$	$[Co]_2/[Zn]_t$	n	$[Co]_1/[Zn]_t$	$[Co]_2/[Zn]_t$	n
0.1	0.2	1.00	0.8	1.2	0.95
0.2	0.7	1.06	0.8	1.4	0.98
0.2	1.3	0.93	1.2	1.4	0.94
0.5	1.5	1.06	1.2	2.0	0.95
0.5	2.0	1.15	1.6	1.8	1.10
0.5	2.5	1.25			Av. 1.05
0.5	3.0	1.28			±0.16

These values are calculated from, and are presented in the same order as the data in Table 2.

Equilibrium constant evaluation. With the Co/Zn ratio unity, three simple equilibrium expressions can be written

$$CoZn \rightleftharpoons Co + Zn \tag{I'}$$

$$2\,CoZn \rightleftharpoons Co_2 + Zn_2 \tag{II}$$

$$Co_2Zn_2 \rightleftharpoons Co_2 + Zn_2 \tag{III}$$

To determine which of these can be used best to describe the equilibrium between the species present in the amalgam, the equilibrium constants for reactions I', II and III were calculated. Provided the data are sufficiently precise, the set of equilibrium constants that shows the least variation with concentration will correspond to the most probable equilibrium constant expression. These equilibrium constants were calculated using the stripping analysis data from Table 2, along with the accumulation coefficients, to calculate the amalgam concentrations. These equilibrium constants are listed in Table 4, and K_2 appears to be much less a function of concentration than the other possibilities. Thus, these data strongly support the conclusions of FICKER AND MEITES[7] with regard to the stoichiometry and equilibrium involved in the

TABLE 4

EQUILIBRIUM CONSTANTS, K_1, K_2, AND K_3, CALCULATED FOR REACTIONS I', II, AND III

[Co]/[Zn]	$K_1 \cdot 10^2$	K_2	$K_3 \cdot 10^2$
0.7	2.84	2.45	2.34
0.8	1.13	2.80	0.57
1.2	1.15	2.00	2.48
1.3	3.95	1.62	1.97
1.4	1.16	1.85	0.56
1.6	1.25	1.91	0.63
1.8	1.21	1.67	0.62
2.0	5.44	1.66	2.57
3.0	4.00	2.55	2.00
Av.	$2.46 \cdot 10^{-2}$	2.05	$1.52 \cdot 10^{-2}$
Rel. Sd. Dv.	65%	21%	60%

Co–Zn intermetallic compound. However, the value of K_2 calculated here is about one order of magnitude smaller than that reported by FICKER AND MEITES.

These results indicate that this general approach is a very useful way of studying intermetallic compounds. However, the inherent limitations on the precision of stripping analysis data make it very difficult to perform additional experiments that would permit more definite conclusions regarding the stoichiometry and the equilibria involved.

KINETIC STUDY OF THE FORMATION OF THE Co–Zn INTERMETALLIC COMPOUND

From qualitative observations made in the anodic stripping experiments described above, it appeared that the Co–Zn intermetallic compound was formed very rapidly in the mixed amalgam. To characterize the reaction rates involved, a kinetic study was carried out.

Kinetic characteristics of the Co–Zn system

The reactions that take place during the formation of the Co–Zn intermetallic compound are not known in enough detail to assign an unambiguous mechanism. For example, in experiments in which the intermetallic compound is formed during a simultaneous deposition of both cobalt and zinc, the reaction might be very complex:

$$2\, Co(II) \xrightarrow{4e} Co_2 \tag{IV}$$

$$2\, Zn(II) \xrightarrow{4e} Zn_2 \tag{V}$$

$$Co_2 + Zn_2 \xrightarrow{k_f} 2\, CoZn \tag{VI}$$

The formation of the Co_2 species was shown to be very rapid in the cyclic triangular wave experiments reported previously[11]. Similar experiments have not yet been carried out with zinc, since the existence of the Zn_2 species was not considered seriously until recently. However, it would be expected to be quite rapid. Further complications involve the reaction between the cobalt and zinc, especially if they are

present at comparable concentration levels, since kinetic data for such second-order electrochemical kinetic systems are not readily evaluated.

In this case, however, it was possible to make use of the unique electrochemical properties of the cobalt system, to avoid the second-order effects. The electrochemical characteristics of the cobalt and zinc systems are shown in the stationary electrode polarograms of Fig. 2. Because of the wide potential separation between the cathodic and anodic branches of the Co(II)–Co amalgam system, it is possible to form a cobalt amalgam on a hanging mercury drop (*e.g.*, at a potential of −1.2 V) and then maintain the amalgam without further reaction at a potential where zinc is not reduced (between −0.2 and −0.8 V). Thus, cobalt amalgam drops can be prepared in a separate cobalt(II) solution, and then these electrodes can be transferred to a fresh zinc(II) solution while holding the electrode at −0.4 V.

These cobalt amalgam drops are available for further reaction with zinc whenever the potential is made sufficiently cathodic to reduce the zinc ions. Provided the zinc concentration in the amalgam is kept low with respect to the cobalt, the reaction scheme can be considered a pseudo first-order chemical reaction following charge transfer, *i.e.*, reaction (V) followed by

$$Zn_2 \xrightarrow[Co_2]{k} 2\,CoZn \tag{VII}$$

Theoretical considerations

Because of the uncertainty regarding the exact nature of reaction (V), the one-step methods of studying chemical reactions initiated by a charge transfer could not be used. Using the generalized notation

$$O + n\,e \rightleftharpoons R \tag{VIII}$$

$$R \xrightarrow{k} Z \tag{IX}$$

these methods depend on generating R under conditions where the electrochemical equilibrium can be shifted significantly by the removal of R from the vicinity of the electrode surface by the chemical reaction[14]. KEMULA AND GALUS[15] used such a one-step method in the only previously reported kinetic investigation of an intermetallic system in mercury. But these one-step methods require that the charge transfer that initiates the chemical reaction be electrochemically reversible, not complicated in any way by charge transfer or extraneous chemical kinetic effects. Such effects prevented application of a one-step method to the Co–Zn system.

An alternative approach is available, however, in the two-step methods, such as cyclic triangular wave voltammetry[16], current reversal chronopotentiometry[17], or the step-functional potentiostatic method[9]. Although any one of the three methods could have been used in principle, the step-functional potentiostatic method seemed to be least susceptible to unknown complications related to reaction (V). In this method, the potential is jumped to a value where the rate of generation of R (the cathodic current) is determined solely by the diffusion of substance O to the electrode surface. Then at some switching time, τ, the potential is suddenly returned to the initial value. The resulting anodic current, which is determined by the diffusion-controlled re-oxidation of R, gives a measure of the unreacted R.

The rate constant can be determined from the difference between the observed anodic current in the kinetic case and the anodic current which would have been observed in the absence of the chemical reaction (Fig. 3). The current–time curves were analysed by measuring the anodic to cathodic current ratios, i_a/i_c, at specific values of t and $t-\tau$, in a direct application of the theory presented previously[9]. The
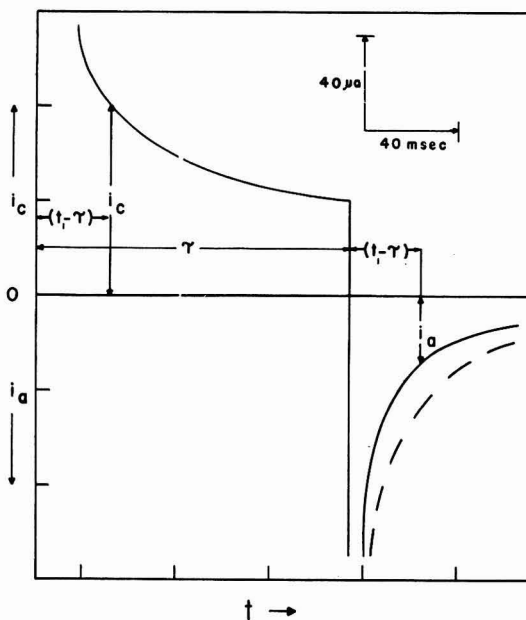
Fig. 3. Typical cathodic–anodic current–time curves for the Zn system. Soln.: $1.00 \cdot 10^{-3}$ M Zn; 0.1 M pyridine–pyridinium chloride, pH 6.0; 1.0 M NaNO$_3$; $10^{-4}\%$ gelatin. Initial potential, E_i, was -0.40 V vs. S.C.E., and the square-wave pulse was -0.80 V; $\tau = 134$ msec. For the anodic portion of the current–time curve, the dashed line is obtained on a pure mercury electrode, the solid line is obtained on a cobalt-amalgam electrode.

rate constants were obtained from working curves in which the current ratios, i_a/i_c, are plotted against the dimensionless parameter, $k\tau$, for various values of the time ratio, $(t-\tau)/\tau$. The time ratios used in this work were selected so that the working curves calculated previously[9] could be used directly.

Experimental procedures

In general, the experimental procedure involved forming a cobalt amalgam drop electrode by pre-electrolysis in a solution containing cobalt(II), transferring this cobalt amalgam drop to a fresh solution containing zinc, then applying the potential change to electrolyze zinc into the cobalt amalgam on the first step, and to reoxidize the unreacted zinc on the second step.

The preparation of the cobalt amalgam followed the general stripping-analysis pre-electrolysis procedures described previously[11]. A constant-potential pre-electrolysis was carried out in a stirred solution containing 2.5×10^{-3} M cobalt(II), 1 M sodium nitrate, 0.1 M pyridine–pyridinium chloride, pH 6.0. The pre-electrolysis potential was -1.20 V vs. S.C.E., and the plating time was 5 min. The electrolysis

conditions were similar to those used in the previous case, and from the magnitude of the plating current, the accumulation coefficient, γ_{Co}, was of the order of 200, as before. Thus, the amalgam concentrations used were extremely high—of the order of 0.5 M.

As discussed previously[11], the stripping analysis behavior of cobalt amalgams becomes very complicated when the cobalt concentration is high. Multiple peaks are observed which have been interpreted as indication of cobalt aggregates or possibly precipitates in the mercury. Unfortunately, high cobalt concentrations were required for the kinetic study to ensure that the chemical reaction remains pseudo first-order. However, in all cases, these concentrated amalgam drops were bright and shiny, and there was no visible evidence of precipitation on the amalgam surface.

After the pre-electrolysis step, the cobalt amalgam drop was removed from the solution and rinsed with distilled water and finally with the test solution. The electrode then was transferred to a second solution containing the zinc ions, 1 M sodium nitrate, 0.1 M pyridine–pyridinium chloride (pH 6.0). Simultaneously, the electrode potential was set at -0.4 V $vs.$ S.C.E. A 30-sec interval was allowed for the solution to come to rest.

The step-functional controlled-potential experiments were carried out by applying a single square pulse of -0.8 V amplitude to the working electrode. Thus the first (cathodic) step was carried out at -1.20 V $vs.$ S.C.E., a potential in the limiting current region for the reduction of zinc ions, and the second (anodic) step was carried out at -0.4 V, a potential in the limiting current region for the oxidation of zinc amalgams. To prove that the cobalt amalgam is not electroactive under these conditions, suitable blanks were measured in the absence of zinc, using both cobalt amalgam and pure mercury hanging drop electrodes. The current–time curves obtained in these measurements were identical, demonstrating the absence of electroactive species in the cobalt amalgam in this potential range.

Although the applied potential signal was of large amplitude, the charging current was small compared to the electrolysis current observed for the 10^{-3} M zinc solutions. Thus, blank corrections were not required.

Results and discussion

Pure mercury electrodes. To characterize the mass transfer process in the Zn^{2+}–Zn amalgam system alone, a quantitative study was made of the cathodic–anodic current–time curves for zinc using exactly the same procedures as in the kinetic studies, but without cobalt present. In these experiments, 4 switching times were used with the 1.0×10^{-3} M zinc solution: 540, 250, 126 and 49 msec. In addition, the two other zinc concentrations used in the kinetic studies (5.0×10^{-4} M, and 2.0×10^{-3} M) were studied with the two switching times actually used in the kinetic studies: 126 and 49 msec. At least three replicate curves were measured for each concentration and switching time.

The cathodic current–time curves were analysed by plotting i_c/C^*_0 vs $1/\sqrt{t}$ for each value of τ. Straight lines were obtained in each case, and the results indicated that the reduction of zinc under the experimental conditions used here is a diffusion-controlled process. The diffusion coefficient, estimated from the slopes of the i_c $vs.$ $1/\sqrt{t}$ plots for all three concentrations was 6.24×10^{-6} cm^2/sec, relative standard deviation 2%.

The anodic current–time curves were analysed by comparing them to the cathodic current–time curves. Current ratios, i_a/i_c, were measured at several values of t and $(t-\tau)$ on each current–time curve, and then these ratios were plotted as a function of $(t-\tau)/\tau$. Typical results obtained for four values of τ are shown in Fig. 4, where the points are experimental values, and the lines are theoretical. The agreement
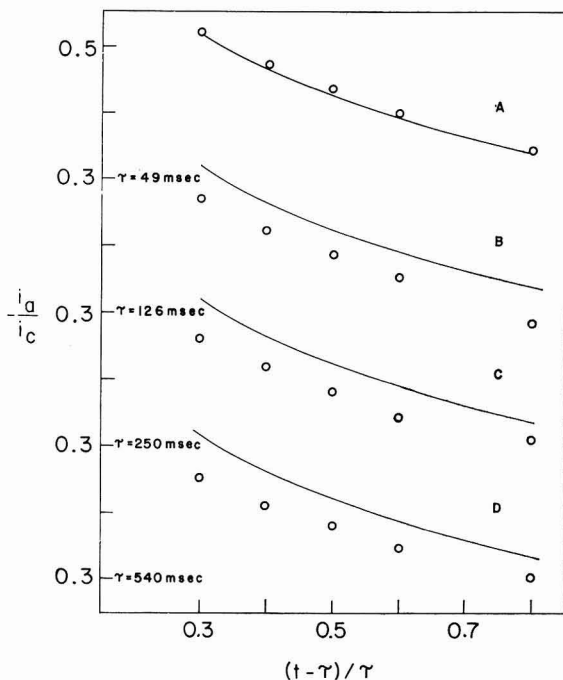
Fig. 4. Comparison of expt. with theory under conditions where the subsequent chemical reaction is absent, *i.e.*, with pure mercury electrodes. (—), theory; (○) exptl.

between experiment and theory is excellent for the shortest switching time (49 msec), and although the experimental current ratios are uniformly low for the other switching times, the agreement is still thought to be satisfactory, since the data are plotted in a manner which emphasizes small deviations from theory. Although these deviations are in the proper direction to be accounted for by convergent cathodic diffusion and divergent anodic diffusion[18,19], the spherical correction terms are not large enough to account for the entire difference. An alternative possibility may involve stirring caused by drop movement on application of the potential step[18]. This also would cause high cathodic currents and low anodic currents, the proper direction to account for the observed deviations from theory. Still another possibility may be related to the postulated dimerization of the Zn(amal) after the reduction. Depending on the time scale for the dimerization, a diminished anodic current might be caused by an unsymmetrical diffusion process. Considering the other uncertainties involved in the kinetic measurements, however, the deviations from pure diffusion theory were relatively unimportant.

Kinetic measurements. For the kinetic measurements with cobalt-amalgam drop electrodes only two switching times were used, 49 and 126 msec, values which were of the same order of magnitude as the half-life of the chemical reaction.

The cathodic curves obtained for the reduction of zinc on a cobalt-amalgam drop were identical with those measured on a pure mercury drop. This is in accord with the assumption that the subsequent chemical reaction between the zinc and cobalt should not affect the diffusion-controlled reduction of the zinc.

To analyse the anodic current–time curves obtained with a cobalt-amalgam drop electrode, the current ratios, i_a/i_c, were obtained by measuring i_a and i_c at values of t such that values of $(t-\tau)/\tau$ were equal to 0.3, 0.4, 0.5, 0.6 and 0.8. To improve the accuracy and convenience of reading the currents from the photographs of the oscilloscope traces, the data were replotted as i *vs.* $1/\sqrt{t}$ for both the cathodic

TABLE 5

KINETIC DATA FOR THE FORMATION OF THE Co–Zn INTERMETALLIC COMPOUND

$[Zn^{2+}]$ $(m/l \cdot 10^3)$	$\tau(msec)$	$(t-\tau)/\tau$	i_a/i_c	$k(t-\tau)$	$Av.\ k$ (sec^{-1})
0.5	49	0.3	0.350	0.126	
		0.4	0.324	0.140	
		0.5	0.294	0.165	
		0.6	0.268	0.180	
		0.8	0.224	0.240	
	126	0.3	0.258	0.228	
		0.4	0.218	0.296	
		0.5	0.191	0.345	
		0.6	0.171	0.407	
		0.8	0.126	0.544	5.61
1.0	49	0.3	0.360	0.120	
		0.4	0.325	0.140	
		0.5	0.304	0.150	
		0.6	0.275	0.174	
		0.8	0.225	0.232	
	126	0.3	0.260	0.225	
		0.4	0.225	0.286	
		0.5	0.193	0.345	
		0.6	0.165	0.418	
		0.8	0.123	0.560	5.66
2.0	49	0.3	0.358	0.120	
		0.4	0.318	0.141	
		0.5	0.300	0.150	
		0.6	0.281	0.168	
		0.8	0.225	0.208	
	126	0.3	0.257	0.229	
		0.4	0.226	0.284	
		0.5	0.193	0.350	
		0.6	0.167	0.420	
		0.8	0.122	0.560	5.60

Each i_a/i_c ratio represents the average of at least eight experiments; a fresh cobalt-amalgam electrode was used in each case.

and anodic current–time curves. From these linear plots, the currents were measured at the five pre-selected values of t and $(t-\tau)$.

The current ratios, i_a/i_c, obtained in this way were used with the working curves to obtain values of the kinetic parameter, $k\tau$. Thus, from each current–time curve, five estimates of $k\tau$ were obtained. These measurements were made for the two switching times on two separate zinc solutions at each concentration, and at least four replicate current–time curves (each on a fresh cobalt-amalgam drop electrode) were obtained in each case. These data are summarized in Table 5.

The values of $k\tau$ were converted to $k(t-\tau)$ in order that the data obtained with the two values of τ could be combined in a form so that they could be processed together. Then plots were made of $k(t-\tau)$ *vs.* $(t-\tau)$, and the rate constant was calculated directly from the slope. In each case, a reasonable straight line which passed through the origin (as required by theory) could be drawn through the experimental points, although the data obtained at short switching times were consistently high (Fig. 5).
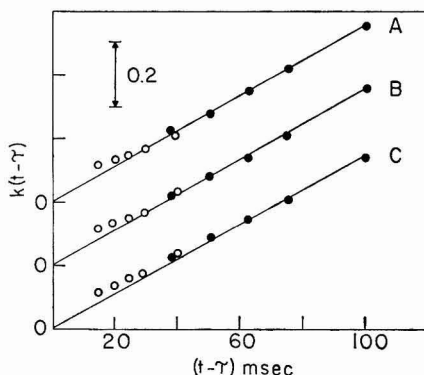
Fig. 5. Exptl. plot of $k(t-\tau)$ *vs.* $(t-\tau)$. Soln.: 0.1 M pyridine–pyridinium chloride, pH 6.0; 1.0 M NaNO$_3$; $10^{-4}\%$ gelatin; with (A), $2.0 \cdot 10^{-3}\ M$ [Zn^{2+}]; (B) $1.0 \cdot 10^{-3}\ M$ [Zn^{2+}]; (C), $0.5 \cdot 10^{-3}\ M$ [Zn^{2+}]. (●), $\tau = 126$ msec; (○) $\tau = 49$ msec.

It is possible to speculate on the sources of error in these experiments. For example, it can be assumed that the same factors that caused the deviation from pure diffusion theory in the study of the zinc system (Fig. 4), are also in operation in the kinetic studies under these conditions. Thus, a range of values of k can be estimated which brackets the values given in Table 5. However, the exact nature of neither the cobalt nor zinc species in the mercury is known with any certainty at this time. Therefore, the kinetic study reported here should be considered as no more than a measure of the rate at which the free zinc disappears. A more detailed evaluation of the rates must await detailed information regarding the form and concentration of the cobalt and zinc species that actually react.

Nevertheless, this study demonstrates that the application of modern methods of electroanalytical chemistry will be of value in the investigation of these complex systems, and the approaches developed in this work will form the basis of extensive new knowledge on mixed amalgams as other intermetallic systems are studied.

ห้องสมุด กรมวิทยาศาสตร์

SUMMARY

Stripping analysis techniques were extended to the study of mixed Co–Zn amalgams in hanging mercury drop electrodes. The composition of the intermetallic compound and the equilibria involved in the amalgam phase were investigated. Rapid and convenient methods were developed using data from anodic stationary electrode polarograms of the mixed amalgams. The results confirmed previous work, and indicated that the intermetallic compound is CoZn, in equilibrium with Co_2 and Zn_2, with $K = [Co_2][Zn_2]/[CoZn]^2 = 2$ (Rel. S. D., 20%).

The rate of formation of the Co–Zn intermetallic compound was measured using the step-functional potentiostatic method. Zinc was deposited on a previously prepared cobalt amalgam electrode, and then, in a second step, the unreacted zinc was reoxidized. The cobalt amalgam concentration was maintained at 0.5 M, and the pseudo first-order rate constant for the disappearance of zinc was 5.6 sec^{-1}.

REFERENCES

1 A. S. RUSSELL, P. V. F. CAZALET AND N. M. IRVIN, J. Chem. Soc., (1932) 841.
2 G. TAMMANN AND W. JANDER, Z. Anorg. Allgem. Chem., 124 (1922) 105.
3 G. N. BABKIN AND M. T. KOZLOVSKII, Izv. Vysshikh. Uchebn. Zavedenii, Khim. i Khim Tekhnol., (1958) 129.
4 A. G. STROMBERG AND V. E. GORODOVYKH, Zh. Neorgan. Khim., 8 (1963) 2355.
5 W. KEMULA AND Z. GALUS, Bull. Acad. Polon. Sci., Ser. Sci. Chim. Geol. Geograph., 7 (1959) 553.
6 W. KEMULA, Z. GALUS AND Z. KUBLIK, ibid., 6 (1958) 661.
7 H. K. FICKER AND L. MEITES, Anal. Chim. Acta, 26 (1962) 172.
8 I. SHAIN, Treatise on Analytical Chemistry, edited by KOLTHOFF AND ELVING, Interscience, New York, 1963, Part I, sec. D-2, chap. 50.
9 W. M. SCHWARZ AND I. SHAIN, J. Phys. Chem., 69 (1965) 30.
10 W. L. UNDERKOFLER AND I. SHAIN, Anal. Chem., 35 (1963) 1778.
11 B. K. HOVSEPIAN AND I. SHAIN, J. Electroanal. Chem., 12 (1966) 397.
12 I. SHAIN AND J. LEWINSON, Anal. Chem., 33 (1961) 187.
13 P. DELAHAY, C. C. MATTAX AND T. BERZINS, J. Am. Chem. Soc., 76 (1954) 5319.
14 D. M. H. KERN, ibid., 75 (1953) 2473; 76 (1954) 1011.
15 W. KEMULA AND Z. GALUS, Bull. Acad. Polon. Sci., Ser. Sci. Chim. Geol. Geograph., 7 (1959) 607.
16 R. S. NICHOLSON AND I. SHAIN, Anal. Chem., 36 (1964) 706.
17 O. DRACKA, Collection Czech. Chem. Commun., 25 (1960) 338.
18 I. SHAIN AND K. J. MARTIN, J. Phys. Chem., 65 (1961) 254.
19 W. G. STEVENS AND I. SHAIN, ibid. 70 (1966) 2276.

THE ANODIC DISSOLUTION OF MERCURY IN SULPHIDE ION SOLUTIONS

R. D. ARMSTRONG, D. F. PORTER AND H. R. THIRSK

Department of Physical Chemistry, University of Newcastle upon Tyne, 1 (England)

(Received May 17th, 1966)

INTRODUCTION

The anodic behaviour of mercury in sulphide solutions has previously been investigated polarographically[1,2] and it has been observed that a dissolution process precedes the formation of an anodic film on the electrode. The nature of the dissolving species has been postulated[2] as HgS_2^{2-}, although its identification has not been attempted.

BARKER AND FAIRCLOTH[3] have measured the capacity of a mercury electrode in contact with 0.5 M Na_2S solution at potentials cathodic to the dissolution region, their results indicating little or no anion adsorption prior to the dissolution reaction, which, however, they have not studied. Recently, KISELEV AND ZHDANOV[4] have measured the capacity for a number of sulphide ion concentrations but have been unable to isolate effects which might indicate anion adsorption, owing to the presence of the dissolution reaction. Again, no attempt was made to identify the nature of the dissolving species or the mechanism of the dissolution reaction. The present experiments were intended to elucidate these factors.

EXPERIMENTAL

Instrumental

The kinetics of the anodic dissolution reaction have been studied using the faradaic impedance method. Figure 1 shows a block diagram of the equipment which incorporated a potentiostat and pulse generator of a design previously described[5]. In order to make electrode impedance measurements, an audio frequency signal generator was used to superpose a sinusoidal signal on the selected d.c. bias potential of the working electrode. The amplitude of this signal was necessarily small since the impedances of faradaic electrode processes show an exponential potential dependence. In practice, a peak-to-peak amplitude of 5 mV was found small enough to produce an undistorted sinusoidal component of the cell current and large enough to minimise the effects of random noise.

The oscillator output was fed into a 1000:1 potential divider which enabled a signal of exactly 1000 times the amplitude of that applied to the working electrode to be displayed on a Tektronix Type 503 oscilloscope. This signal was applied to the calibrated horizontal amplifier of the oscilloscope whilst the vertical amplifier displayed the periodic component of the cell-current arising from the applied sinusoidal

potential. The current was measured as the potential across a calibrated 1000-Ω resistor in series with the cell.

Since the signals applied to the horizontal and vertical oscilloscope amplifiers were of the same frequency, the resultant Lissajous figure took the general form of an
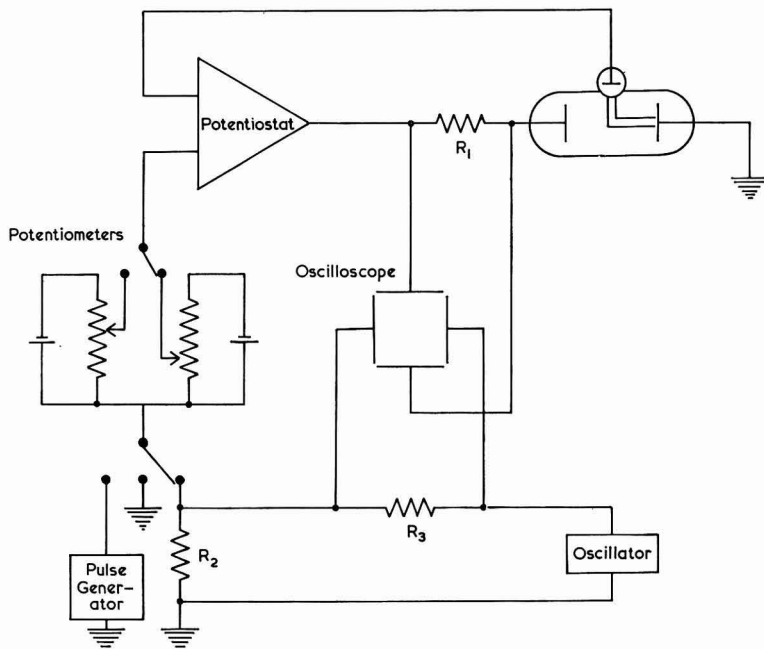
Fig. 1. Block diagram of potentiostatic equipment. $R_1 = 1000\ \Omega$, $R_2 = 100\ \Omega$, $R_3 = 100\ k\Omega$.

ellipse the parameters of which were governed by the impedance of the electrode. Measurement of the ellipse yielded directly the magnitude, $|Z|$, and phase shift, θ, of the impedance in the normal way.

Impedance measurements have been made in this manner at frequencies of 15 to 2000 c/sec. The upper frequency limit is determined by the ohmic drop in solution, between the tip of the Luggin capillary and the working electrode surface, which becomes comparable with the electrode impedance at frequencies above 2000 c/sec. The potentiostat itself may be operated at frequencies up to 15 kc/sec above which instrumental limitations introduce a phase shift.

Some additional measurements have been obtained using a conventional a.c. bridge[6] to measure the impedance of a hanging mercury drop electrode in M Na_2S solution. This method gives useful data over a frequency range extending to 100 kc/sec.

Electrochemical cells

For the potentiostatic experiments, the cell was of the type previously used in these laboratories for kinetic studies of the formation of solid phases on liquid substrates and has been described in detail elsewhere[7]. The upturned mercury drop forming the renewable working electrode surface had an area of the order of 10^{-1} cm^2; the exact value was determined by measurement with a travelling microscope and checked

by comparing the measured differential capacity in M NaOH solution with the data of PAYNE[8].

Potentials were measured by reference to a mercury/mercuric oxide electrode in M NaOH solution *via* a Luggin capillary and a liquid junction formed at a three-way tap.

The cell used for the a.c. bridge measurements[6] incorporated a hanging mercury drop electrode and concentric cylindrical platinum-foil counter electrode. Again, a three-way tap enabled the formation of a liquid junction with the reference electrode section.

Materials

Mercury was purified by prolonged agitation in contact with dilute nitric acid followed by two successive distillations *in vacuo*.

AnalaR-grade reagents were used throughout and solutions of sodium sulphide were prepared, in an atmosphere of purified nitrogen, from de-oxygenated triply distilled water in order to minimise oxidation.

Solutions

The sulphide ion solutions in which the dissolution reaction has been studied are listed in Table 1 with the concentrations of the ionic species present, the ionic strengths and the potentials of the liquid junctions formed with M NaOH solution.

The calculation of the ionic concentrations requires a knowledge of the equilibrium constant, K_{HS^-}, for the dissociation

$$HS^- \rightleftharpoons H^+ + S^{2-}$$
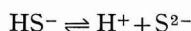
Values of K_{HS^-} at 25° reported in the literature vary considerably[9] between the limits of 6.3×10^{-13} and 1.2×10^{-15} mole l^{-1}. ELLIS AND GOLDING[10] have observed

TABLE 1

CALCULATED IONIC CONCENTRATIONS AND LIQUID JUNCTION POTENTIALS

Soln.	$[S^{2-}]$ (mole l^{-1})	$[HS^-]$ (mole l^{-1})	$[OH^-]$ (mole l^{-1})	$[Cl^-]$ (mole l^{-1})	$[Na^+]$ (mole l^{-1})	Ionic strength (mole l^{-1})	Liquid junction potential with M NaOH (mV)
(a) Using $K_{HS^-} = 1.0 \cdot 10^{-14}$							
M Na$_2$S	0.382	0.618	0.618	—	2.0	2.382	−6.8
0.5 M Na$_2$S+ M NaOH	0.275	0.225	1.225	—	2.0	2.275	+1.7
0.5 M Na$_2$S+ M NaCl	0.134	0.366	0.366	1.0	2.0	2.134	−6.7
(b) Using $K_{HS^-} = 2.5 \cdot 10^{-15}$							
M Na$_2$S	0.172	0.828	0.828	—	2.0	2.172	−1.9
0.5 M Na$_2$S+ M NaOH	0.128	0.372	1.372	—	2.0	2.128	+4.3
0.5 M Na$_2$S+ M NaCl	0.050	0.450	0.450	1.0	2.0	2.050	−4.7

that the inconsistencies may well arise through the instability of alkaline sulphide solutions in air and claim an accuracy of $\pm 20\%$ in their value of 1.0×10^{-14} mole l^{-1} obtained by spectrophotometric measurements in oxygen-free solutions.

Thus Table 1 gives the ionic concentrations for the solutions used in the present work, calculated on the basis of (a) $K_{HS^-} = 1.0 \times 10^{-14}$ mole l^{-1}, (b) $K_{HS^-} = 2.5 \times 10^{-15}$ mole l^{-1}. The latter value gave the best stoichiometric consistency in the subsequent results and hence the concentrations shown in Table 1(b) were used throughout this work.

The liquid junction potentials were calculated from the Henderson equation using an estimated typical value of 70 cm^2 Ω^{-1} equiv.$^{-1}$ for the limiting equivalent conductivity of the S^{2-} ion, for which no data is available.

All measurements were made at room temperature, $24 \pm 1°$.

POTENTIOSTATIC EXPERIMENTS

Some preliminary measurements were made by observing current–time transients for the dissolution reaction in M Na_2S solution. The potential of the working electrode was initially held at -1.10 V (Hg/HgO), *i.e.*, negative to the potential at which dissolution occurs. An anodic step pulse was then applied by means of the pulse generator. Pulse heights of 200–300 mV resulted in a current falling with time. Higher potentials produced more complex transients owing to an anodic electrocrystallisation reaction, but for the present work attention was limited to the range in which dissolution occurred without film formation.

The current–time transients indicate that the reaction is not entirely diffusion controlled since the current did not show a linear dependence on $t^{-\frac{1}{2}}$.

Attempts were made to obtain the pseudo-steady state dissolution current at $t = 0$ by extrapolation of the current against $t^{\frac{1}{2}}$ but this proved impracticable since a linear extrapolation is not possible over the time scale of the transients (100 μsec–100 msec).

FARADIC IMPEDANCE MEASUREMENTS

Faradaic impedance measurements were made in the potential region of the anodic dissolution reaction in each solution. The impedance was measured at each of several fixed potentials, at frequencies of 15–2000 c/sec. The working electrode was held at a cathodic potential (-1.40 V on Hg/HgO) between the readings.

Values of $|Z|$ and θ obtained in this manner were used to calculate the resistive and capacitative components of the equivalent series circuit[11] of the electrode impedance at each potential and frequency, using

$$R_s = |Z| \cos \theta \tag{1}$$

$$\frac{1}{\omega C_s} = |Z| \sin \theta \tag{2}$$

These quantities were plotted against $\omega^{-\frac{1}{2}}$, where ω is the angular frequency, after the method proposed by RANDLES[12]. The dependence on $\omega^{-\frac{1}{2}}$ is given by[11]

$$R_s = \left(\frac{RT}{nF}\right) \left\{ \frac{1}{i_0} + \frac{1}{2^{\frac{1}{2}}nF\omega^{\frac{1}{2}}} \left[\left(\frac{1}{C_O D_O^{\frac{1}{2}}}\right) + \left(\frac{1}{C_R D_R^{\frac{1}{2}}}\right) \right] \right\} \tag{3}$$

$$\frac{1}{\omega C_s} = \left(\frac{RT}{nF}\right)\left\{\frac{1}{2^{\frac{1}{2}}nF\omega^{\frac{1}{2}}}\left[\left(\frac{1}{C_O D_O^{\frac{1}{2}}}\right) + \left(\frac{1}{C_R D_R^{\frac{1}{2}}}\right)\right]\right\} \tag{4}$$

where i_0 is the exchange current density; C_O, C_R are the surface concentrations of the oxidised and reduced species respectively and D_O, D_R are the respective diffusion co-efficients. Since $C_R \gg C_O$ in these experiments, we may put $(C_R D_R^{\frac{1}{2}})^{-1}=0$. Equations (3) and (4) then represent a pair of parallel lines, the slope of which yields C_O. The intercept of R_s at $\omega^{-\frac{1}{2}} = 0$ corresponds to the charge transfer resistance, R_{ct}, whence i_0 is calculated:

$$R_{ct} = \left(\frac{RT}{nF}\right)\frac{1}{i_0} \tag{5}$$

Figure 2 shows a typical experimental plot of R_s and $1/(\omega C_s)$ against $\omega^{-\frac{1}{2}}$. The linearity of such plots indicates that the slow step of the reaction is heterogeneous. Values of C_O and i_0 at each potential were calculated assuming $D_O = 10^{-5}$ cm^2 sec^{-1}, $n = 2$.

Deviations from linearity as $\omega^{-\frac{1}{2}} \to 0$, which are most marked at the most negative dissolution potentials, are attributed to the increasing contribution of the double-
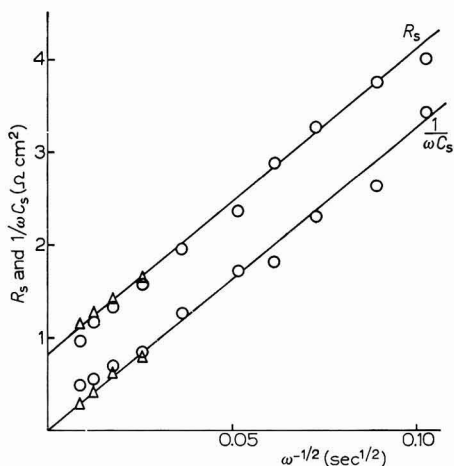
Fig. 2. Typical plot of R_s and $1/\omega C_s$ against $\omega^{-\frac{1}{2}}$. 0.5 M Na$_2$S + M NaOH, $E = -0.90$ V (Hg/HgO). $\triangle$, Points corrected for double-layer capacity ($C_{dl} = 16.5$ μF cm^{-2}).

layer capacity to the electrode admittance as the frequency is increased. A correction for this effect has been applied in all cases where the faradaic impedance is $>5\%$ of that of the double-layer capacity.

In these cases, the equivalent series circuit is transformed to the equivalent parallel circuit, and after subtraction of the double-layer capacity from the total capacity, transformed back to a series circuit which now represents the faradaic path only.

The magnitude of the double-layer capacity required to effect a correction to linearity is in the range 16.5–20 μF cm^{-2}, i.e., values rising only slowly with potential above that measurable at potentials just cathodic to the dissolution range. The use of such values for the double-layer capacity is further justified later.

RESULTS AND DISCUSSION

Nature of the dissolving species

The concentration of the dissolving species, C_O, is plotted as its logarithm against the electrode potential in Fig. 3. The resultant linear slope for each of the solutions gives $2.3\ RT/nF = 0.032$ V, so that $n = 2$.

By comparing the values of $\log C_O$ in the three solutions at a fixed potential, it is possible to determine which of these ions present in solution is involved in the dissolution reaction. No consistent stoichiometry is obtained for any ion or combination
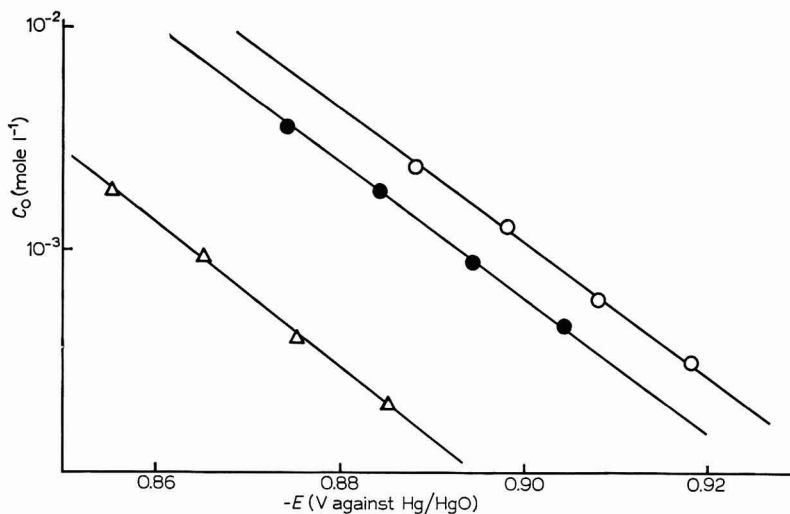
Fig. 3. Potential dependence of C_O (corrected for liquid junction potentials). [Solns.: (o), M Na₂S; (●), 0.5 M Na₂S + M NaOH; (△), 0.5 M Na₂S + M NaCl.

of ions except in the case of S^{2-}, for which $(\partial \log C_O/\partial \log [S^{2-}])_E = 2.1 \pm 0.1$ (Fig. 4). Hence the results indicate that dissolution occurs as the ion HgS_2^{2-} and the overall process is

$$Hg + 2\ S^{2-} \rightleftharpoons HgS_2^{2-} + 2\ e$$
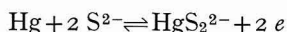
Accurate comparison of the experimentally determined C_O-values with those obtained from equilibrium data is not possible owing to the uncertainty in the latter. The equilibrium constant for

$$Hg^{2+} + 2\ S^{2-} \rightleftharpoons HgS_2^{2-}$$
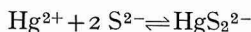
has been reported[9,13] with values from 3.6×10^{50} to 8.5×10^{54} mole⁻² l². The present results are consistent with a value of $\sim 1 \cdot 10^{54}$ mole⁻² l². Equilibrium data for other complex ionic species[13] indicate that none is present at a concentration of $> 10^{-5} \cdot [HgS_2^{2-}]$.

KNOX[14] has reported that HgS dissolves in aqueous Na₂S as the HgS_2^{2-} ion, ot give a yellow solution. In the present work, however, no evidence has been found that

solutions of this ion are coloured. In a qualitative macroscopic experiment, M Na$_2$S solution was electrolysed at a large ($\sim$16 cm^2) mercury pool anode. At potentials where the dissolution was proceeding at the bare anodic mercury surface there was an
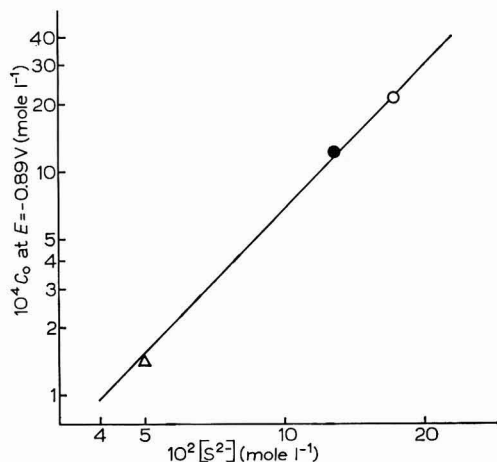
Fig. 4. Logarithmic dependence of C_0 at fixed potential on [S^{2-}] as calculated in Table 1(b). Solns.: (○), M Na$_2$S; (●), 0.5 M Na$_2$S + M NaOH; (△), 0.5 M Na$_2$S + M NaCl.
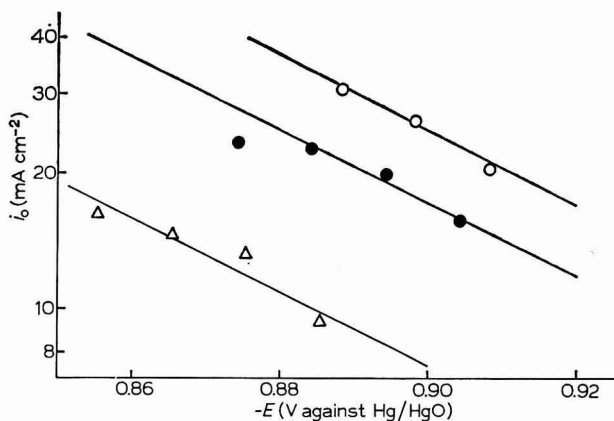
Fig. 5. Potential dependence of i_0 (corrected for liquid junction potentials). Solns.: (○), M Na$_2$S; (●), 0.5 M Na$_2$S + M NaOH; (△), 0.5 M Na$_2$S + M NaCl.

absence of coloration, even on prolonged electrolysis. However, at potentials considerably above that at which a black solid film (probably HgS) formed on the surface, a yellow coloration was produced.

A similar yellow anodic product was observed using a platinum anode and has been attributed to the formation of polysulphides[15,16]. It appears likely that such compounds were present as impurities in the solutions of KNOX and that these, rather than the HgS$_2^{2-}$ species, were responsible for the yellow coloration.

Mechanism of the electrode reaction

When the exchange current density, i_0, for a given solution is plotted logarithmically against electrode potential, E, the anodic Tafel line (slope b_a) is obtained provided that the dissolution reaction is zero order in HgS_2^{2-}. Since (Fig. 5)

$$\left(\frac{\partial \log i_0}{\partial E}\right)_{[S^{2-}], [HS^-], [OH^-]} = \frac{1}{b_a} = (140 \pm 40 \text{ mV})^{-1}$$

a rate-determining step involving a single electron transfer is indicated. At fixed potential a consistent reaction order is found only for S^{2-}. Therefore the reaction is zero order in OH^- and HS^- and first order in S^{2-} since (Fig. 6)

$$\left(\frac{\partial \log i_0}{\partial \log [S^{2-}]}\right)_E = 0.95 \pm 0.10$$
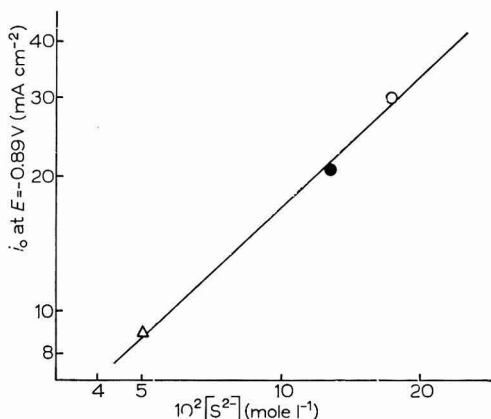
Fig. 6. Logarithmic dependence of i_0 at fixed potential on $[S^{2-}]$. Solns.: ($\circ$), M Na$_2$S; ($\bullet$), 0.5 M Na$_2$S + M NaOH; ($\triangle$), 0.5 M Na$_2$S + M NaCl.

This implies a heterogeneous rate-determining step having the mechanism

$$Hg + S^{2-} \rightarrow HgS^- + e$$

followed by an overall fast step

$$HgS^- + S^{2-} \rightleftharpoons HgS_2^{2-} + e$$
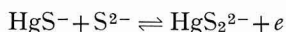
which may be heterogeneous or in part homogeneous.

Such a mechanism invokes the existence of singly-charged Hg^+ for which there is little evidence. The intermediate may, however, be present in the adsorbed state, as has been suggested in the case of HgCN as an intermediate in the dissolution of mercury in solutions containing the CN^- ion[17].

The cathodic Tafel line consistent with the foregoing results and proposed mechanism should have a slope of 43 ± 4 mV decade^{-1}. An attempt was made to check this by plotting $\log i_0$ against E at a fixed $[HgS_2^{2-}]$ (Fig. 7). The initial fast pre-equilibrium step of the reverse reaction should result in a reaction order of -1 for S^{2-}. Hence Fig. 7 does not show the true cathodic Tafel line since there is a non-zero order species present in varying concentration. VETTER[18] has shown that for this case:

$$\left(\frac{\partial \log i_0}{\partial E}\right)_{[\mathrm{HgS_2}^{2-}]} = -\frac{1}{b_c} + \frac{nFx_c}{2.3\, RT\nu} \tag{6}$$

where b_c is the cathodic Tafel slope, x_c is the cathodic reaction order and ν the stoichiometric number of the species which is present in varying concentration. Since for S^{2-}, $x_c = -1$, $\nu = -2$ we should expect to obtain

$$\left(\frac{\partial \log i_0}{\partial E}\right)_{[\mathrm{HgS_2}^{2-}]} = -(140 \pm 40 \text{ mV})^{-1}$$

Experimentally this was found to be $-(160 \pm 20 \text{ mV})^{-1}$, in agreement within experimental error.
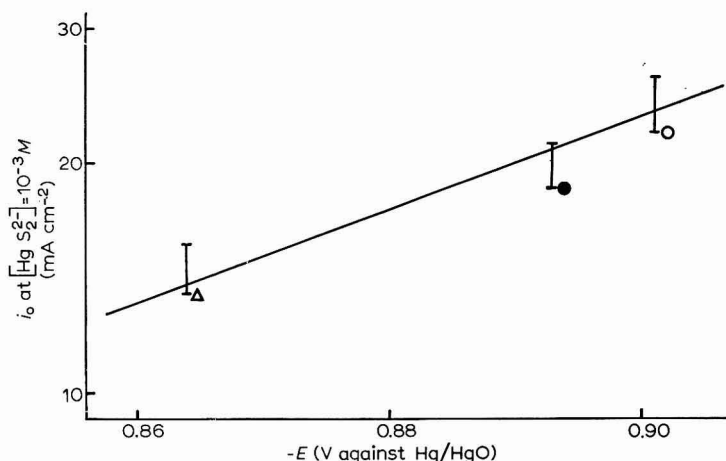
Fig. 7. Potential dependence of i_0 at fixed $[\mathrm{HgS_2}^{2-}]$. Solns.: (○), M Na$_2$S; (●), 0.5 M Na$_2$S + M NaOH; (△), 0.5 M Na$_2$S + M NaCl.

DOUBLE-LAYER CAPACITY MEASUREMENTS

The capacity of the electrode double layer was measured using the potentiostat at potentials cathodic to the dissolution reaction, at a frequency of 1000 c/sec. These results are in general agreement with those of BARKER AND FAIRCLOTH[3] for 0.5 M Na$_2$S solution, although we consider that the values of the capacities, which these authors recorded at the most positive potentials, are partially composed of a faradaic pseudocapacity and are not necessarily indicative of a continuously rising double-layer capacity, C_{dl}, with potential.

In addition, a.c. bridge measurements have been made at more positive potentials and at frequencies up to 80 kc/sec, in an attempt to separate C_{dl} from the faradaic pseudocapacity of the dissolution reaction. The impedance of the electrode in M Na$_2$S solution was measured as R_s and C_s, the components of its equivalent series circuit. The potential dependence of these quantities at frequencies of 1, 40 and 80 kc/sec (Figs. 8 and 9) shows the following features:

(i) R_s increases with potential in the dissolution region and reaches a maximum the position and height of which are frequency dependent.

The potential at which this maximum occurs corresponds approximately to that at which the faradaic and double-layer impedances become equal for a given frequency.
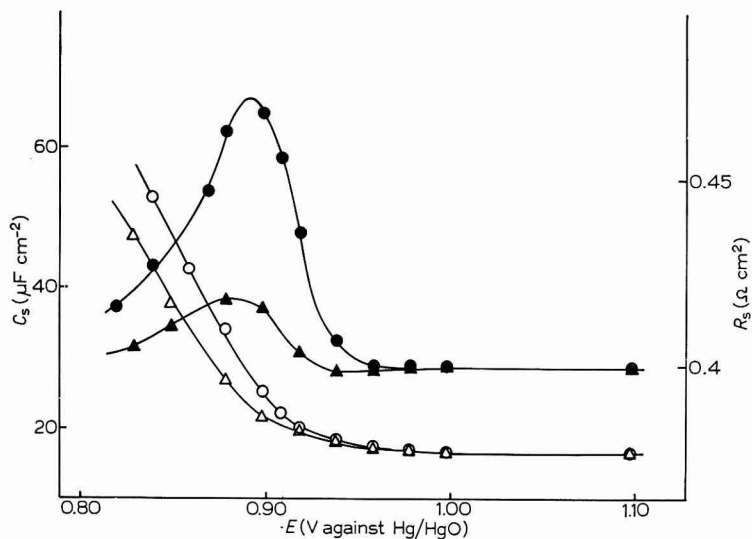
Fig. 8. A.c. bridge measurements. Potential dependence of R_s (solid points) and C_s (open points) in M Na$_2$S solution. Frequencies: ($\circ$), 40 kc/sec; ($\triangle$), 80 kc/sec.
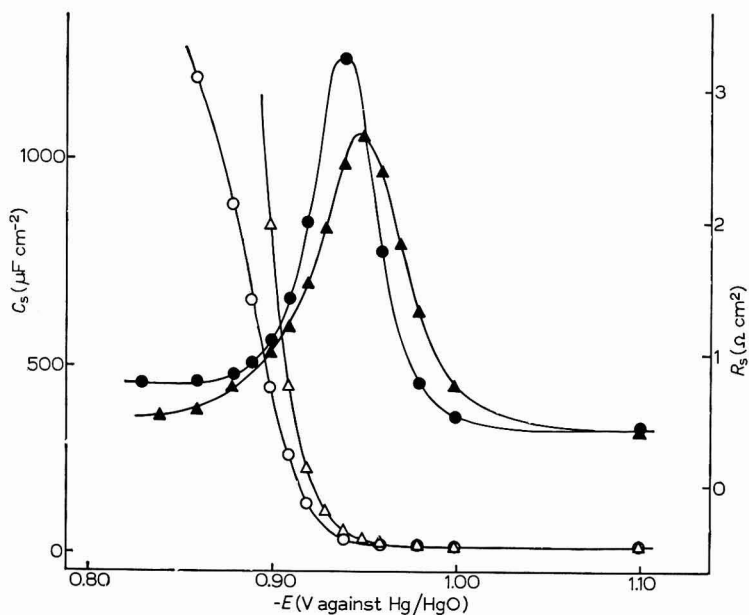
Fig. 9. Comparison of potentiostatic impedance measurements ($\triangle$, $\blacktriangle$) and a.c. bridge measurements ($\circ$, $\bullet$) at 1 kc/sec. Potential dependence of R_s (solid points) and C_s (open points).

(ii) C_s increases with potential in the dissolution region, sharply at 1 kc/sec and progressively less sharply as the frequency is increased.

These measurements show that at 80 kc/sec the double-layer capacity is measurable to potentials < -0.94 V (Hg/HgO) and that up to this potential C_{dl} does not rise above 20 μF cm^{-2}.

The consistency of the results obtained by the a.c. bridge and those obtained using the potentiostat is shown in Fig. 9 where values of R_s and C_s computed from the measurements made with the potentiostat are compared with those obtained directly with the bridge, at 1 kc/sec.

ELECTROCAPILLARY CURVE AND ADSORPTION OF ANIONS

The electrocapillary curve of mercury in 0.5 M K$_2$S solution shows a maximum at a rather negative potential (~ -0.810 V Hg/HgO)[19]. This has previously been interpreted[20] in terms of the strong specific adsorption of S^{2-} or HS^{-} ions. However, as KISELEV AND ZHDANOV have pointed out[4], when GOUY measured the interfacial tension for this system an appreciable current flowed through the cell at potentials in the region of the observed e.c.m. The present measurements indicate that in this potential region the mercury is dissolving as HgS$_2$$^{2-}$. The question therefore arises as to what extent the shape of the electrocapillary curve is indicative of specific anion adsorption in the presence of the reversible electrode reaction.

MOHILNER[21] has shown that in the presence of a reversible electrode process the electrocapillary equation in this case becomes

$$\left(\frac{\partial \gamma}{\partial E}\right) = q^\beta - 2F\Gamma_{HgS_2{}^{2-}} \tag{7}$$

where q^β is the charge in the solution side of the interphase and $\Gamma_{HgS_2{}^{2-}}$ is the surface excess of HgS$_2$$^{2-}$ with respect to water. Thus a maximum can be obtained in the electrocapillary curve in the presence of a reversible dissolution reaction if $q^\beta = 2F\Gamma_{HgS_2{}^{2-}}$. Now q^β may be obtained from the double-layer capacity measurements as

$$q^\beta = \int_0^{\Delta E} C_{dl}.\,d(\Delta E) \tag{8}$$

where ΔE is the potential of the solution cathodic to the P.Z.C. If there is no specific adsorption, C_{dl} does not vary markedly with potential, and we may write

$$q^\beta = K\Delta E \tag{9}$$

where K is the integral capacity. The potential of the observed e.c.m. in 0.5 M K$_2$S solution is -0.810 V (Hg/HgO)[19] and that of the P.Z.C. of mercury in the absence of adsorption is -0.300 V (Hg/HgO)[22]. Hence at the e.c.m. $\Delta E = 0.510$ V. Substitution of this value in eqn. (9) together with $K = 16.5$ μF cm^{-2} yields $q^\beta = 8.4$ μC cm^{-2}.

Assuming that HgS$_2$$^{2-}$ is not specifically adsorbed in the region of the e.c.m. we may also write[21]

$$\Gamma_{HgS_2{}^{2-}} = n_{01}\int_0^\infty \{\exp[2F\phi(x)/RT] - 1\}\,dx \tag{10}$$

where n_{01} is the concentration of HgS_2^{2-} at the electrode surface in moles cm^{-3} and the remaining terms are as defined by MOHILNER.

Integration of eqn. (10) has not been attempted for the case of mixed electrolytes (of which sodium sulphide solution is one), but an approximate order of magnitude calculation may be performed using the integrated form for a $Z:Z$ electrolyte, given by[21]

$$2F\Gamma_{HgS_2^{2-}} = n_{01}\left(\frac{RT\varepsilon}{2\pi n_0}\right)^{\frac{1}{2}}\left[\exp\left(-\frac{2F\phi_2}{2RT}\right) - 1\right]$$ (11)

where the symbols are again as defined by MOHILNER.

If we now approximate the 0.5 M K_2S solution to a 0.25 M 2:2 electrolyte (which has approximately the same ionic strength), we substitute in eqn. (11) as follows: $n_0 = 0.25 \times 10^{-3}$ mole cm^{-3}; $n_{01} = 6.45 \times 10^{-5}$ mole cm^{-3} ($[HgS_2^{2-}]$ at observed e.c.m.); $\varepsilon = 80 \cdot 4\pi \cdot 8.85 \cdot 10^{-14}$ Fcm^{-1}; $\phi_2 = -0.032$ V. The equation then yields $2F\Gamma_{HgS_2^{2-}} = 1.9$ μC cm^{-2}.

Thus the value of $2F\Gamma_{HgS_2^{2-}}$ seems too small to account entirely for the observed electrocapillary curve without assuming any specific anion adsorption. Our own impedance measurements indicate that in 0.5 M Na_2S solution there is no specific adsorption at potentials < -0.860 V (Hg/HgO). However, it is possible that at more positive potentials there is a sudden rise in the double-layer capacity as has been observed in a number of other systems[23].

Capacity at the limit of anodic polarisation

It has already been stated[23] and should again be stressed here, that a pseudo-capacity is observed only if a solution-soluble species (*e.g.*, HgS_2^{2-}) is formed on anodic polarisation, and the presence of such a species is not a necessary condition for the formation of a solid anodic phase.

GRAHAME et al.[24] have suggested that specific anion adsorption at the mercury electrode involves covalent bonding, though this view has been disputed by several authors[25,26]. GRAHAME supports this by comparing the capacities in different electrolytes at the limit of anodic polarisation for which the double-layer capacity is measurable. Thus he finds an approximately linear logarithmic relationship between these capacities and the mercurous ion concentrations of the salts corresponding to the anion in question. It would appear, however, that this procedure is not valid since the limit of anodic polarisation frequently depends on the stability constant of the soluble species formed rather than on the solubility product of the solid anodic phase.

Thus, in the present case, the limit of anodic polarisation occurs when the dissolution reaction provides a detectable contribution to the electrode admittance and, at this potential, no indication of adsorption is shown by the double-layer capacity measurements, as would be expected from the extremely low solubilities of HgS and Hg_2S, on the basis of GRAHAME's correlation.

SUMMARY

The anodic dissolution of mercury in sulphide ion solutions has been studied by the faradaic impedance method, using *in situ* generation of the dissolving species. The mercury passes into solution as the soluble complex ion HgS_2^{2-}. The rate-determining step in the dissolution reaction has been identified as a heterogeneous single-electron transfer process which is first order in $[S^{2-}]$ and a reaction mechanism is proposed on this basis. Double-layer capacity measurements have been made in the presence of the dissolution reaction and these indicate the absence of any strong specific anion adsorption at the electrode. The shape of the electrocapillary curve for sulphide solutions is discussed in the light of these observations.

REFERENCES

1 J. REVENDA, *Collection Czech. Chem. Commun.*, 6 (1934) 453.
2 I. M. KOLTHOFF AND C. S. MILLER, *J. Am. Chem. Soc.*, 63 (1941) 1405.
3 G. C. BARKER AND R. L. FAIRCLOTH, *Advances in Polarography*, Vol. 1, Pergamon Press, Oxford, 1960, p. 313.
4 B. A. KISELEV AND S. I. ZHDANOV, *Elektrokhimiya*, 1 (1965) 159.
5 A. BEWICK AND M. FLEISCHMANN, *Electrochim. Acta*, 8 (1963) 89.
6 W. P. RACE, unpublished work.
7 M. FLEISCHMANN AND H. R. THIRSK, *Electrochim. Acta*, 9 (1964) 757.
8 R. PAYNE, *J. Electroanal. Chem.*, 7 (1964) 343.
9 *Stability Constants of Metal-Ion Complexes*, Chemical Society Special Publication No. 17, 1964, pp. 215–224.
10 A. J. ELLIS AND R. M. GOLDING, *J. Chem. Soc.*, (1959) 127.
11 P. DELAHAY, *Advances in Electrochemistry*, Vol. 1, Interscience New York, 1961.
12 J. E. B. RANDLES, *Discussions Faraday Soc.*, 1 (1947) 11.
13 G. SCHWARZENBACH AND M. WIDMER, *Helv. Chim. Acta*, 46 (1963) 2613.
14 J. KNOX, *Trans. Faraday Soc.*, 4 (1908) 29.
15 H. GERISCHER, *Z. Elektrochem.*, 54 (1950) 540.
16 W. R. FETZER, *J. Phys. Chem.*, 32 (1928) 1787.
17 M. PÉREZ-FÉRNANDEZ AND H. GERISCHER, *Z. Elektrochem.*, 64 (1960) 477.
18 K. J. VETTER, *Transactions of the Symposium on Electrode Processes, Philadelphia, 1959*, J. Wiley, New York, 1961, p. 47.
19 G. GOUY, *Ann. Chim. Phys.*, (7) 29 (1903) 145.
20 A. N. FRUMKIN, *Kinetics of Electrode Processes*, Moscow, University Press, 1952.
21 D. M. MOHILNER, *J. Phys. Chem.*, 66 (1962) 724.
22 D. C. GRAHAME, E. M. COFFIN, J. I. CUMMINGS AND M. A. POTH, *J. Am. Chem. Soc.*, 74 (1952) 1207.
23 R. D. ARMSTRONG AND M. FLEISCHMANN, *J. Polarog. Soc.*, 11 (1965) 31.
24 D. C. GRAHAME, M. A. POTH AND J. I. CUMMINGS, *J. Am. Chem. Soc.*, 74 (1952) 4422.
25 S. LEVINE, G. M. BELL AND D. CALVERT, *Can. J. Chem.*, 40 (1962) 518.
26 J. O'M. BOCKRIS, M. A. DEVANATHAN AND K. MÜLLER, *Proc. Roy. Soc. London*, 274A (1963) 55.

BIMETALLIC ELECTRODE SYSTEMS IN POLAROGRAPHY

CATHODE RAY POLAROGRAPHIC STUDY USING SILVER AND SILVER AMALGAM CATHODES AND MOLYBDENUM ANODE*

V. T. ATHAVALE, M. R. DHANESHWAR and R. G. DHANESHWAR

Analytical Division, Atomic Energy Establishment, Trombay, Bombay 28 (India)
(Received April 7th, 1966)

Solid wire electrodes are easy to make and therefore convenient to use in micro cells and in continuous analysis. However, the reduction waves are often unreliable and are difficult to interpret owing to ill-defined diffusion conditions. Almost all the work reported in recent years deals with platinum electrodes, rotating or stationary[1], and graphite electrodes[2,3]. These are used mainly for anodic waves. With the improvement in instrumentation which gives fast sweep voltages, the subject of metal indicator electrodes needs re-examination.

The platinum electrode is used extensively as a redox indicator electrode in potentiometry, and for the oxidation or reduction of many ions in polarography. The silver electrode, however, is primarily responsive to silver ions in potentiometry and it is, therefore, of interest to study the behaviour of silver and silver amalgam electrodes in polarography. Silver is an attackable electrode; platinum is a noble electrode.

The study of silver ion reduction by polarography is not easy since mercuric ion is reduced at almost the same half-wave potential and therefore interferes. Furthermore, neither calomel nor mercury pool reference electrodes can be used in silver polarography.

A detailed study of silver ion reduction using the DME-Mo system in d.c. polarography shows how to reduce the interference of the mercury wave to a considerable extent[4]. In general, it has been found that the molybdenum electrode behaves as a reference electrode in almost all aqueous and non-aqueous solutions[5,6].

The present study has been carried out using silver or silver amalgam as indicator electrode, and molybdenum as a reference electrode.

EXPERIMENTAL

Apparatus

D.c. polarograph. A semi-manual Du-Bellay polarograph manufactured by M/s. Association Ouvriers des Instruments de Précision, Paris.

Cathode-ray polarograph. A K-1000 model manufactured by the Southern Instruments Ltd., Richmond, Surrey, U.K.

Electrodes. (a) Platinum wire (19 s.w.g.) electrode prepared by sealing the wire in a Pyrex-glass tube (internal diameter 0.5 in., length 3.5 in.) so that 1 in. of the wire

---

* Presented to the 53rd Session of the Indian Science Congress held at Chandigarh, January 1966.

jutted out of the tube and $\frac{1}{2}$ in. of the wire remained inside. The tube was filled with mercury for electrical contact. (b) Molybdenum wire (25 s.w.g.) electrode, 15 mm long. (c) Silver electrode (28 s.w.g.) prepared by sealing the wire in soft-glass tubing. The length of the silver wire was 7 mm. (d) Silver amalgam electrode prepared by dipping the cleaned silver electrode (5-mm long) in doubly-distilled mercury for about a minute and then washing the amalgamated wire with distilled water[7].

Cleaning of the electrodes. The molybdenum electrode was washed with distilled water, dried on a filter paper, rubbed with emery paper (No. 0), rewashed in distilled water and dried. The silver electrode was cleaned by dipping it for 1 min in 1:4 nitric acid and washed with distilled water. The silver amalgam electrode was cleaned with distilled water, only.

Polarographic cell. This was similar to that described earlier[5]; a 50-ml beaker was fitted with a rubber bung containing a number of holes for inserting various electrodes, and an inlet and outlet for nitrogen. The cell was kept in a thermostat with a constant temperature of 30° ±0.1°. Nitrogen, purified by passing through a vanadous sulphate train, was passed for 20 min before any measurements were taken.

The current–voltage curves on the cathode-ray polarograph were measured by a delayed-trace technique.

Reagents

Silver nitrate solution, 0.1 M, was prepared by dissolving 16.989 g of the dry BDH AnalaR-grade salt in distilled water, making up the solution to 100 ml and storing in an amber-coloured bottle in the dark.

All other solutions were prepared from AnalaR-grade salts.

RESULTS

Polarographic waves for 1.0 mM silver in 0.1 M sulfosalicylic acid as supporting electrolyte were taken on a Du-Bellay d.c. polarograph using the silver and molybdenum electrode system. As no steady current could be obtained for any potential, all the work was carried out on a K-1000 cathode-ray polarograph.

Silver peaks in different supporting electrolytes

For obvious reasons the silver electrode cannot be used in very acidic solutions. The supporting electrolytes tried were therefore mildly acidic or neutral, *viz.*, 1/2-saturated salicylic acid, 0.1 M potassium nitrate, 0.1 M sulfosalicylic acid and 0.1 M potassium thiocyanate. As it is clear from Table 1, only 0.1 M sulfosalicylic acid seemed to be at all suitable. Although silver waves were obtained for all the supporting electrolytes except thiocyanate, the linearity between current and concentration was obtained only in sulfosalicylic acid.

Sulfosalicylic acid supporting electrolyte was found to be suitable also for silver amalgam and platinum electrodes.

Silver and other cation reductions on platinum, silver and silver amalgam cathodes

KOLTHOFF AND LINGANE[8] have reported that a silver wave is obtained on a platinum cathode. However, the wave is not well formed and is practically without base.

With a platinum cathode and molybdenum anode, S-shaped silver waves were obtained in 0.1 M sulfosalicylic acid for 2.0 mM and 1.0 mM silver, but no wave was detected for 0.5 mM. The results in Table 2A indicate that the half-wave potential changes considerably for different silver concentrations.

TABLE 1

SILVER PEAKS IN DIFFERENT SUPPORTING ELECTROLYTES
Cathode — Ag wire; Anode — Mo wire

No.	Supporting electrolyte	Ag concn. $\cdot 10^{-3}$ M	E_p (V)	i_p (μA)	Remarks
1	$\frac{1}{2}$-satd. salicylic acid	1.0	−0.25	12.6	S-shaped curve
2	$\frac{1}{2}$-satd. salicylic acid	0.5	−0.25	10.2	S-shaped curve
3	0.1 M potassium nitrate	1.0	−0.24	14.4	S-shaped curve
4	0.1 M potassium nitrate	0.5	−0.28	15.0	S-shaped curve
5	0.1 M potassium thiocyanate	1.0	slight ppt. is obtained		
6	0.1 M sulfosalicylic acid	1.0	−0.57	2.5	Peak
7	0.1 M sulfosalicylic acid	0.5	−0.57	1.25	Peak

When an S-shaped curve is obtained, E_p is taken as $E_{\frac{1}{2}}$ in the usual sense.

TABLE 2

SILVER AND OTHER CATION WAVES FOR PLATINUM, SILVER AND SILVER AMALGAM CATHODES
(A) Ag peaks for Pt cathode and Mo anode

No.	Ag concn. $\cdot 10^{-3}$ M	E_p (V)	i_p (μA)	Remarks
1	2.0	−0.57	6.8	S-shape
2	1.0	−0.37	3.5	S-shape
3	0.5	Wave merges with blank wave		

(B) Ag and other cation waves for Ag and Ag–Hg cathode and Mo anode

No.	Cation	Cathode	E_p (V)	i_p (μA)	Remarks
4	Ag^+	Ag	−0.57	2.5	Peak
5	Ag^+	Ag–Hg	+0.12	3.60	Sharp peak
6	Hg^{2+}	Ag	−0.40	6.6	S-shape
7	Hg^{2+}	Ag–Hg	−0.28	7.8	Peak
8	Cu^{2+}	Ag–Hg	−0.10	2.5	Peaks are not
			−0.30	3.0	reproducible
9	Cu^{2+}	Ag	No peak is obtained		
10	$Cd^{2+}, Cr^{6+}, Fe^{3+}$ Ni^{2+}, Zn^{2+}	Ag or Ag–Hg	Peaks are not obtained. Sometimes a trace that is visible for the 1st sweep vanishes during subsequent sweeps.		

The concns. of all cations is 10^{-3} M in 0.1 M sulfosalicylic acid.

Silver and other cation (such as copper, cadmium, nickel, iron, chromium and zinc) reductions were tried using silver and silver-amalgam cathodes in 0.1 M sulfosalicylic acid. The concentration of all cations was 1.0 mM. Silver peaks were obtained for both electrodes, but were sharper for the amalgam electrodes. The peak potentials were quite far apart, +0.12 V for the amalgam electrode and −0.57 V for the silver electrode (Table 2B). In d.c. polarography, the mercury wave interferes

with the silver wave for all supporting electrolytes, complexing as well as non-com-plexing, because their standard potentials are practically the same[9]. With silver and amalgam cathodes, the mercuric reduction occurred at -0.40 and -0.28 V, respec-tively, with an S-shaped wave for the silver electrode but a peak for the amalgam electrode. Moreover, the current was found to be proportional to the mercuric ion concentration for 1.0 mM and 0.5 mM, but below 0.5 mM the wave merged with the blank. Thus mercury and silver waves are reasonably separated using the silver cathode, and widely separated with the silver amalgam cathode. For the silver elec-trode, a peak was obtained for silver and an S-shaped wave for mercury, thereby fur-ther reducing the possibility of mercury interference.

No waves were obtained for copper, cadmium, zinc, iron and chromium on a silver electrode. For the amalgam electrode, persistent but irreproducible copper peaks were obtained. For almost all the cations there were traces of peaks in the initial one or two sweeps, but these quickly faded in subsequent sweeps.

As silver is reduced at $+0.12$ V in the case of the amalgam electrode, there was no necessity for passing nitrogen. In the case of the silver electrode, it was not possible to eliminate the oxygen wave entirely, even after passing purified nitrogen for a prolonged time. The oxygen wave, however, is S-shaped and the silver reduction is a peak which sits on top of the oxygen wave and there was, therefore, no interference from the oxygen wave. This oxygen wave has been studied in detail and the findings will be reported later.

Linearity of peak current with concentration

Perfect linearity was obtained for $2\cdot10^{-3}$–$0.25\cdot10^{-3}$ M silver for the silver electrode and for $1\cdot10^{-3}$–$0.25\cdot10^{-3}$ M for the silver amalgam cathode. For $2\cdot10^{-3}$ M, no peak was obtained in the case of the amalgam electrode (Table 3). Silver peaks were obtained for both electrodes at all concentrations, indicating the reversibility of the electrode reaction throughout. The peak potentials remained nearly constant over

TABLE 3

CHANGES IN PEAK CURRENT AND POTENTIAL WITH SILVER CONCENTRATION
Anode — Mo wire

No.	Cathode — Ag wire		concn. Ag^+ $\cdot 10^{-3}$ M	Cathode — Ag–Hg wire	
	E_p (V)	i_p (μA)		E_p (V)	i_p (μA)
1	-0.60	5.0	2.0	no peak	
2	-0.57	2.5	1.0	$+0.12$	3.60
3	-0.57	1.25	0.5	$+0.13$	1.80
4	-0.54	0.63	0.25	$+0.16$	0.90
5	merges with blank wave		0.10	no peak	

Supporting electrolyte, 0.1 M sulfosalicylic acid.

the range of silver concentration, confirming the reversibility of the electrode reaction and the performance of the molybdenum electrode as reference electrode.

A tungsten wire electrode was tried as a reference electrode. Although silver peaks were obtained with the tungsten electrode, no linearity was observed between

peak heights and silver concentration. This may be due to the formation of an adhering silver coating on the tungsten electrode at higher silver concentrations.

SUMMARY

Silver and silver amalgam cathodes were used in conjunction with molybdenum wire as a reference electrode, on a cathode-ray polarograph. Only silver and mercury ion reduction peaks were obtained for the silver electrode; for the amalgam electrode copper peaks were also obtained. Mercury and silver peaks do not interfere with each other. The linearity of peak current with silver concentration was studied.

REFERENCES

1 I. M. KOLTHOFF AND J. J. LINGANE, *Polarography*, Vol. I, Interscience Publishers, New York, 1955, 2nd ed., p. 339.
2 V. M. GAYLOR, A. L. CONRAD AND J. H. LANDERL, *Anal. Chem.*, 29 (1957) 224.
3 P. J. ELVING AND D. L. SMITH, *Proceedings of the Feigl Anniversary Symposium*, Elsevier Publishing Co., London, 1963, p. 204.
4 R. G. DHANESHWAR AND A. V. KULKARNI, to be published in *Indian J. Chem.*
5 V. T. ATHAVALE, S. V. BURANGEY AND R. G. DHANESHWAR, *J. Electroanal. Chem.*, 9 (1965) 169.
6 V. T. ATHAVALE, S. V. BURANGEY AND R. G. DHANESHWAR, *Proceedings of SAC Conference, Nottingham, U.K., July 1965*, W. Heffer and Sons, Ltd., Cambridge, England, 1966, p. 446.
7 E. BISHOP AND R. G. DHANESHWAR, *Analyst*, 88 (1963) 424.
8 I. M. KOLTHOFF AND J. J. LINGANE, *Analyst*, 88 (1963) 405.
9 A. I. VOGEL, *A Text Book of Quantitative Inorganic Analysis*, Longmans Green & Co., London, 1953, 2nd ed., p. 80.

ELECTROMETRIC DETERMINATION OF CRITICAL MICELLE CONCENTRATION OF SOAP SOLUTIONS

WAHID U. MALIK AND A. K. JAIN

Chemical Laboratories, University of Roorkee, Roorkee (India)

(Received July 1st, 1966)

Surface-active agents are characterized by the deviation in their ideal behaviour above a narrow concentration range, referred to as critical micelle concentration, which is characteristic for each material. Any method that measures the deviation from the ideal behaviour can be used to determine the c.m.c.* of the surfactant. The change in boiling point, freezing point, solubility, refractivity, light scattering, solubilization, electrical conductance, colour of dyes and surface tension have been widely used to determine this property.

Surprisingly, metal, metal–surfactant electrodes have been rarely used in determining the c.m.c. of surfactants. WALTON[1] employed a mercury, mercurous dodecanesulphonate electrode for determining the activity coefficient of dodecanesulphonic acid. The same electrode was employed by TARTAR[2] and co-workers for studying the transference numbers of 1-dodecanesulphonic acid and by VAN VOORST VADER[3] for determining the c.m.c. and pre-association of the surfactant ions of sodium dodecyl sulphonate. Since most of the heavy-metal salts of the higher fatty acids are insoluble in water, it was decided to carry out systematic studies on a number of metal, metal soap electrode systems using metals such as copper, nickel, cobalt, and mercury. In this paper, the suitability and the performance of cobalt, cobalt soap electrodes in determining the c.m.c. of the potassium salts of lauric, myristic, palmitic and stearic acids, is discussed. The effect of urea on the micelle formation of potassium laurate and myristate in aqueous solutions has also been investigated by this technique.

EXPERIMENTAL

Reagents

Lauric, myristic, palmitic and stearic acids were reagent-grade (B.D.H.) products purified by repeated crystallization from alcohol.

Potassium laurate, myristate, palmitate, stearate. Potassium soaps were obtained by refluxing equivalent amounts of fatty acids and potassium hydroxide in alcohol for 10–12 h on a water bath. These soaps were further purified by extraction within a soxhlet. Finally, the soaps were crystallized from alcohol.

Cobalt laurate, myristate, palmitate and stearate. These cobalt soaps were prepared by direct metathesis at 50–55° from the corresponding sodium soaps (1.5%,

---

* c.m.c. = critical micelle concentration.

500 ml) and cobalt sulphate solution (1.0%, 500 ml). The precipitated cobalt soaps were washed with distilled water and then with ethanol to remove free precipitant. They were analysed for metal content.

Preparation of cobalt electrodes

Cobalt electrodes were prepared by depositing cobalt on platinum wires by the electrolysis of a solution containing 8% cobalt sulphate and 2.5% ammonium sulphate. The electrodes were connected to a 4-V battery and a current of 25 mA was passed for 3 h.

E.m.f. measurements

A Cambridge portable potentiometer was used for e.m.f. measurements. The following cell was set up:

$$\text{Co/CoD}_2(s), \text{KD}(c) \,|\, \text{satd. KCl salt bridge} \,||\, \text{satd. KCl, Hg}_2\text{Cl}_2(s) \,|\, \text{Hg}$$
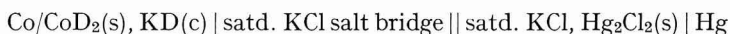
D stands for laurate, myristate, palmitate, and stearate. Standard solutions of potassium soaps were prepared in doubly-distilled water and transferred to conical flasks. Excess cobalt laurate, myristate, palmitate and stearate were added to potassium laurate, myristate, palmitate and stearate solutions, respectively. The capped conical flasks were placed in a thermostat at $35 \pm 0.1°$. When the solutions were saturated with cobalt soap, they were transferred to half-cells provided with cobalt electrodes. A saturated calomel electrode was attached through a saturated potassium chloride salt bridge. Some solid cobalt soap was always added to the half-cells to make certain that the soap solution was saturated with respect to cobalt soap. Since the cobalt, cobalt soap electrode was rather slow in coming to equilibrium, each solution was allowed to stand for some time before the final e.m.f. reading was taken.

RESULTS AND DISCUSSION

The concentration ranges of potassium laurate, myristate, palmitate and stearate investigated were 0.001–0.1 M, 0.00025–0.05 M, 0.0001–0.0075 M and 0.0001–0.002 M, respectively. Curves A, B, C and D (Figs. 1 and 2) are the plots between cobalt, cobalt laurate; cobalt, cobalt myristate; cobalt, cobalt palmitate and cobalt, cobalt stearate electrode potentials and the logarithm of the concentrations of potassium laurate, myristate, palmitate and stearate, respectively. The electrode reaction taking place at the cobalt, cobalt soap electrode is as follows:

$$\text{CoD}_2 + 2\,e \rightleftharpoons \text{Co} + 2\,\text{D}^-$$
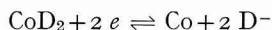
The electrode potential is given by the following equation,

$$E_{\text{CoD}_2 \rightarrow \text{Co}} = E^0_{\text{CoD}_2 \rightarrow \text{Co}} - \frac{2.303\,RT}{F} \log a_{\text{D}^-} \tag{1}$$

where a_{D^-} is the activity of the detergent anions. Curves A, B, C and D give breaks which can provide useful information about the nature of the soap solution. In dilute solutions, *i.e.*, below the c.m.c., the soaps deviate only slightly from the ideal behaviour of an electrolyte. They behave as moderately strong electrolytes. Increase in the soap concentration results in increase in the activity of the detergent anions. The
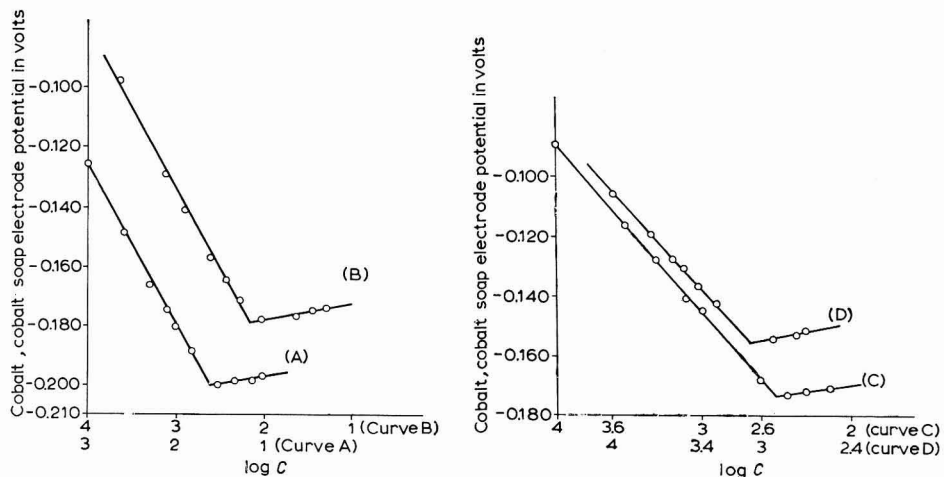
Figs. 1-2. Plots between cobalt, cobalt soap electrode potential and logarithm of potassium soap concn. at 35°. (A), potassium laurate; (B), potassium myristate; (C), potassium palmitate; (D), potassium stearate.

electrode potential equation (1) shows that the reduction potential of the cobalt, cobalt soap electrode changes to more negative values with increase in concentration. Therefore, the first linear branch in curves A, B, C and D corresponds to the increase in activity of the detergent anions. However, at concentration ranges above the c.m.c., the behaviour of the soap is non-ideal due to the micellization of detergent anions and the increase in the soap concentration does not result in increase in the activity of the detergent anions. Therefore, the concentration of detergent anions above the c.m.c. remains almost constant and so does the electrode potential and these breaks in the curves thus correspond to the c.m.c. of the soaps. The c.m.c. values determined by this method are given in Table 1 and compared with those obtained by other methods.

TABLE 1

COMPARATIVE C.M.C. VALUES OF POTASSIUM SOAPS

Soap	Temp. (°C)	c.m.c. · 10^3 (M)	Method of determination
Potassium laurate	35	25.12	Laurate ion activity (e.m.f. method)
	35	27.00	Interferometric method[4]
	25.8	24.00	Spectral dye method[5]
	50	24.50	Solubilization method[6]
Potassium myristate	35	6.918	Myristate ion activity (e.m.f. method)
	35	7.000	Interferometric method[4]
	25.8	6.000	Spectral dye method[5]
	30	7.000	Solubilization method[6]
Potassium palmitate	35	3.162	Palmitate ion activity (e.m.f. method)
Potassium stearate	35	0.8710	Stearate ion activity (e.m.f. method)
	50	< 1.000	Solubilization method[6]
	60	< 0.800	Solubilization method[6]

From Table 1 it is seen that the c.m.c. values of the soaps, determined by the e.m.f. method agree well with those found by other methods. This agreement may be taken as evidence that the activity of detergent anions in the soap solutions is, in fact, being measured.

Our results indicate that the cobalt, cobalt soap electrode potential remains practically constant after the c.m.c. This shows that after the c.m.c. there is no further change in the concentration of detergent anions on the addition of more soap; the excess of soap goes into solution in the form of micelles.

The changes in the c.m.c. values of potassium laurate and myristate solutions in the presence of different amounts of urea are given in Table 2. The ratio of the

TABLE 2

EFFECT OF UREA ON THE C.M.C. OF POTASSIUM SOAPS AT 35°

Soap	Urea (M)	c.m.c. · 10^3 (M)	$C.m.c./c.m.c._{(0)}$
Potassium laurate	0	25.12	1
	0.5	26.30	1.04
	1	28.18	1.12
	2	33.11	1.31
	3	36.31	1.44
	4	42.66	1.69
Potassium myristate	0	6.918	1
	0.5	7.244	1.04
	1	7.586	1.09
	2	8.511	1.23
	3	9.333	1.34
	4	10.470	1.51
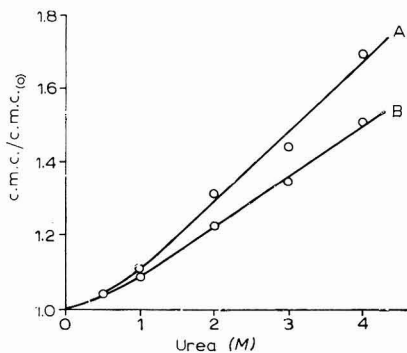
Fig. 3. Effect of urea on the c.m.c. of potassium laurate and myristate solns. at 35°. (A), potassium laurate; (B), potassium myristate.

c.m.c. in the presence of urea to the c.m.c. in the absence of urea, c.m.c./c.m.c.$_{(0)}$, has been adopted as a convenient way of representing the data[7]. Small concentrations of urea have little influence on the micelle formation of soaps but higher concentrations bring about a marked increase in the c.m.c. of the soaps. From Fig. 3, it is evident that there is almost a linear relationship between c.m.c./c.m.c.$_{(0)}$ and urea concentra-

tion in the range 1–4 M of urea. These results are in agreement with those reported by earlier workers[7,8].

Recent investigations[7-10] have shown the importance of water structure on micelle formation. The current hypothesis for micelle formation is based on the "iceberg structure" of water[11]. According to FRANK AND EVANS[11], the water molecules become more ordered around the non-polar solute, with an increasing extent of hydrogen bonding in this region. Thus, in the case of soap solutions, the hydrocarbon chains of the detergent anions are surrounded by a water structure (so-called "iceberg structure") and represent a comparatively low energy state[10]. The non-polar detergent anions surrounded by "iceberg" water structure are curled up tightly and internal movements are consequently restricted[9]. This concomitant restriction of motion provides a driving force for aggregation which is an entropy effect at lower temperatures[10]. Therefore, the more ordered the "iceberg structure" around the detergent anions, the greater will be the driving force for aggregation. It is anticipated, therefore, that structure-promoting substances should enhance the tendency of micellization and consequently decrease the c.m.c. of the surfactants, whereas substances that break up the "iceberg" water structure around detergent anions should retard the tendency of micellization and consequently increase the c.m.c. The effect of urea can be explained in the light of the "iceberg" picture of water structure around the non-polar detergent anions. RUPLEY[12] observed that aqueous solutions of urea exhibit anomalously low viscosities and he explained this behaviour by suggesting that urea disrupts the water structure. On this basis, urea, as a water-structure-breaking substance, should increase the c.m.c.

SUMMARY

The variation of detergent anion activity with concentration in solutions of potassium laurate, myristate, palmitate and stearate has been studied using the cobalt, cobalt soap electrode. The detergent anion activity increases at first, reaches a maximum at the c.m.c. and thereafter remains almost constant. The constant value of the activity above the c.m.c. shows that the excess of soap added goes into solution in the form of micelles. The c.m.c. values of potassium laurate, myristate, palmitate and stearate are 2.512×10^{-2} M, 6.918×10^{-3} M, 3.162×10^{-3} M and 8.71×10^{-4} M, respectively. In the presence of urea, the micellization of potassium laurate and myristate takes place at higher concentrations.

REFERENCES

1 H. F. WALTON, J. Am. Chem. Soc., 68 (1946) 1180.
2 L. L. NEFF, O. L. WHEELER, H. V. TARTAR AND E. C. LINGAFELTER, J. Am. Chem. Soc., 70 (1948) 1989.
3 F. VAN VOORST VADER, Trans. Faraday Soc., 57 (1961) 110.
4 H. B. KLEVENS, J. Colloid Sci., 2 (1947) 301.
5 W. D. HARKINS, J. Am. Chem. Soc., 69 (1947) 1428.
6 I. M. KOLTHOFF AND W. STRICKS, J. Phys. Colloid Chem., 52 (1948) 915.
7 P. MUKERJEE AND A. RAY, J. Phys. Chem., 67 (1963) 190.
8 W. BRUNNING AND A. HOLTZER, J. Am. Chem. Soc., 83 (1961) 4865.
9 E. D. GODDARD, C. A. J. HOEVE AND G. C. BENSON, J. Phys. Chem., 61 (1957) 593.
10 E. D. GODDARD AND G. C. BENSON, Can. J. Chem., 35 (1957) 987.
11 H. S. FRANK AND M. W. EVANS, J. Chem. Phys., 13 (1945) 507.
12 J. A. RUPLEY, J. Phys. Chem., 68 (1964) 2002.

PULSE POLAROGRAPHY
II*. EXPERIMENTAL VERIFICATION OF THE DIFFUSION EQUATION INCLUDING THE SHIELDING EFFECT

A. W. FONDS, A. A. A. M. BRINKMAN AND J. M. LOS

Laboratory of Physical Chemistry, Free University, Amsterdam (The Netherlands)

(Received April 22nd, 1966)

INTRODUCTION

In normal pulse polarography the potential is applied to the dropping mercury electrode after the latter has grown for a time, t_1. The diffusion equation, valid in this case, was derived by BRINKMAN AND LOS[1], who showed that the exact solution could be well approximated (deviation less than 1%) by the closed form expression

$$i_\mathrm{d} = 7.06 \cdot 10^4 n D^{1/2} c^* m^{2/3} t_1^{1/6} \frac{(1+\vartheta)^{4/3}}{\{(1+\vartheta)^{7/3} - 1\}^{1/2}}$$

$$\times \left[1 + 4.4 D^{1/2} m^{-1/3} t_1^{1/6} \frac{\{(1+\vartheta)^{7/3} - 1\}^{1/2}}{(1+\vartheta)} \right] \tag{1}$$

where ϑ is the ratio of the time t, elapsed between voltage application and measurement of i_d, the instantaneous current, to the time t_1 of drop growth prior to voltage application. All units are in c.g.s. (*e.g.*, c^* in moles cm^{-3}), save i_d, which is in amperes.

The factor before the square brackets gives the current without correction for the spherical shape of the drop. This part of eqn.(1) is exact, as can be seen by considering the problem for the plane, expanding electrode, which problem is solvable by Laplace transformation[2]. It is worth noting that the expanding character of the electrode has hardly any influence on this result. The Cottrell equation (valid for the plane, *non*-expanding electrode), which BARKER AND GARDNER have used[3], deviates less than $100\vartheta/3\%$ from the exact solution for the plane, expanding electrode, and since ϑ is generally of the order of 10^{-2} this deviation is negligible.

The second term within the square brackets constitutes the spherical correction, which is certainly not negligible as it may add as much as 10% to the current (even for small values of ϑ, if the rate of flow of mercury is small).

Because of the important contribution of the spherical correction term to the current, it proved to be necessary to evaluate the effect of shielding on this term.

SHIELDING EFFECT

For the theoretical treatment of the shielding effect we have followed MATSUDA[4],

---

* Part I, see ref. 1.

who was the first to incorporate this effect in the diffusion current equation of normal polarography. A detailed discussion of MATSUDA's approach has been given by MARKOWITZ AND ELVING[5]. MATSUDA assumes a finite thickness of the diffusion layer, δ, implying a homogeneous solution from δ onward.

The diffusion equation to be solved is

$$\frac{\partial c}{\partial t} = D \frac{1}{r^2} \frac{\partial}{\partial r}\left(r^2 \frac{\partial c}{\partial r}\right) - \frac{\alpha^3}{3r^2} \frac{\partial c}{\partial r} \tag{2}$$

where

$$\alpha = \left(\frac{3m}{4\pi d}\right)^{1/3}$$

d being the density of mercury.

The boundary conditions are

$$t > 0; \quad r = r_0 \qquad :c = 0 \tag{3a}$$

$$t = 0; \quad r \geqslant \alpha t_1^{1/3} \quad :c = c^* \tag{3b}$$

$$t > 0; \quad r = r_0 + \delta \quad :c = c^*; \quad \frac{\partial^n c}{\partial r^n} = 0, \quad n = 1, 2, 3, \dots. \tag{3c}$$

where r_0, the drop radius, is given by

$$r_0 = \alpha (t_1 + t)^{1/3} \tag{4}$$

We now multiply both sides of eqn.(2) by r^2 and integrate with respect to r from r_0 to $r_0 + \delta$. The right-hand side thus yields

$$Dr^2 \left(\frac{\partial c}{\partial r}\right)\Big]_{r_0}^{r_0+\delta} - \frac{\alpha^3}{3} c \Big]_{r_0}^{r_0+\delta} = -Dr_0^2 \left(\frac{\partial c}{\partial r}\right)_{r=r_0} - \frac{\alpha^3 c^*}{3} \tag{5}$$

while the integral of the left-hand side is derived from the equality

$$\frac{\partial}{\partial t} \int_{r_0}^{r_0+\delta} (c^* - c) r^2 \, \mathrm{d}r$$

$$= - \int_{r_0}^{r_0+\delta} \left(\frac{\partial c}{\partial t}\right) r^2 \, \mathrm{d}r + (c^* - c_{r=r_0+\delta})(r_0 + \delta)^2 \frac{\partial(r_0+\delta)}{\partial t} - (c^* - c_{r=r_0}) r_0^2 \frac{\partial r_0}{\partial t}$$

$$= - \int_{r_0}^{r_0+\delta} \left(\frac{\partial c}{\partial t}\right) r^2 \, \mathrm{d}r - c^* r_0^2 \frac{\partial r_0}{\partial t} = - \int_{r_0}^{r_0+\delta} \left(\frac{\partial c}{\partial t}\right) r^2 \, \mathrm{d}r - \frac{\alpha^3 c^*}{3} \tag{6}$$

where conditions (3c) and eqn.(4) have been used.

Integration of eqn.(2) therefore produces the equation

$$\frac{\partial}{\partial t} \int_{r_0}^{r_0+\delta} (c^* - c) r^2 \, \mathrm{d}r = Dr_0^2 \left(\frac{\partial c}{\partial r}\right)_{r=r_0} \tag{7}$$

which can be transformed by putting $x = r - r_0$ to

$$\frac{\partial}{\partial t} \int_0^{\delta} (c^* - c)(r_0 + x)^2 \, \mathrm{d}x = Dr_0^2 \left(\frac{\partial c}{\partial x}\right)_{x=0} \tag{8}$$

We now expand $(c^* - c)$ as a power series in x/δ

$$c^* - c = \frac{c^* r_0}{r_0 + x} \left\{ 1 + \sum_{j=1} A_j \left(\frac{x}{\delta}\right)^j \right\} \tag{9}$$

Assuming that six coefficients A_j will suffice (which was shown by Matsuda[4] to be correct in normal polarography), we find the A_j's from the six simultaneous equations

$$c(\delta, t) = c^*; \quad \left(\frac{\partial c}{\partial x}\right)_{x=\delta} = 0; \quad \left(\frac{\partial^2 c}{\partial x^2}\right)_{x=\delta} = 0; \quad \left(\frac{\partial^3 c}{\partial x^3}\right)_{x=\delta} = 0; \quad \left(\frac{\partial^4 c}{\partial x^4}\right)_{x=\delta} = 0 \tag{10a}$$

$$\left(\frac{\partial^2 (r_0 + x) c}{\partial x^2}\right)_{x=0} = 0 \tag{10b}$$

The eqns.(10a) are part of the boundary conditions (3c). In conjunction with eqn.(9) they lead to the equations $\Sigma A_j = -1$; $\Sigma j A_j = 0$; $\Sigma j(j-1)A_j = 0$; $\Sigma j(j-1)(j-2)A_j = 0$; $\Sigma j(j-1)(j-2)(j-3)A_j = 0$.

Equation (10b) can be obtained by substitution of $x = r - r_0$ into eqn.(2) and putting $x = 0$. It leads to $A_2 = 0$. Combination with the other 5 equations in A_j gives $A_1 = -3$; $A_3 = 10$; $A_4 = -15$; $A_5 = 9$ and $A_6 = -2$. Substitution of these A_j-values into eqn.(9) makes integration of the left-hand side of eqn.(8) possible. The result is

$$\frac{\partial}{\partial t} \left(\frac{3}{14} r_0^2 \delta + \frac{1}{28} r_0 \delta^2\right) = D r_0^2 \left(\frac{3}{\delta} + \frac{1}{r_0}\right) \tag{11}$$

In order to solve this equation we transform to $\vartheta = t/t_1$ and expand δ as

$$\delta = \sqrt{Dt_1} \sum_{j=0} \beta_j(\vartheta) \{\alpha^{-1} D^{1/2} t_1^{1/6}\}^j \tag{12}$$

which is substituted into eqn.(11). Comparing the coefficients of equal powers of D, α or t_1, we find the following differential equation for β_0

$$(1+\vartheta)^{2/3} \beta_0 \frac{d\beta_0}{d\vartheta} + \frac{2\beta_0^2}{3(1+\vartheta)^{1/3}} = 14(1+\vartheta)^{2/3} \tag{13}$$

subject to the condition $\beta_0 = 0$ for $\vartheta = 0$, since then $\delta = 0$ must apply. The solution of eqn.(13) is

$$\beta_0 = 2\sqrt{3} \, \frac{\{(1+\vartheta)^{7/3} - 1\}^{1/2}}{(1+\vartheta)^{2/3}} \tag{14}$$

For β_1 we obtain

$$\frac{d\beta_1}{d\vartheta} + \left[\frac{7(1+\vartheta)^{4/3}}{6\{(1+\vartheta)^{7/3} - 1\}} + \frac{2}{3(1+\vartheta)}\right] \beta_1 = \frac{2\{(1+\vartheta)^{7/3} - 1\}}{(1+\vartheta)^{8/3}} \tag{15}$$

with the condition $\beta_1 = 0$ for $\vartheta = 0$. The solution is

$$\beta_1 = \frac{2}{\{(1+\vartheta)^{7/3} - 1\}^{1/2} (1+\vartheta)^{2/3}} \int_0^\vartheta \frac{\{(1+x)^{7/3} - 1\}^{3/2}}{(1+x)^2} \, dx \tag{16}$$

The current can now be found from $(\partial c/\partial x)_{x=0}$, which gives in combination with eqns.(9) and (11)

$$i_d = 4\pi n F c^* \frac{\partial}{\partial t} \left(\frac{3}{14} r_0^2 \delta + \frac{1}{28} r_0 \delta^2\right) \tag{17}$$

Transformation from t to ϑ and substitution of eqns.(12) and (14) — omitting terms with $j \geq 2$ — gives

$$i_d = 7.06 \cdot 10^4 n D^{1/2} c^* m^{2/3} t_1^{1/6} \frac{(1+\vartheta)^{4/3}}{\{(1+\vartheta)^{7/3} - 1\}^{1/2}}$$

$$\times \left[1 + 4.4 D^{1/2} m^{-1/3} t_1^{1/6} \frac{\{(1+\vartheta)^{7/3} - 1\}^{1/2}}{(1+\vartheta)} \right.$$

$$\left. \times \left\{ 1 + \frac{3}{14} (1+\vartheta)^{1/3} \frac{d\beta_1}{d\vartheta} + \frac{\beta_1}{7(1+\vartheta)^{2/3}} - \frac{3\{(1+\vartheta)^{7/3} - 1\}}{7(1+\vartheta)^{7/3}} \right\} \right] \quad (18)$$

Comparison with eqn.(15) leads to the reduction

$$i_d = 7.06 \cdot 10^4 n D^{1/2} c^* m^{2/3} t_1^{1/6} \frac{(1+\vartheta)^{4/3}}{\{(1+\vartheta)^{7/3} - 1\}^{1/2}}$$

$$\times \left[1 + 4.4 D^{1/2} m^{-1/3} t_1^{1/6} \frac{\{(1+\vartheta)^{7/3} - 1\}^{1/2}}{(1+\vartheta)} \left\{ 1 - \frac{(1+\vartheta)^{5/3}}{4\{(1+\vartheta)^{7/3} - 1\}} \beta_1 \right\} \right] \quad (19)$$

Comparison with the exact current equation (1) shows that both solutions are the same if the term in β_1 were dropped in eqn.(19). Therefore, as in normal polarography, MATSUDA's method gives too small a value for the spherical correction.
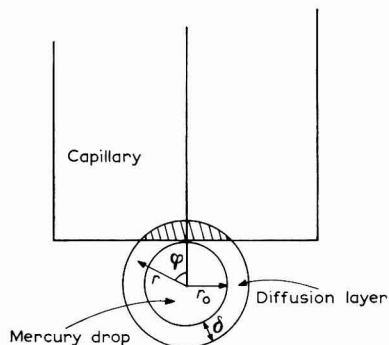
Fig. 1. Model of the dropping mercury electrode after MATSUDA[4].

In order to find the shielding correction, we now calculate the current from the model represented in Fig. 1, where we have taken into account that the upper part of the diffusion layer is covered by the tip of the capillary. The current is now given by

$$i_d = nF \frac{d}{dt} \int_{r_0}^{r_0+\delta} \int_0^{2\pi} \int_{\cos^{-1}(r_0/r)}^{\pi} (c^* - c) r^2 \sin \varphi \, d\varphi \, d\Psi \, dr \quad (20)$$

where r, φ and Ψ are spherical coordinates. The integrations over φ and Ψ are straightforward, yielding $(1 + r_0/r)$ and 2π, respectively. We now substitute eqn. (9) into eqn. (20) and transform again to $x = r - r_0$

$$i_d = 2\pi nF \frac{d}{dt} \int_0^\delta c^* r_0 (2r_0 + x) \left\{ 1 + \sum_{j=1}^{6} A_j \left(\frac{x}{\delta}\right)^j \right\} dx$$

Introduction of eqns. (12), (14) and (15) leads, precisely as in the preceding case, to

$$i_d = 7.06 \cdot 10^4 n D^{1/2} c^* m^{2/3} t_1^{1/6} \frac{(1+\vartheta)^{4/3}}{\{(1+\vartheta)^{7/3}-1\}^{1/2}}$$

$$\times \left[1 + 4.4 D^{1/2} m^{-1/3} t_1^{1/6} \frac{\{(1+\vartheta)^{7/3}-1\}^{1/2}}{(1+\vartheta)} \right.$$

$$\left. \times \left\{ \frac{1}{2} - \frac{(1+\vartheta)^{5/3}}{4\{(1+\vartheta)^{7/3}-1\}} \beta_1 + \frac{3\{(1+\vartheta)^{7/3}-1\}}{14(1+\vartheta)^{7/3}} \right\} \right] \qquad (21)$$

Comparison of eqns.(21) and (19) shows that incorporation of the shielding effect gives a decrease in the relative spherical correction of

$$4.4 D^{1/2} m^{-1/3} t_1^{1/6} \frac{\{(1+\vartheta)^{7/3}-1\}^{1/2}}{(1+\vartheta)} \left\{ \frac{2}{7} + \frac{3}{14}(1+\vartheta)^{-7/3} \right\} \qquad (22)$$

Subtraction of this shielding correction from the relative spherical correction of the exact current equation (1) gives

$$i_d = 7.06 \cdot 10^4 n D^{1/2} c^* m^{2/3} t_1^{1/6} \frac{(1+\vartheta)^{4/3}}{\{(1+\vartheta)^{7/3}-1\}^{1/2}}$$

$$\times \left[1 + 4.4 D^{1/2} m^{-1/3} t_1^{1/6} \frac{\{(1+\vartheta)^{7/3}-1\}^{1/2}}{(1+\vartheta)} \left(\frac{5}{7} - \frac{3}{14}(1+\vartheta)^{-7/3} \right) \right] \qquad (23)$$

Equation (23) which constitutes the *complete diffusion equation for the instantaneous current* can be simplified by putting

$$\frac{5}{7} - \frac{3}{14}(1+\vartheta)^{-7/3} \sim \frac{1}{2}(1+\vartheta)$$

which is justified within 1% (of the total current) for ϑ-values up to 0.5. For very small ϑ-values we notice that the shielding correction amounts to reducing the spherical correction to one-half of its original value.
We finally obtain

$$i_d = 7.06 \cdot 10^4 n D^{1/2} c^* m^{2/3} t_1^{1/6} \frac{(1+\vartheta)^{4/3}}{\{(1+\vartheta)^{7/3}-1\}^{1/2}}$$

$$\times [1 + 2.2 D^{1/2} m^{-1/3} t_1^{1/6} \{(1+\vartheta)^{7/3}-1\}^{1/2}] \qquad (24)$$

In order to find the average current we integrate eqn.(24) from ϑ' to ϑ''

$$\overline{i_d} = 6.05 \cdot 10^4 n D^{1/2} \frac{c^* m^{2/3} t_1^{1/6}}{(\vartheta''-\vartheta')} \left[\{(1+\vartheta)^{7/3}-1\}^{1/2} + 1.1 D^{1/2} m^{-1/3} t_1^{1/6} (1+\vartheta)^{7/3} \right]\Big|_{\vartheta'}^{\vartheta''} \qquad (25)$$

If so desired, the factor $\{(1+\vartheta)^{7/3}-1\}^{1/2}$ can be further approximated by $(1+\vartheta/3) \cdot \sqrt{(7\vartheta/3)}$, which is correct within 1% for ϑ-values up to 0.9.

EXPERIMENTAL

Chemicals

The following reagent-grade depolarizer salts were used: $TlNO_3$, $PbCl_2$,

$ZnSO_4 \cdot 7H_2O$, $CdCl_2$ and $CdSO_4 \cdot 8/3H_2O$, all after complete dehydration. In all solutions twice-distilled water was used.

KCl was purified by twice recrystallizing from pure water, followed by drying in vacuum over P_2O_5 and heating for 3 h in an oven at 600°. Available standard solutions of HCl were used without further purification.

Mercury for the dropping mercury electrode (DME) and the mercury pool electrode—used as a counter electrode in all experiments—was purified by bubbling air through the metal, followed by filtration, distillation under air and finally distillation under an atmosphere of nitrogen.

Apparatus

The experiments were carried out using a fully transitorized pulse polarograph, which was constructed in this laboratory. This instrument is capable of measuring instantaneous currents. A diagram is given in Fig. 2.
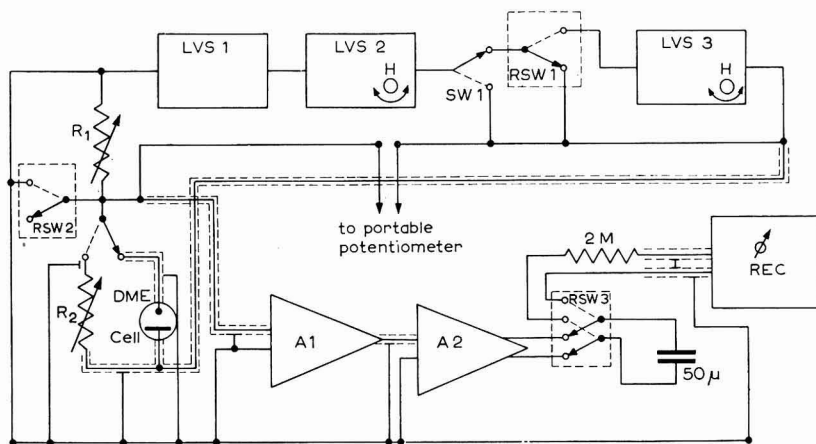
Fig. 2. Schematic diagram of the pulse polarograph: (LVS1), stabilized low voltage supply with a 0.5-V step-wise attenuator, range: $+1.5$ to -2.0 V; (LVS2), stabilized low voltage supply, range: 0 to -1.0 or -2.0 V (continuously, monitored by Helipot); (LVS3), stabilized low voltage supply, range: 0 to -0.5 or -1.0 V (continuously, monitored by Helipot); (H), Helipot motor-driven potentiometer; (A1), Sanborn 860-4200 Wide Band Amplifier (voltage amplifier); (A2), current amplifier; (R1), load resistor: 10, 50, 100, 500, 1000, or 5000 Ω; (R2), decade resistance box for calibration purposes; (RSW1, RSW2 and RSW3), relay switches; (SW1), switch: pulse voltage on or off; (DME), dropping mercury electrode; (REC), Kipp Micrograph BD2 recorder (1-sec response).

By means of the low voltage supplies, LVS1 and LVS2, a starting potential for the DME can be chosen, while a rectangular pulse voltage, obtained from the low voltage supply, LVS3, is superimposed by means of the relay switch, RSW1. LVS3 is monitored by a motor-driven potentiometer (Helipot) so that the pulse height may increase or decrease linearly with a rate of 37.5 or 75 mV/min alternatively, depending on the chosen range (0.5 or 1 V). The potential, E, of the DME with respect to a mercury pool electrode or a reference electrode and the cell current, i, as functions of time may be characterized as in Figs. 3a,b.

Each time cycle (duration t_0) begins and ends with the fall of a mercury drop, which is induced by a solenoid-operated mechanical knocker. The closing of the relay

switch, which activates this knocker (not shown in Fig. 2), is controlled by a free-running multivibrator with a variable time constant. At the same time this multi-vibrator triggers a series of three monostable multivibrators, which control the activation of all other relay switches.
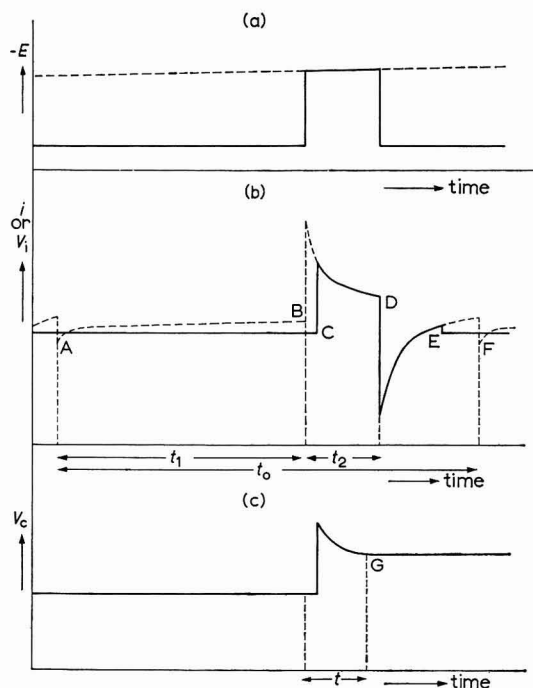
Fig. 3. (a), Potential of the DME *vs.* time.
(b), Cell current (- - - - -) and amplifier input signal (————) *vs.* time: (A and F), fall of the mercury drop; (B), start, and (D), end of the pulse application; (C), opening, and (E), closing of the short-circuit of the amplifier input by RSW2.
(c), Storage capacitor voltage *vs.* time: (G), the capacitor is switched from the amplifier output to the recorder by RSW3.

The voltage drop, V_i, across resistor R_1, which is proportional to the cell current, is amplified by a voltage amplifier, A_1, while the current amplifier, A_2, feeds the amplified signal into a storage capacitor of 50 μF. Since A_1 and A_2 are both wide band amplifiers and since A_2 has an output impedance of less than 1 Ω, the charge and voltage response of the storage capacitor is nearly instantaneous and proportional to the cell current at any time of the capacitor's measuring period. In order to prevent overloading of the amplifier system and to achieve a better initial response of the cell to the pulse voltage, resistor R_1 is kept short-circuited by relay switch RSW2 during each cycle until the initial sharp current peak has passed (*e.g.*, until 10 msec after pulse application).

At the time t (just shorter than the pulse time, t_2), the storage capacitor is disconnected from the amplifier circuit by means of relay switch RSW3 and its voltage measured by a recorder with a series resistance of 2 MΩ. The amplifier input signal,

V_i, and the corresponding capacitor voltage, V_c, are given in Figs. 3b and 3c, respectively.

The recorder is provided with a pen-lift relay so that a single point is plotted on the chart about 1 sec after the time t has passed, while an automatic interrupter of its balancing system shortly thereafter causes the indicator to stay in the vicinity of its last plot. Chart speeds of 2 and 6 cm/min were used. In this way a pulse polarogram will consist of a series of points in the familiar shape of a stepped wave, provided the starting potential is properly chosen before the onset of the wave. A typical polarogram is shown in Fig. 4.
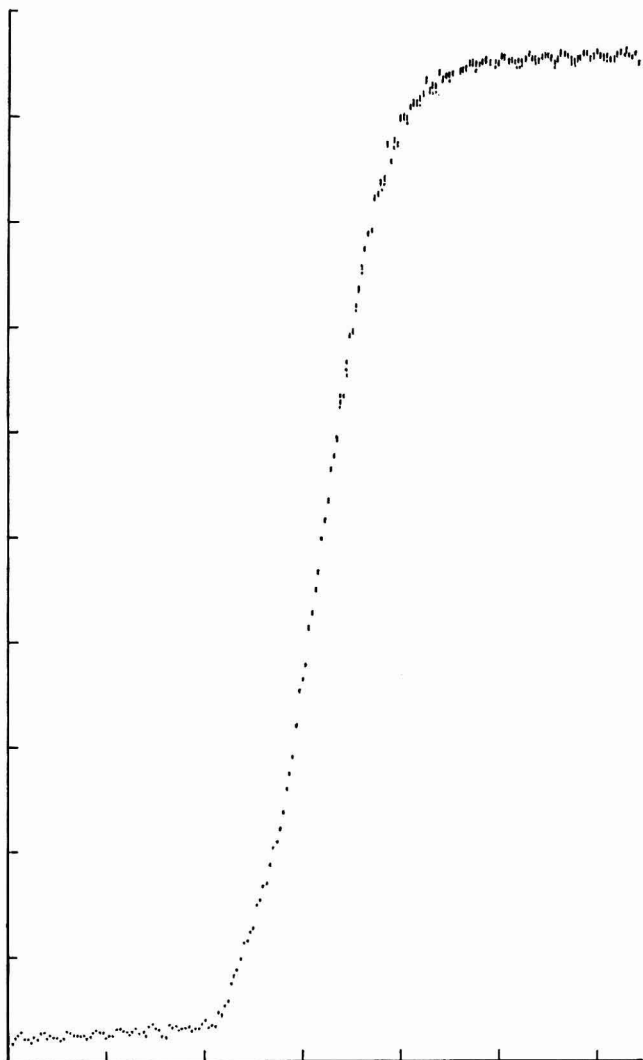
Fig. 4. Pulse polarogram of $2.03 \cdot 10^{-3}$ M Tl(I) in 0.2 M KCl: Starting potential, -0.300 V; $t_1 = 3$ sec; $t = 0.090$ sec; horiz., 75 mV/div.; vert., 5 μA/div.

The drop time, t_0, the delay time, t_1 and the pulse current measuring time, t, which were variable, were calibrated with a precision of about 0.2% by means of a Tektronix Type 502 Dual Beam Oscilloscope and a Venner TSA 3336 Time and Frequency Measuring Equipment.

Dropping mercury electrode

Several capillaries of different shape were used (see Table 1). Preliminary investigations showed that the inside of a capillary has to be siliconated in order to

TABLE 1

Siliconated capillary	Shape of the tip	Surface around the orifice
I	Cylindrical	Siliconated
IV	Cylindrical	Not siliconated
VI	Cylindrical	Not siliconated
IIA	Conical	Siliconated

prevent the solution from entering into the capillary. However, as a result of this procedure the surface around the orifice is also siliconated. This could give rise to a decrease of the diffusion currents by as much as 10%, especially with capillaries with a small rate of flow of mercury. Probably the silicon layer around the orifice inhibits the contact of the solution with the mercury drop, especially when the drop is small. In order to avoid this, the tip of the capillary was broken off after siliconation. Capillaries of which the orifice looked ragged under a microscope, were rejected.

In the case of the capillary with a perfect conical tip (IIA) and also in the case of the one cylindrical capillary which had a large rate of mercury flow (I), the silicon layer around the orifice apparently did not cause any trouble.

RESULTS AND DISCUSSION

Tables 2, 3 and 4 show the observed instantaneous diffusion currents (i_{obs}) of Tl(I) in 0.2 M KCl; Pb(II) in 0.1 M KCl+0.1 M HCl, and Zn(II) in 1 M KCl+ $5 \cdot 10^{-4}$ M HCl together with the calculated values i_a, i_b and i_c, where:

i_a denotes the diffusion current calculated for an expanding plane electrode (no spherical correction), *i.e.*, the factor before the square brackets in eqn.(1);

i_b denotes the diffusion current calculated for the expanding spherical electrode, neglecting the shielding correction, *i.e.*, eqn. (1);

i_c denotes the diffusion current calculated for the expanding spherical electrode with incorporation of the shielding effect, *i.e.*, eqn. (23).

Tracer diffusion coefficients[6,7] were used in the calculations. The close relationship between polarographic and tracer diffusion coefficients has been pointed out by BEARMAN[8] and was established experimentally by LOS AND MURRAY[9] at an earlier date.

Comparing the significant differences between the values in the columns for i_a and i_b, it is obvious that it is not correct to neglect the spherical correction in pulse polarography, as is tacitly implied by BARKER AND GARDNER[3] and by PARRY AND OSTERYOUNG[10].

TABLE 2

Tl(I) in 0.2 M KCl; $D_{Tl(I)} = 17.9 \cdot 10^{-6}$ cm² sec⁻¹; temp.: 25.0 ± 0.1°

$c^* \cdot 10^3$ (moles l⁻¹)	Cap.	t_1 (sec)	t (sec)	ϑ	m (mg sec⁻¹)	i_a (μA)	i_b (μA)	i_c (μA)	i_{obs} (μA)	$\frac{i_{obs}-i_b}{i_b}$ (%)	$\frac{i_{obs}-i_c}{i_c}$ (%)
2.005	I	4	0.036	0.009	3.918	130.67	133.51	132.10	131.4	−1.6	−0.5
		3	0.036	0.012	3.869	107.28	109.85	108.58	107.8	−1.9	−0.7
		2	0.036	0.018	3.881	82.52	84.77	83.67	82.6	−2.6	−1.3
		2	0.090	0.045	3.848	53.24	55.51	54.42	53.9	−2.9	−0.9
		2	0.540	0.270	3.848	26.29	28.71	27.72	28.4	−1.1	+2.5
		0.9	0.090	0.100	3.839	32.85	34.62	33.81	33.4	−3.5	−1.2
2.030	IIA	3	0.036	0.012	1.993	69.79	71.88	70.85	71.9	+0.0	+1.5
		3	0.090	0.030	1.993	44.92	47.02	46.00	46.7	−0.7	+1.5
		1.5	0.090	0.060	1.965	28.84	30.51	29.72	29.9	−2.0	+0.6
		1.5	0.540	0.360	1.978	15.05	16.87	16.16	16.84	−0.2	+4.2
1.939	VI	4	0.036	0.009	0.9304	48.46	50.16	49.32	49.1	−2.1	−0.4
		4	0.090	0.0225	0.9304	31.06	32.77	31.93	31.7	−3.2	−0.7
		4	0.540	0.135	0.9304	14.05	15.82	15.06	15.38	−2.8	+2.1
		2.4	0.036	0.015	0.9194	34.40	35.83	35.13	35.9	+0.3	+2.1
		2.4	0.090	0.0375	0.9194	22.24	23.68	22.99	22.9	−3.3	−0.4
		2.4	0.540	0.225	0.9194	10.680	12.204	11.565	11.78	−3.5	+1.8
		1.5	0.036	0.024	0.9234	25.44	26.67	26.07	26.3	−1.4	+0.9
		1.5	0.090	0.060	0.9234	16.65	17.89	17.31	17.14	−4.2	+1.0
		1.5	0.540	0.360	0.9234	8.650	10.001	9.474	9.62	−3.8	+1.5

TABLE 3

Pb(II) in 0.1 M KCl + 0.1 M HCl; $D_{Pb(II)} = 9.63 \cdot 10^{-6}$ cm² sec⁻¹; temp.: 25.0 ± 0.1°

$c^* \cdot 10^3$ (moles l⁻¹)	Cap.	t_1 (sec)	t (sec)	ϑ	m (mg sec⁻¹)	i_a (μA)	i_b (μA)	i_c (μA)	i_{obs} (μA)	$\frac{i_{obs}-i_b}{i_b}$ (%)	$\frac{i_{obs}-i_c}{i_c}$ (%)
2.079	I	2	0.036	0.018	3.946	126.91	129.44	128.20	129.8	+0.3	+1.2
		2	0.090	0.045	3.946	82.38	84.93	83.71	84.0	−1.1	+0.3
		1.5	0.090	0.060	3.909	68.54	70.86	69.76	70.9	+0.1	+1.6
		1.5	0.540	0.360	3.935	35.76	38.29	37.30	37.8	−1.3	+1.3
		0.9	0.036	0.040	4.025	77.14	79.10	78.16	78.6	−0.6	+0.6
		0.9	0.090	0.100	4.038	51.67	53.67	52.76	54.1	+0.8	+2.5
		0.9	0.540	0.600	4.028	30.05	32.32	31.51	32.2	−0.4	+2.2
2.079	IIA	4	0.036	0.009	1.670	112.55	114.93	113.75	114.4	−0.5	+0.6
		4	0.090	0.0225	1.670	72.13	74.53	73.36	73.6	−1.2	+0.3
		3	0.036	0.012	1.661	92.85	95.01	93.94	94.1	−1.0	+0.2
		3	0.090	0.030	1.661	59.77	61.95	60.89	61.0	−1.5	+0.2
		3	0.540	0.180	1.665	27.93	30.21	29.23	29.8	−1.4	+2.0
		3	1.08	0.360	1.665	22.62	25.01	24.08	24.7	−1.2	+2.6
		2	0.090	0.045	1.652	46.10	48.01	47.09	47.2	−1.7	+0.2
		2	0.540	0.270	1.652	22.76	24.80	23.97	24.2	−2.4	+1.0
1.993	IV	4.5	0.036	0.008	0.5891	58.21	59.89	59.06	59.8	−0.2	+1.3
		4.5	0.090	0.020	0.5891	37.25	38.94	38.11	38.1	−2.2	−0.0
		4.5	0.540	0.120	0.5891	16.68	18.42	17.64	17.68	−4.0	+0.2
		3	0.036	0.012	0.5841	44.35	45.81	45.09	45.2	−1.3	+0.2
		3	0.090	0.030	0.5841	28.54	30.01	29.30	29.0	−3.4	−1.0
		3	0.540	0.180	0.5870	13.36	14.90	14.24	14.06	−5.6	−1.3
		1.5	0.036	0.024	0.5811	28.16	29.33	28.76	28.7	−2.1	−0.2
		1.5	0.090	0.060	0.5811	18.44	19.62	19.06	18.76	−4.4	−1.6
		1.5	0.540	0.360	0.5878	9.65	10.94	10.43	10.24	−6.4	−1.8
		1.5	1.08	0.720	0.5878	8.48	9.87	9.39	9.16	−7.2	−2.4
		0.9	0.036	0.040	0.5804	20.33	21.32	20.84	20.7	−2.9	−0.7
		0.9	0.090	0.100	0.5834	13.64	14.65	14.19	13.96	−4.7	−1.6

TABLE 4

Zn(II) in 1 M KCl$+5\cdot10^{-4}$ M HCl; $D_{\text{Zn(II)}} = 8.18\cdot10^{-6}$ cm^2 sec^{-1}; temp.: $25.0 \pm 0.1°$

$c*\cdot10^3$ (moles l^{-1})	Cap.	t_1 (sec)	t (sec)	ϑ	m (mg sec^{-1})	i_a (μA)	i_b (μA)	i_c (μA)	i_{obs} (μA)	$\dfrac{i_{obs}-i_b}{i_b}$ (%)	$\dfrac{i_{obs}-i_c}{i_c}$ (%)
1.931	I	2.4	0.036	0.015	3.153	105.33	107.30	106.33	104.3	−2.8	−1.9
		2.4	0.090	0.0375	3.039	66.44	68.40	67.45	67.8	−0.9	+0.5
		0.9	0.036	0.040	3.139	55.95	57.38	56.69	56.2	−2.1	−0.9
		0.9	0.090	0.100	3.017	36.43	37.86	37.21	37.5**	−1.0	+0.8
1.931	IV	4.5	0.036	0.008	0.5877	51.90	53.28	52.60	52.5	−1.5	−0.2
		4.5	0.090	0.020	0.5877	33.22	34.61	33.93	34.6	−0.0	+2.0
		4.5	0.540	0.120	0.5877	14.87	16.30	15.66	15.7**	−3.7	+0.3
		4.5	1.08	0.240	0.5885	11.62	13.10	12.49	12.3**	−6.9	−1.5
		2	0.036	0.018	0.5738	30.04	31.09	30.59	30.4	−2.2	−0.6
		2	0.090	0.045	0.5738	19.50	20.56	20.05	20.2	−1.8	+0.7
		2	0.540	0.270	0.5774	9.67	10.80	10.34	10.1**	−6.5	−2.3
2.112	IIA	3	0.036	0.012	1.828	92.68	94.61	93.66	94.6	−0.0	+1.0
		3	0.090	0.030	1.828	59.65	61.59	60.65	61.7	+0.2	+1.7
		2.4	0.540	0.225	1.828	24.87	26.78	25.98	26.6	−0.7	+2.4

** Since at the start of the hydrogen wave the horizontal diffusion-current plateau of the Zn(II) wave had not yet been reached, these values of i_{obs} are only approximate.

TABLE 5

Cd(II) in 0.1 M KCl; temp.: $25.0\pm0.1°$

Depolarizer salt	$c*\cdot10^3$ (moles l^{-1})	Cap.	t_1 (sec)	t (sec)	ϑ	m (mg sec^{-1})	i_{obs} (μA)	$D^{\frac{1}{2}}\cdot10^3$ (cm sec$^{-\frac{1}{2}}$)	$D\cdot10^6$ (cm^2 sec^{-1})
CdCl$_2$	0.996	IV	4	0.036	0.009	0.6139	25.9	2.863	8.20
			4	0.090	0.0225	0.6139	16.38	2.806	7.87
			4	0.540	0.135	0.6118	7.60	2.794	7.81
			1.5	0.090	0.060	0.6031	8.77	2.797	7.82
CdSO$_4$	0.848	I	2.4	0.036	0.015	3.742	51.9	2.788	7.77
			2.4	0.090	0.0375	3.742	34.0	2.809	7.89
CdSO$_4$	0.848	IV	4	0.036	0.009	0.6065	21.9	2.822	7.96
			4	0.090	0.0225	0.6065	14.14	2.818	7.94
			4	0.036	0.009	0.2906	13.40	2.807	7.88
			4	0.090	0.0225	0.2891	8.46	2.750	7.56
CdSO$_4$	0.3733	I	2.4	0.036	0.015	3.392	21.1	2.800	7.84
			2.4	0.090	0.0375	3.392	13.86	2.827	7.99
			2.4	0.540	0.225	3.392	6.81	2.833	8.03
			1.5	0.036	0.024	3.335	15.30	2.778	7.72
			1.5	0.090	0.060	3.335	10.26	2.827	7.99
			1.5	0.540	0.360	3.335	5.47	2.834	8.03
CdSO$_4$	0.3733	IV	4	0.036	0.009	0.5892	9.34	2.833	8.03
			4	0.090	0.0225	0.5892	6.03	2.858	8.17
			4	0.540	0.135	0.5892	2.82	2.828	8.00
			2	0.036	0.018	0.5879	5.90	2.810	7.90
			2	0.090	0.045	0.5879	3.83	2.784	7.75
			2	0.540	0.270	0.5879	1.98	2.805	7.87

For the capillaries with cylindrical tip (I, IV and VI), incorporation of the shielding effect (i_c) gives better agreement with i_{obs}, except for capillary I in the case of Pb(II). Capillary I had a siliconated bottom (see Table 1) and we have the experience with such capillaries that very slowly-growing mercury drops adhere to the bottom part. For the capillary with a conical tip (IIA), the calculated currents, i_c, including the shielding effect, are clearly overcorrected, as must be expected.

Table 5 contains the diffusion coefficients calculated from the observed pulse polarographic diffusion currents of Cd(II) in 0.1 M KCl, using eqn.(23). This results in an average value of $D_{Cd(II)} = (7.91 \pm 0.11) \cdot 10^{-6}$ cm^2 sec^{-1}.

MACERO AND RULFS[11] obtained from diffusion experiments with $2.39 \cdot 10^{-3}$ M CdCl$_2$ in 0.1 M KCl, an average value of $(6.93 \pm 0.03) \cdot 10^{-6}$ cm^2 sec^{-1}. This suggests that their correction for initial mixing was not correct. The concentrations of Cd(II) in our experiments were less than those used by MACERO AND RULFS, because concentrations greater than 10^{-3} M gave rise to rather extended maxima in the diffusion currents, but this difference in concentration cannot likely account for a deviation of about 14%.

Moreover, the same authors obtained the diffusion coefficients of a number of electroactive ions in supporting electrolyte solutions, using a calibrated Cottrell technique[12]. The Cottrell-cell was calibrated with a mM solution of CdCl$_2$ in 0.1 M KCl, taking $D_{Cd(II)} = 7.00 \cdot 10^{-6}$ cm^2 sec^{-1}, obtained from diaphragm cell meas-

TABLE 6

DIFFUSION COEFFICIENTS IN 0.1 M KCl AT 25°

Electroactive species	$D \cdot 10^6$ (cm^2 sec^{-1})		
	According to ref. 10	Recalculated	According to refs. 6, 7
Cd(II)	(7.00)*	(7.91)*	
Pb(II)	8.62	9.74	9.70
Tl(I)	15.8	17.9	18.4

* Calibrating values, used for the calculations.

TABLE 7

SHAPES OF PULSE POLAROGRAMS AND HALF-WAVE POTENTIALS (vs. MERCURY POOL ELECTRODE, 25.0±0.1°)

Soln.	No. of log plots	Av. value of slope (mV)	Av. value of $-E_{\frac{1}{2}}$ (V)
Tl(I) in 0.2 M KCl	8	59 ± 1	0.541 ± 0.002
Pb(II) in 0.1 M KCl+0.1 M HCl	6	31.7 ± 0.8	0.473 ± 0.003
Cd(II) in 0.1 M KCl	5	31.7 ± 0.8	0.661 ± 0.001

urements[13]. Their results for Pb(II) and Tl(I) in 0.1 M KCl are listed in Table 6 together with the values recalculated with $D_{Cd(II)} = 7.91 \cdot 10^{-6}$ cm^2 sec^{-1} and also the tracer values obtained by WANG[6,7] AND POLESTRA[7]. The agreement between the recalculated values and the tracer diffusion coefficients is markedly better.

The shape of the pulse polarograms of Tl(I), Pb(II) and Cd(II) in the stated supporting electrolyte solutions was in agreement with the Nernst equation: plots of

$\log(i_d - i)/i$ vs. E were fairly linear. The average slopes (not corrected for ohmic drop) of these lines and the average values of the half-wave potentials $(E_{\frac{1}{2}})$ with respect to the mercury pool electrode are listed in Table 7.

In Fig. 5 the curves obtained for Zn(II) by plotting $\log(i_d - i)/i$ vs. E are given for three different pulse times. It is interesting to note that the shapes of the curves are similar to the shapes found by KORYTA[14] for Zn(II) in $NaNO_3$ solutions. It seems
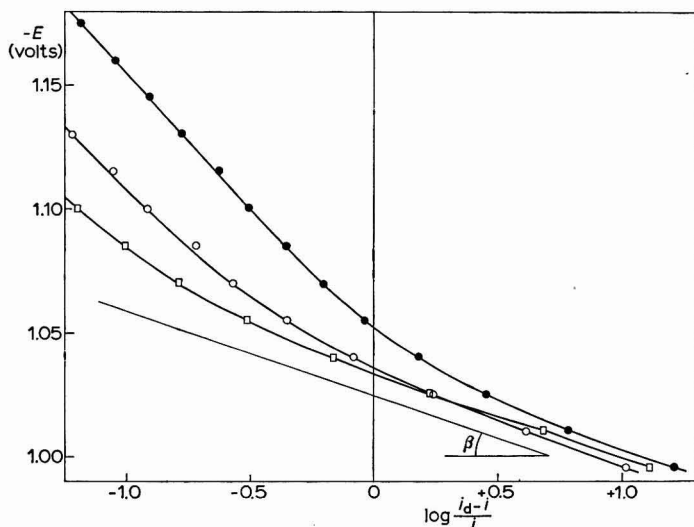
Fig. 5. Plots of log $(i_d - i)/i$ vs. potential for Zn(II) in 1 M KCl + 5·10^{-4} M HCl; pulse times: (●), 0.036; (○), 0.090; (□), 0.540 sec. β, theoretical slope angle for a reversible 2-electron polarogram.

that the wave tends to become more "reversible" when the pulse time increases.

In some instances, slight maxima were found in the pulse polarograms. They were situated in the usual region at the beginning of the diffusion current plateau. A relation between these maxima and the maxima usually encountered in normal polarography could not be detected, neither in shape nor occurrence.

SUMMARY

The effect of the shielding of the mercury drop by the tip of the capillary on the diffusion equation in pulse polarography was evaluated. The modified diffusion

equation for instantaneous currents was tested, using a pulse polarograph constructed from solid state components. The apparatus has been described.

The agreement between theoretical and experimental values of the diffusion current was proved to be satisfactory for the ions, Tl(I), Pb(II) and Zn(II), provided tracer diffusion coefficients were used in the calculations. The diffusion coefficient of Cd(II) was determined.

REFERENCES

1 A. A. A. M. BRINKMAN AND J. M. LOS, *J. Electroanal. Chem.*, 7 (1964) 171.
2 K. E. REINERT, *Z. Elektrochem.*, 66 (1962) 390; H. D. F. COLE, P. DELAHAY AND G. G. SUS-BIELLES, *Collection Czech. Chem. Commun.*, 30 (1965) 3987, have recently given the same derivation, unfortunately obscured by numerous misprints.
3 G. C. BARKER AND A. W. GARDNER, A.E.R.E. – C/R 2297, 1961.
4 H. MATSUDA, *Bull. Chem. Soc. Japan*, 26 (1953) 342.
5 J. M. MARKOWITZ AND P. J. ELVING, *Chem. Rev.*, 58 (1958) 1066.
6 J. H. WANG, *J. Am. Chem. Soc.*, 76 (1954) 1528.
7 J. H. WANG AND F. M. POLESTRA, *J. Am. Chem. Soc.*, 76 (1954) 1584.
8 R. J. BEARMAN, *J. Phys. Chem.*, 66 (1962) 2072.
9 J. M. LOS AND D. W. MURRAY, *Advances in Polarography*, Vol. II, Pergamon Press, London, 1960, p. 437.
10 E. P. PARRY AND R. A. OSTERYOUNG, *Anal. Chem.*, 37 (1965) 1634.
11 D. J. MACERO AND C. L. RULFS, *J. Electroanal. Chem.*, 7 (1964) 328.
12 D. J. MACERO AND C. L. RULFS, *J. Am. Chem. Soc.*, 81 (1959) 2942.
13 C. L. RULFS, *J. Am. Chem. Soc.*, 76 (1954) 2071.
14 J. KORYTA, *Electrochim. Acta*, 6 (1962) 67.

COMPORTEMENT DES HALOGENURES MERCUREUX AU COURS DE LA CHRONOAMPEROMETRIE PAR REDISSOLUTION CATHODIQUE

J. P. PERCHARD,

Laboratoire de Spectrochimie Moléculaire, Faculté des Sciences de Paris

M. BUVET et R. MOLINA

Commissariat à l'Energie Atomique, S.E.A., Fontenay-aux-Roses (Hauts de Seine)

(Reçu le 23 mai, 1966)

A. PRINCIPE

Le potentiel d'oxydation du mercure en présence d'halogènures se trouve déplacé vers les valeurs négatives par suite de la formation d'un précipité d'halogènure mercureux, Hg_2X_2, à l'électrode. En régime polarographique, les courbes $i=f(E)$
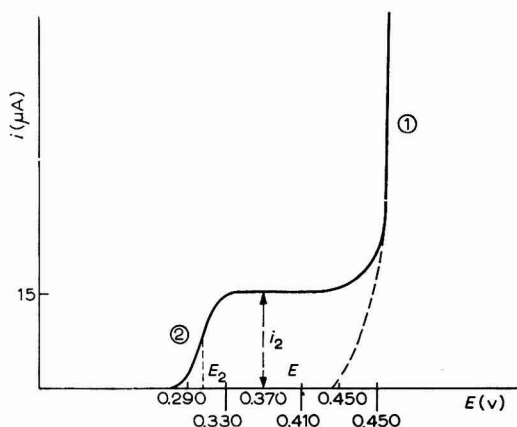
Fig. 1. Courbe $i = f(E)$ relative à l'oxydation du mercure en présence d'halogènure, en régime polarographique, milieu $HClO_4$, 0.1 N–$[Cl^-] = 10^{-4}$ M.

présentent la forme schématisée sur la Fig. 1. La partie de courbe (1) correspond à la réaction électrochimique:

$$2\,Hg\downarrow \rightleftharpoons Hg_2{}^{2+} + 2\,e \tag{1}$$

suivie de la réaction chimique:

$$Hg_2{}^{2+} + 2X^- \rightleftharpoons \downarrow Hg_2X_2$$
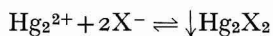
La partie (2) à la réaction:

$$2\,Hg\downarrow + 2\,X^- \rightleftharpoons \downarrow Hg_2X_2 + 2\,e \tag{2}$$

dont le courant limite de diffusion, i_2, est proportionnel à la concentration des ions X^- en solution.

La goutte pendante est placée à un potentiel, E_P, tel que la réaction (2) ait lieu et atteigne ce courant limite alors que la vitesse d'oxydation du mercure suivant la réaction (1) est négligeable. Après un certain temps d'électrolyse à ce potentiel, on laisse reposer la solution et on effectue un balayage du potentiel vers les valeurs négatives. L'halogénure mercureux déposé sur la goutte est réduit, ce qui se traduit par l'apparition d'un minimum d'intensité sur la courbe $i = f(E)$.

Dans ce cas particulier, aucune solution mathématique précise n'a été apportée à l'équation différentielle de diffusion. Nous avons étudié l'influence de différents paramètres sur la valeur du courant minimum obtenu.

B. ÉTUDE EXPÉRIMENTALE

Il est nécessaire de déterminer de façon très précise les conditions expérimentales puisque nous montrerons que de faibles modifications de certains paramètres entraînent des variations importantes des résultats. Dans l'annexe expérimentale est décrit le montage particulier de la cellule d'électrolyse qui élimine les risques de pollution des solutions. Nous préciserons ici les raisons qui ont guidé notre choix quant à l'électrolyte support et au potentiel de préélectrolyse.

1. Choix de l'électrolyte support

La condition essentielle que doit remplir l'électrolyte support est de ne pas complexer les ions mercureux, ce qui aurait pour effet de rendre le mercure plus facilement oxydable. Dans ces conditions la vague (2) risquerait d'être masquée par celle correspondant au nouveau complexe.

Nous avons tracé les polarogrammes d'oxydation du mercure en présence de nitrate de sodium, puis d'acide acétique et d'acide perchlorique. Les potentiels d'oxydation observés sont sensiblement les mêmes, ce qui indique que dans nos conditions opératoires ces trois composés complexent peu le mercure et peuvent donc être considérés comme électrolytes supports satisfaisants. Pour des concentrations de 10^{-1} M, leur teneur en bromure et iodure est négligeable; celle en chlorure peut atteindre 1 à $2 \cdot 10^{-6}$ M.

2. Choix du potentiel de préélectrolyse

Le choix de E_P doit être tel que seule la réaction (2) ait lieu car on veut constituer le dépôt à la surface même de l'électrode. Si E_P est trop élevé, les réactions (1) et (2) ont lieu simultanément et une fraction de l'halogénure mercureux précipite au sein de la solution et non à l'électrode. Au contraire, si E_P est trop petit, le courant de préélectrolyse est faible et la quantité d'halogénure déposée est également faible. Nous avons vu plus haut que le potentiel de préélectrolyse, E_P, doit être supérieur au potentiel de demi-vague, E_2, caractéristique de la réaction (2). On sait que E_2 croît lorsque le produit de solubilité de l'halogénure croît et lorsque la concentration de ce dernier décroît. La zone optimale de potentiels de préélectrolyse est donc la plus réduite pour les solutions diluées de l'halogénure le plus soluble. La Fig. 2 illustre ces phénomènes pour les cas comparés de I⁻ et Cl⁻.

Notre exposé est divisé en deux parties:

(i) la première se rapporte aux résultats les plus simples, obtenus pour des concentrations en halogénures supérieures à 10^{-5} M;
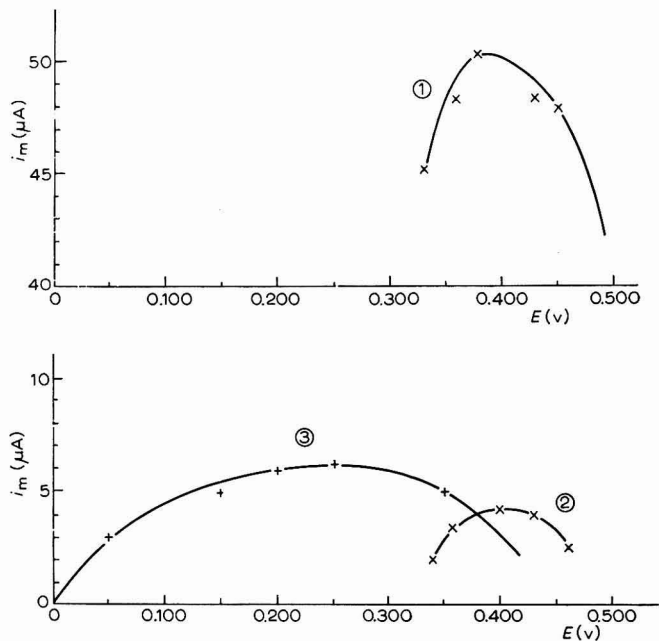
Fig. 2. Courbes $i_m = f(E_P)$, en milieu $HClO_4$, 10^{-1} M. (1) $[Cl^-] = 5 \cdot 10^{-4}$ M; (2) $[Cl^-] = 5 \cdot 10^{-5}$ M; (3) $[I^-] = 5 \cdot 10^{-5}$ M. Surface de goutte: 1.356 mm²; préélectrolyse de 30 sec; repos de 30 sec; $V = 1$ V/min.

(ii) la seconde à ceux obtenus aux concentrations inférieures.

Dans le premier cas, en effet la courbe $i = f(E)$ tracée lors de la réduction ne présente en général qu'un seul minimum, tandis que dans le second plusieurs pics successifs apparaissent. Nous avons cherché à interpréter ce phénomène en étudiant de façon détaillée l'exemple de l'iodure, puis nous avons tenté d'étendre nos conclusions aux solutions de bromure et de chlorure.

C. RÉSULTATS OBTENUS POUR DES CONCENTRATIONS SUPÉRIEURES À 10^{-5} M

Nous avons vérifié, sur une solution de chlorure 4.76×10^{-5} M, la proportionnalité entre l'intensité minimale, i_m, d'une part, le temps de préélectrolyse (Fig. 3), la racine carrée de la vitesse de balayage (Fig. 4) et la surface de la goutte (Fig. 5) d'autre part.

La proportionnalité entre i_m et $V^{\frac{1}{2}}$ indiquerait que la vitesse de dissolution du dépôt est limitée par la diffusion des ions Cl^- de l'électrode vers la solution. D'autre part, la croissance du courant lors du balayage cathodique ne peut être imputée à une consommation complète de l'halogénure déposé puisque plusieurs balayages successifs sont nécessaires pour observer la disparition du pic caractéristique. Rappelons qu'aucune solution mathématique n'a été apportée à ce problème de diffusion.

En outre, la proportionnalité de i_m à la surface de l'électrode prouve que le chlorure mercureux ne diffuse pas dans la goutte de mercure: en effet, on sait que lorsque l'espèce électroactive diffuse dans le mercure, le courant i_m est proportionnel au diamètre de l'électrode sphérique.
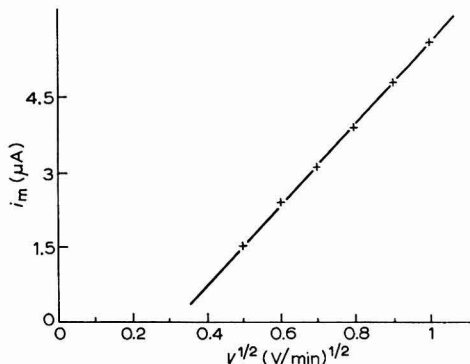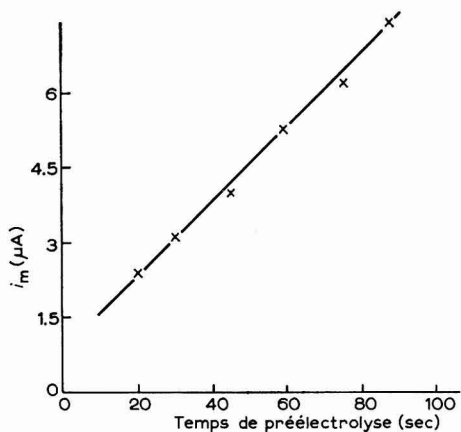
Fig. 3. Courbe $i_m = f(t)$ pour une soln. de chlorure $4.76 \times 10^{-5} M$, en milieu acide perchlorique, $10^{-1} M$. Gouttes de 1.356 mm^2; repos 30 sec au potentiel de préélectrolyse; $+0.400$ V; $V = 0.5$ V/min.

Fig. 4. Courbe $i_m = f(V)^{\frac{1}{2}}$. Gouttes de 1.356 mm^2; 30 sec de préélectrolyse à 0.400 V; repos 30 sec circuit fermé.
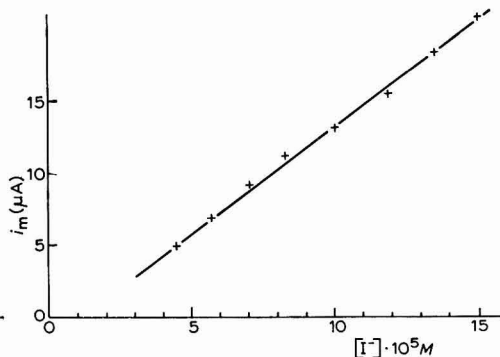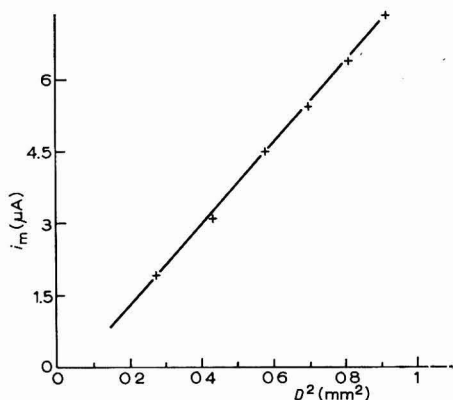
Fig. 5. Courbe $i_m = f(D^2)$. 30 sec de préélectrolyse à $+0.400$ V; repos 30 sec circuit fermé; $V = 0.5$ V/min.

Fig. 6. Courbe $i_m = f(C)$ pour I$^-$. Gouttes de 1.356 mm^2; 30 sec de préélectrolyse à $+0.250$ V; repos 30 sec; $V = 0.9$ V/min.

La relation linéaire entre i_m et la concentration de la solution en bromure ou iodure est vérifiée avec une précision de l'ordre de 3% (Fig. 6); dans le cas de concentrations en chlorure comprises entre 10^{-4} et $10^{-5} M$, les pics apparaissent tantôt simples, tantôt doubles. Dans le second cas, la séparation entre les deux pics, de hauteurs à peu près égales, varie en sens inverse de la concentration et passe de 40 mV environ pour $[Cl^-] = 2 \cdot 10^{-5} M$ à 10 mV pour $[Cl^-] = 9 \cdot 10^{-5} M$. Quand la concentration est supérieure à $10^{-4} M$, on observe toujours un seul pic.

Les deux droites de la Fig. 7 ont été tracées avec les pics doubles (a) et les pics simples (b), un peu plus élevés. On constate que ces droites d'étalonnage sont assez

peu différentes. Dans le cas du pic simple, le potentiel E_m correspondant à i_m varie avec la concentration; la relation $E_m = f \log[Cl^-]$ est linéaire, la pente de la droite correspondante étant voisine de -0.064. Le déplacement est donc voisin de celui de E_2 de la vague polarographique (2) de la Fig. 1.
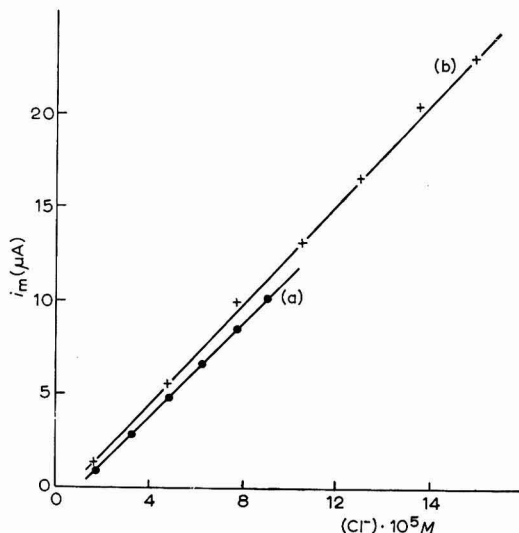
Fig. 7. Courbe $i_m = f(C)$ pour Cl^-. Gouttes de 1.356 mm^2; 30 sec de préélectrolyse à $+0.400$ V; repos 30 sec circuit fermé; $V = 1$ V/min. (a), Pics dédoublés; (b), pics simples.

D. RÉSULTATS OBTENUS POUR DES CONCENTRATIONS INFÉRIEURES À 10^{-5} M

Pour des concentrations en halogènures inférieures à 10^{-5} M, les vérifications des diverses lois sont rendues beaucoup plus difficiles par la présence de deux pics dans le cas du bromure, de l'iodure, et parfois de trois dans celui du chlorure.

(a) *Cas de l'ion I^-*

Pour des concentrations voisines de 10^{-5} M, on observe deux pics lors de la réduction du dépôt de Hg_2I_2. Le premier qui apparaît, dans l'ordre des potentiels décroissants (sens du balayage des potentiels) a une hauteur qui croît avec le temps de préélectrolyse (Fig. 8). Le second des deux pics correspond à un potentiel de -0.11 V. Nous avons vérifié que l'intensité, i_m, du premier pic varie linéairement avec la surface de la goutte et avec la racine carrée de la vitesse de balayage des potentiels. Pour des temps de préélectrolyse supérieurs à 30 sec, ce pic est de beaucoup le plus important et masque le second.

Pour des concentrations inférieures à 10^{-6} M, on n'observe lors de la réduction que le second des deux pics, situé au potentiel de -0.11 V.

Une étude systématique faisant intervenir les différents paramètres prouve qu'on reste dans le domaine de la limitation du courant par diffusion. En effet, la hauteur, i_m, du pic varie linéairement avec la racine carrée de la vitesse de balayage et la surface de la goutte. Par conséquent, ici encore, la diffusion de l'iodure mercureux dans la goutte de mercure reste négligeable. Les relations entre i_m et le temps de
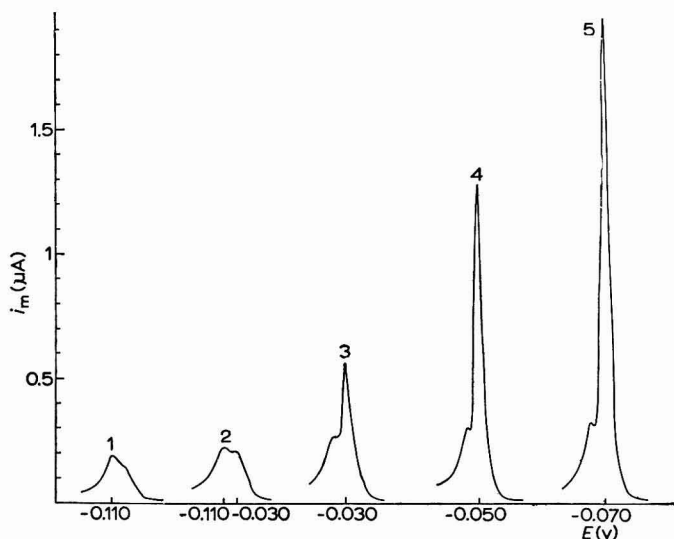
Fig. 8. Courbes $i = f(E)$ pour différentes valeurs du temps de préélectrolyse, t. Concn. en iodure, 1.17×10^{-5} M; Milieu NaNO$_3$, 10^{-1} M; gouttes de 2.19 mm²; préélectrolyse à +0.250 V; repos 30 sec; $V = 0.9$ V/min; T = 22°; temps de préélectrolyse: (1), 5; (2), 10; (3), 30; (4), 60; (5), 100 sec.
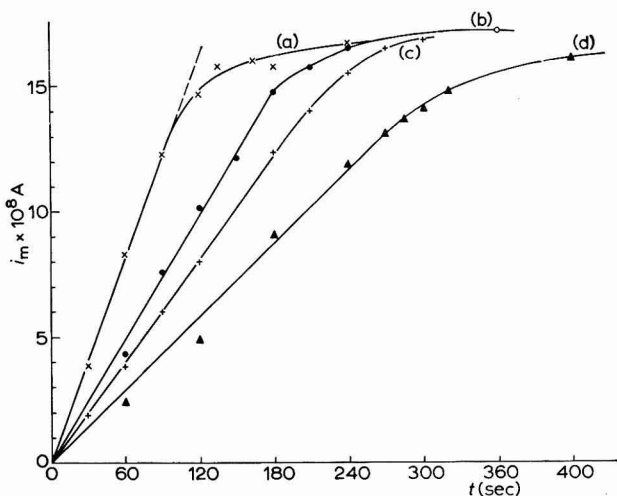
Fig. 9. Courbe $i_m = f(t)$. Gouttes de 2.19 mm²; repos 30 sec; $V = 0.9$ V/min. [I⁻]: (a), 7.27; (b), 4.31; (c), 3.80; (d), 2.81 $\times$ 10^{-7} M. T = 23°.

préélectrolyse, t, d'une part, la concentration de la solution, C, d'autre part, sont plus complexes puisqu'elles ne restent linéaires que pour des faibles valeurs des variables (Figs. 9 et 10). Pour des valeurs supérieures de celles-ci on observe une limitation de i_m. Cette constatation a déjà été faite par KEMULA, KUBLIK ET TARASZEWSKA[1] qui n'en ont pas donné d'explication.

Nous exposerons maintenant certains résultats quantitatifs obtenus à partir

des relations $i_m = f(t)$ et $i_m = f(C)$ qui permettent d'interpréter l'existence de ce pic et sa limitation.

En désignant par t_1 le temps maximal de préélectrolyse pour lequel la relation linéaire entre i_m et t est vérifiée, nous observons que le produit $t_1 \cdot C$ est constant (Tableau 1): il est possible de relier C au courant de préélectrolyse, i; nous constatons que le produit $i \cdot t_1$ est constant, aux incertitudes de mesure près. Cette quantité
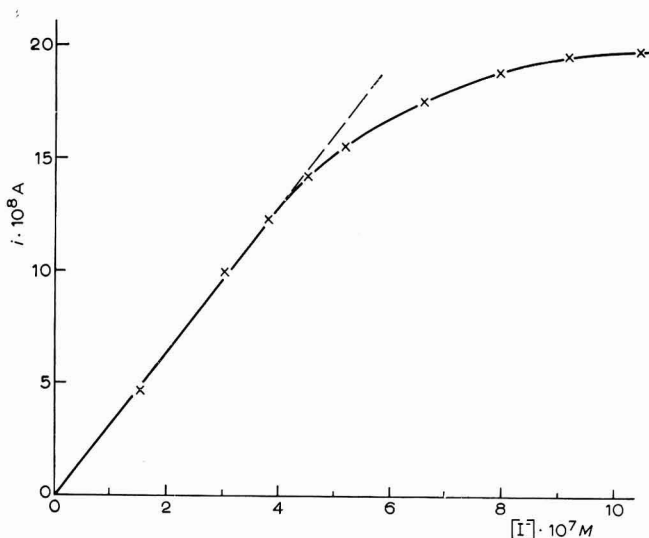
Fig. 10. Courbe $i_m = f(C)$ relative à I^-. Gouttes de 2.19 mm²; préélectrolyse de 3 min à +0.250 V; repos 30 sec; $V = 0.9$ V/min; T = 22°.

TABLEAU 1

RELATION ENTRE LA CONCENTRATION EN IODURE, LE COURANT D'OXYDATION ET LE TEMPS LIMITE DE PRÉÉLECTROLYSE, t_1, POUR LEQUEL LA COURBE $i_m = f(t)$ EST UNE DROITE

$[I^-] \cdot 10^7$ M	t_1 (sec)	$t_1 \cdot [I^-]$	$i_{pré.}$ 10^8 A	$i_{pré.} \cdot t_1 (\mu C)$
2.81	276	7.75	0.50	1.38
3.80	200	7.60	0.60	1.20
4.31	180	7.76	0.70	1.26
4.53	165	7.47	0.73	1.20
7.27	100	7.27	1.10	1.10
14.80	54	7.99	2.30	1.24
36.10	21	7.58	5.80	1.22

d'électricité limite exprime, d'après la loi de Faraday, le nombre de molécules formées au temps t_1. Avec nos conditions expérimentales nous avons trouvé $i \cdot t_1 = 1.23 \mu C$, ce qui revient à dire qu'il s'est formé au cours de la préélectrolyse 3.75×10^{12} molécules d'iodure mercureux, Hg_2I_2. En admettant que toutes ces molécules se sont fixées sur la goutte, nous avons calculé la surface occupée par chacune d'elle dans l'hypothèse d'une couche monomoléculaire; la surface totale de la goutte est $S = 2.19$ mm² et la surface disponible par molécule, 58.4 Å².

Nous savons que l'iodure mercureux cristallise dans le système quadratique[2,3] et que les paramètres de la maille sont:

$$a = 4.92 \text{ Å}, \qquad b = 11.62 \text{ Å}$$

La projection de la face rectangulaire correspond, étant donné la structure du réseau, à la surface occupée par une molécule, soit:

$$ab = 57 \text{ Å}^2$$

La concordance entre les deux valeurs permet de supposer que le pic étudié correspond effectivement à la réduction d'un dépôt monomoléculaire d'iodure mercureux fixé sur la goutte.

Nous avons étendu nos vérifications expérimentales à des solutions refroidies à $6.0 \pm 0.2°$. Dans ces conditions, nous observons vers -0.14 V un pic dont la hauteur, pour des concentrations inférieures à $2 \cdot 10^{-6}$ M, atteint une limite égale à celle observée en opérant à température ordinaire. De la même façon, le produit $t_1 \cdot C$ conserve pour diverses concentrations une valeur constante mais très supérieure à celle calculée à température ordinaire, toutes conditions expérimentales identiques par ailleurs: 13.3 contre 7.54×10^{-5} M sec. Par contre, le produit $i_1 \cdot i$, i désignant le courant de préélectrolyse, conserve une valeur constante indépendante de la température, soit ici 1.2 μC. Ces résultats s'expliquent par la variation notable du coefficient de diffusion avec la température. A température plus basse le courant de préélectrolyse, i, décroît et le temps pour constituer le dépôt monomoléculaire est plus grand. Il en résulte que le produit $t_1 \cdot C$ devient supérieur tandis que le produit $t_1 \cdot i$, qui représente toujours le même nombre de molécules déposées, reste constant.

En résumé, le calcul de la surface moléculaire fournit le même résultat que l'on opère à 6° ou à 22°. On est donc amené à admettre que Hg_2I_2 est suffisamment insoluble pour rester quantitativement fixé à la surface de l'électrode. La variation de la hauteur du pic avec la température est donc due à la variation du coefficient de diffusion et non à celle du produit de solubilité.

Remarque. On observe également une discontinuité dans le régime de diffusion dès que la couche monomoléculaire s'est formée: à 22° comme à 6°, une fois le temps de préélectrolyse limite t_1 atteint, le courant de préélectrolyse croît de 20% puis redevient constant (Fig. 11).

L'existence d'un dépôt monomoléculaire orienté de Hg_2Br_2 et Hg_2Cl_2 sur le mercure avait été mise en évidence par BOULT ET THIRSK[4] par observation au microscope électronique et étude de diffraction électronique de pellicules décollées de la surface de mercure. En ce qui concerne l'iodure mercureux, ces mêmes auteurs avaient conclu de leurs essais que la couche n'est plus orientée et qu'en outre elle est constituée d'un mélange d'iodures mercureux et mercurique, ainsi que d'oxyde HgO, probablement en raison de la faible stabilité de Hg_2I_2 en présence d'un excès d'iodure. Le fait qu'ils formaient leur dépôt dans des solutions au moins 10^4 fois plus concentrées en iodure que les nôtres permet de justifier la divergence des conclusions.

Une fois la couche monomoléculaire formée, d'autres couches se déposent, mais nous ne pouvons préciser si la croissance du dépôt s'effectue au niveau de la goutte de mercure ou par empilement des couches les unes au-dessus des autres: autrement dit, si ce sont les ions I^- ou Hg_2^{2+} qui diffusent à travers le dépôt déjà constitué. D'après BOULT ET THIRSK, l'épaississement du film a lieu au niveau de l'interface solution –

Hg_2I_2, les ions mercureux quittant le mercure là où il existe des *trous* dans la couche de Hg_2I_2.

Du point de vue électrochimique, la couche monomoléculaire possède des propriétés particulières, que l'on doit vraisemblablement rattacher à la nature de la liaison entre atomes de mercure et molécules d'iodure mercureux.
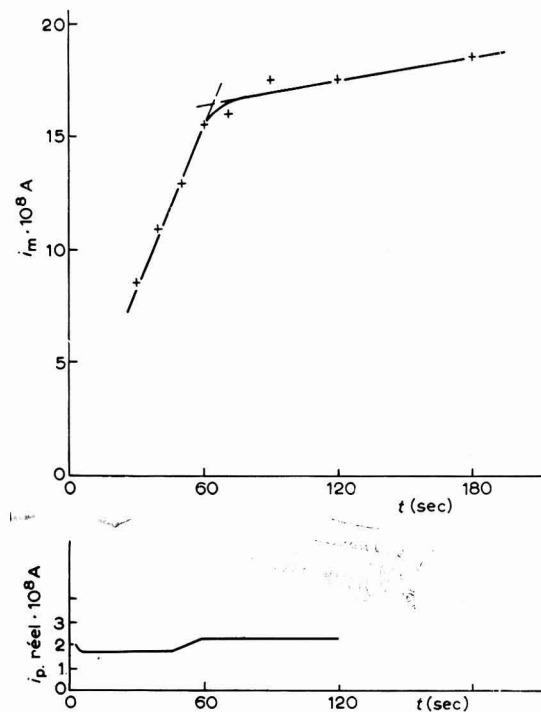
Fig. 11. Courbe i_m et $i_{pré.} = f(t)$ pour une soln. d'iodure de concn. 2.12×10^{-6} M en milieu $NaNO_3$, 10^{-1} M. Gouttes de 2.19 mm²; préélectrolyse à $+0.250$ V; repos 30 sec; $V = 0.9$ V/min; $T = 6°$.

En effet, au cours de la réduction d'un dépôt polymoléculaire, on met en évidence l'existence de deux pics (Fig. 8). Le pic observé au potentiel de -0.11 V et de hauteur sensiblement constante quel que soit le temps de préélectrolyse correspondrait à la réduction de la couche de Hg_2I_2 fixée sur le mercure. Le second pic observé vers les potentiels positifs, suit les lois classiques de la chronoampérométrie et peut être attribué à la réduction de la partie supérieure du dépôt d'iodure mercureux.

(b) *Cas de l'ion Br⁻*

Aux faibles concentrations en bromure, nous avons utilisé l'acide acétique 10^{-1} M comme électrolyte support; le potentiel d'oxydation optimal se situe au voisinage de $+0.330$ V; en l'absence de bromure, le courant de préélectrolyse résiduel est inférieur à 10^{-9} A, dans nos conditions opératoires.

A température ordinaire des séries de mesures ont été effectuées sur des solutions de bromure de concentrations variant entre 10^{-7} et 10^{-6} M. Un pic caractéristique, vers $+0.170$ V, est observé lors de la réduction du dépôt. Pour toute concen-

tration inférieure à $7 \cdot 10^{-7}$ M, la courbe $i_m = f(t)$ est linéaire pour les faibles valeurs de t, passe par un maximum de l'ordre de 0.05 μA et décroît. Aux concentrations supérieures, la croissance du pic n'est plus aussi limitée mais devient non reproductible de sorte que nous n'avons pu faire d'étude systématique. Nous constatons cependant qu' à concentration égale, les courants d'oxydation sont voisins de ceux observés pour l'iodure, mais que la hauteur, i_m, des pics est 3 ou 4 fois moins élevée. Nous pensons que cette différence doit être liée à la solubilité plus grande du bromure mercureux, dont une partie ne se fixe pas à la surface de la goutte là où elle a été formée mais diffuse dans la solution où elle n'est pas réduite au cours du balayage cathodique.

C'est pourquoi nous avons cherché à diminuer le produit de solubilité du bromure mercureux pour fixer un plus grand nombre de molécules à la surface de la goutte.

En refroidissant la solution au voisinage de 6° nous avons observé une décroissance de 20–30% du courant d'oxydation que nous expliquons par une diminution du coefficient de diffusion des ions bromures. Par contre, le pic à la réduction dont le
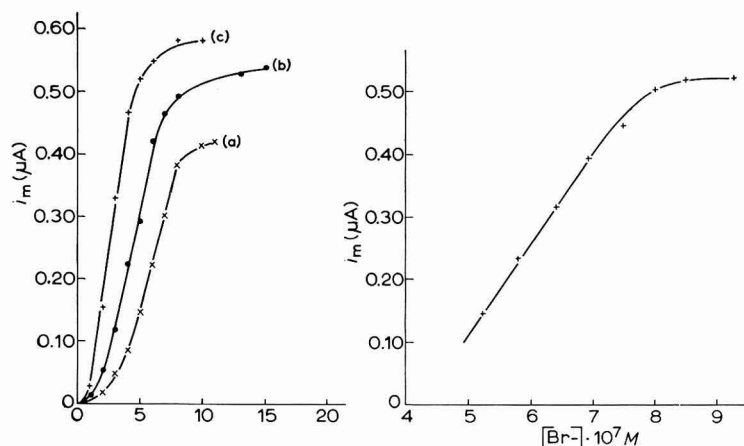
Fig. 12. Courbes $i_m = f(t)$ pour diverses concns. de bromure, milieu CH₃COOH, 10^{-1} M. Gouttes de 2.19 mm²; préélectrolyse à +0.330 V; repos 30 sec; $V = 0.9$ V/min. [Br⁻]: (a) = 5.22; (b) = 6.30; (c) = 9.23 × 10^{-7} M. T = 6.5°.

Fig. 13. Courbe $i_m = f(C)$, milieu CH₃COOH, 10^{-1} M. Gouttes de 2.19 mm²; préélectrolyse de 5 min à +0.330 V; repos 30 sec; $V = 0.9$ V/min; T = 6.5°.

maximum se situe vers +0.12 V, s'est notablement élevé et suit, dans certaines conditions, les lois de la chronoampérométrie linéaire:

(a) La relation $i_m = f(t)$ est linéaire dans un certain domaine de t (Fig. 12). La limitation observée pour des temps croissants de préélectrolyse est de l'ordre de 0.6 μA.

(b) La relation $i_m = f(C)$, où C désigne la concentration en ions bromures, est linéaire aux faibles concentrations (Fig. 13); puis la pente diminue progressivement.

(c) Enfin, nous avons vérifié avec une bonne précision la loi $i_m = kV^{\frac{1}{2}}$, V désignant la vitesse de variation du potentiel.

Pour les concentrations supérieures à 10^{-6} M, nous avons mis en évidence le dédoublement du pic pour les durées croissantes de préélectrolyse (Fig. 14).

Cette série d'observations est comparable aux résultats obtenus pour l'iodure

dans la même zone de concentration: seule diffère la hauteur limite du pic, environ trois fois plus haute dans le cas du bromure. Par analogie nous concluerons que le pic précédemment étudié est relatif à la réduction de la couche monomoléculaire de bromure mercureux liée au mercure. Nous n'avons pu prouver ce résultat par un calcul de surface moléculaire probablement pour la raison que le produit de solubilité n'est pas suffisamment faible pour identifier la quantité de Hg₂Br₂ formé à celle déposée sur la goutte.
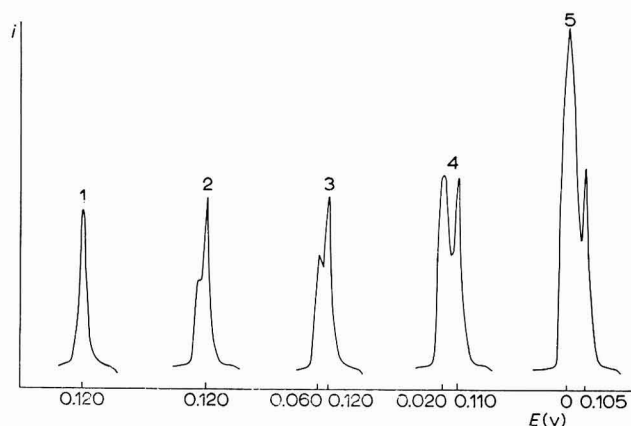
Fig. 14. Courbes $i = f(E)$ pour différentes valeurs du temps de préélectrolyse, t. Concn. en bromure, $2.38 \times 10^{-6}\ M$, milieu CH₃COOH, $10^{-1}\ M$. Gouttes de 2.19 mm²; préélectrolyse à $+0.330$ V; repos 30 sec; $V = 0.9$ V/min; T $= 7°$. Temps de préélectrolyse (1), 2; (2), 3; (3), 4; (4), 7; (5), 12 min.

L'étude de la zone de concentration comprise entre 10^{-5} et $10^{-6}\ M$ est rendue complexe, à température ordinaire, par l'apparition successive de trois pics pour des temps croissants de préélectrolyse. Nous nous limiterons à la description des phénomènes observés. Pour les temps courts de l'ordre de 30 sec un premier pic est observé à un potentiel de $+0.170$ V; puis une épaule apparaît vers $+0.20$ V et ce second pic tend à se substituer ou masquer le premier; l'égalité entre les deux est atteinte pour des valeurs de l'ordre de 0.13 μA, quelle que soit la concentration de la solution. Une fois le premier pic disparu, le second croît tandis que son potentiel tend vers $+0.160$ V; il apparaît alors un troisième pic, vers $+0.13$ V, dont la croissance est rapide et qui, pour des concentrations de l'ordre de $10^{-5}\ M$ et des temps d'oxydation égaux ou supérieurs à la minute, masque le second et subsiste seul.

Une étude détaillée de chacun des pics est rendue difficile par la proximité des potentiels de leurs maxima. Il est possible que l'existence des deux premiers soit liée à la réduction de la couche monomoléculaire, mais il ne nous paraît pas possible d'interpréter le dédoublement.

(c) *Cas de l'ion Cl⁻*

KEMULA et collaborateurs[1], expérimentant à température ordinaire, ont trouvé que pour des concentrations inférieures à $10^{-5}\ M$ le pic relatif à la réduction de chlorure mercureux est très peu élevé et pratiquement indépendant de la concentration. Lorsque celle-ci atteint une certaine valeur la croissance du pic est très rapide et

linéaire. Ces auteurs considèrent la concentration limite comme le seuil d'apparition de précipité sur la goutte, c'est-à-dire la valeur pour laquelle le produit de solubilité est atteint. BALL, MANNING ET MENIS[5] indiquent, au contraire, qu'ils ont pu travailler à la concentration de $6 \cdot 10^{-6} M$ sans observer d'anomalie.

Nous avons repris l'étude de ce domaine de concentrations et retrouvé les résultats de KEMULA. En effet, le pic observé présente une hauteur pratiquement indépendante de la concentration jusqu'à une valeur voisine de $8 \cdot 10^{-6} M$. Au-delà de cette valeur, on retrouve les phénomènes exposés précédemment.

Nous avons pu observer que la hauteur de ce pic est également indépendante du temps de préélectrolyse; elle varie linéairement avec la surface de la goutte.

Ces faits peuvent amener à penser que ce pic n'est pas dû à la redissolution d'un dépôt de chlorure mercureux; dans une étude récente du comportement des halogénures en polarographie, BIEGLER[6] a pu montrer que, pour le chlorure en particulier, il apparaît lors du balayage vers les potentiels positifs, un pic qui ne correspond pas à une réaction électrochimique mais que l'auteur attribue à un phénomène électrique dû à une capacité différentielle élevée (en raison d'une adsorption spécifique des ions chlorures quand le potentiel est suffisamment positif).

Il semble donc hasardeux d'attribuer ce pic au phénomène de redissolution d'une monocouche de chlorure mercureux. Cependant, nous avons réalisé plusieurs expériences dont les conclusions identiques peuvent militer en faveur de cette hypothèse. Après avoir constitué un dépôt important d'halogénure par une oxydation de quatre minutes à $+0.4$ V dans une solution de Cl$^-$, $9.8 \times 10^{-6} M$, on procède à des balayages cathodiques successifs. Au bout de 8–10 balayages, on constate que seul subsiste le pic précédemment observé. Pour les balayages ultérieurs, la hauteur de ce pic décroît lentement. Cette décroissance lente peut être interprétée par le fait que le retour au potentiel initial reconstitue une partie du dépôt précédemment réduit.

CONCLUSION

Pour les concentrations en halogénures inférieures à $10^{-5} M$, l'interprétation des phénomènes ne nous apparaît nette que pour le cas des ions I$^-$. Nous avons pu mettre en évidence la formation d'une monocouche orientée de Hg$_2$I$_2$ lors de l'oxydation d'une électrode de mercure dans des solutions d'iodure en concentration inférieure à $10^{-6} M$. La redissolution de cette monocouche est caractérisée, en chronoampérométrie linéaire, par un pic distinct de ceux auxquels donne naissance la redissolution des autres couches de Hg$_2$I$_2$.

L'interprétation des phénomènes a pu être faite dans le cas de l'iodure, en raison de la plus grande insolubilité de l'iodure mercureux qui permet d'aboutir à des résultats quantitatifs cohérents. L'étude des bromures et chlorures apparaît plus complexe.

Du point de vue analytique, nous pouvons conclure que les dosages de chlorure, bromure et iodure sont possibles à température ordinaire aux concentrations supérieures ou égales à $10^{-5} M$ pour les deux premiers et à $10^{-7} M$ pour le troisième. La sensibilité est accrue par refroidissement des solutions, probablement en raison de la diminution du produit de solubilité des halogénures mercureux. Mais, même dans ce cas, les phénomènes restent complexes en raison de la multiplicité des pics observés à la réduction du dépôt.

E. APPLICATION AU DOSAGE DES CHLORURES

Les conclusions que nous venons de tirer de l'étude précédente limitent, dans le cas particulier des chlorures, la sensibilité de la méthode au voisinage de 10^{-5} M. Elle est donc compétitive, de ce point de vue, avec la méthode classique de distillation du chlore après oxydation. On peut cependant affirmer que sa mise en oeuvre est moins délicate et beaucoup plus rapide.

Mode opératoire

L'équipement utilisé est décrit dans l'annexe expérimentale. La prise d'essai est introduite dans la cellule de mesure et le volume amené à 20 ml par de l'eau bidistillée. On acidifie par quelques gouttes de $HClO_4$, 11 N. La solution est ensuite dégazée durant une dizaine de minutes par un barbottage d'argon saturé d'eau. Dans la suite des opérations, on maintient une circulation d'argon au-dessus de la solution. On forme ensuite une goutte de mercure correspondant à deux divisions de la vis micrométrique ($d=0.66$ mm) et procède à la préélectrolyse à $+0.400$ V, durant 30 sec, la solution étant agitée par un barreau magnétique à la vitesse de 850 tours/min. On arrête l'agitation, le potentiel de l'électrode étant maintenu à la valeur $+0.400$ V. Au bout de 30 sec de repos, on déclenche le balayage cathodique de potentiel à la vitesse de 1 V/min. On obtient alors un pic de courant dont le potentiel se situe entre $+0.200$ et $+0.220$ V.

La courbe d'étalonnage est tracée dans les mêmes conditions en utilisant une solution de chlorure de potassium préalablement recristallisé: en effet, ce sel contient souvent comme impureté du chlorure de sodium. On obtient une droite dont on trouvera un exemple à la Fig. 7.

Domaine d'application

Jusqu'à présent, cette méthode a été utilisée dans les échantillons suivants:

Eau provenant de la fusion de glaces de l'Antarctique, prélevées à différentes distances de la côte. Leurs concentrations en chlorure varient entre 10^{-5} et 10^{-4} M.

Eau de réacteur piscine. Les concentrations déterminées varient également entre 10^{-5} et 10^{-4} M.

Solutions de corrosion.

Solutions de nitrate d'uranyle, de concentration voisine de 400 g/l en uranium. Dans ce cas, la prise d'essai (de 5 ou 10 ml) est amenée à 20 ml par HNO_3, N. Les conditions opératoires restent les mêmes. On a pu ainsi déterminer, sans séparations préalables, des teneurs de 2.5 p.p.m. de chlorure (exprimées par rapport à l'uranium).

Solution de nitrate d'aluminium, en milieu HNO_3, N. La limite de sensibilité atteinte dans ce cas est de 70 p.p.m. (exprimée par rapport à l'aluminium).

Ions gênants

On peut en distinguer deux types:

(i) Les anions susceptibles de former un sel mercureux de solubilité inférieure ou égale à celle du chlorure; l'ion carbonate répond à ces conditions, pour cette raison il n'est pas possible de déplacer le pic dû à la réduction de UO_2^{2+} en complexant cet

élément en milieu carbonate, de façon à disposer d'une plus grande plage de potentiels permettant de doser les halogénures autres que Cl⁻.

(ii) Les cations susceptibles d'être réduits au potentiel de préélectrolyse. Le rendement de l'oxydation du mercure en chlorure mercureux est alors très faible, voir nul si le cation est en grande concentration. Il faut alors procéder à une séparation.

Par exemple, les solutions de Al(III) contenaient comme impureté Fe(III). Ce cation est réduit au potentiel choisi pour l'oxydation du mercure (+0.400 V) et perturbe donc cette oxydation. La séparation en a été effectuée par électrolyse sur nappe de mercure, au potentiel de −1 V.

Reproductibilité

Pour chaque échantillon on effectue deux déterminations indépendantes. Chaque détermination est prise comme valeur moyenne de 3 balayages de potentiels. Les limites de confiance de la valeur moyenne au niveau de 95%, sont alors calculées par la formule:

$$\bar{x} \pm \frac{t\sigma}{\sqrt{2}}$$

Etant donné le grand nombre d'échantillons traités, la valeur de t (coefficient de Student) est très voisine de 2.

Dans ces conditions, nous avons obtenu pour le terme $t\sigma/\sqrt{2}$, la valeur 0.12×10^{-5} M pour des concentrations de chlorure comprises entre 10^{-5} et $3 \cdot 10^{-5}$ M. Au-delà de cette concentration et jusqu'à 10^{-4} M, la reproductibilité garde une valeur constante de 4%.

ANNEXE EXPÉRIMENTALE

I. ÉLECTRODE INDICATRICE

La difficulté essentielle de la méthode de chronoampérométrie linéaire réside dans la définition et la reproductibilité de l'électrode indicatrice. Le mercure constitue un matériau de choix puisque, contrairement aux électrodes solides, sa surface apparente est identique à sa surface active du point de vue électrochimique.

STREULI ET COOKE[7], qui furent parmi les premiers à étudier cette méthode, utilisèrent une large surface plane de mercure; depuis, divers dispositifs ont été envisagés: électrode plane en platine amalgamé[3], surface annulaire de mercure facilement renouvelable[5], goutte calibrée fixée sur un fil de platine ou d'or[9,10] et enfin goutte pendante qui reste suspendue au capillaire[1]. Nous avons utilisé un tel dispositif, commercialisé par la firme Metrohm. Le capillaire, dont la paroi interne a été siliconée, est surmonté d'un petit réservoir étanche (Fig. 15). dont la partie supérieure est constituée d'un piston métallique au déplacement mesuré par vis micrométrique graduée tous les 18°. Pour former une goutte de taille définie, il suffit de déplacer le piston en tournant la vis d'un certain nombre de divisions. Après usage, la goutte est détachée en donnant un léger choc à l'ensemble. Ceci constitue la mise au zéro précédent la formation d'une nouvelle goutte de mercure.

Nous avons déterminé, par mesure optique, le diamètre, D, des gouttes en fonction de l'angle de rotation de la vis exprimé en degrés (Tableau 2). Le volume, v,

de la goutte est égal à celui du mercure chassé par le piston dont le déplacement est égal à $\alpha l/360$, l, étant le pas de vis. Nous pouvons écrire, si la goutte est de forme sphérique:

$$v = \frac{\alpha\, l}{360}\, s = \frac{D^3}{6} \quad \text{ou} \quad \alpha = KD^3$$

s, désignant la section du piston.
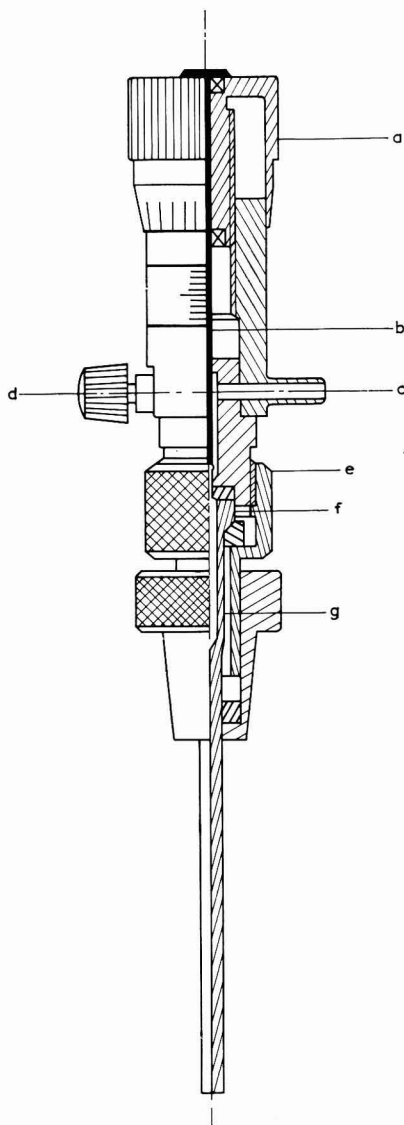
Fig. 15. Schéma de l'électrode à goutte pendante. (a), Vis micrométrique; (b), piston; (c), canalisation permettant de faire le vide; (d), connexion électrique; (e), bague de serrage; (f) extrémité supérieure du capillaire; (g), réservoir à mercure, de volume voisin de 0.18 ml.

Finalement, α est proportionnel au cube du diamètre de la goutte, tant que celle-ci est sphérique.

Nous avons vérifié cette relation pour des gouttes de faibles dimensions plongées dans l'eau (Fig. 16); en abscisse est porté non pas l'angle de rotation mais plus simplement le nombre de divisions, n, dont a tourné la vis micrométrique. On peut en conclure que les gouttes de diamètre inférieur à 1 mm sont peu déformées sous l'effet de la pesanteur et des forces de tension superficielle.

TABLEAU 2

DIAMÈTRE MOYEN DES GOUTTES EN FONCTION DU NOMBRE DE DIVISIONS N DU MICROMÈTRE ET DE L'ANGLE DE ROTATION DE CE DERNIER

N	D (mm)	α (degrés)	S (mm^2)
1	0.522	18	0.856
2	0.657	36	1.356
3	0.760	54	1.814
4	0.835	72	2.190
5	0.900	90	2.545
6	0.963	108	2.913
7	1.013	126	3.223
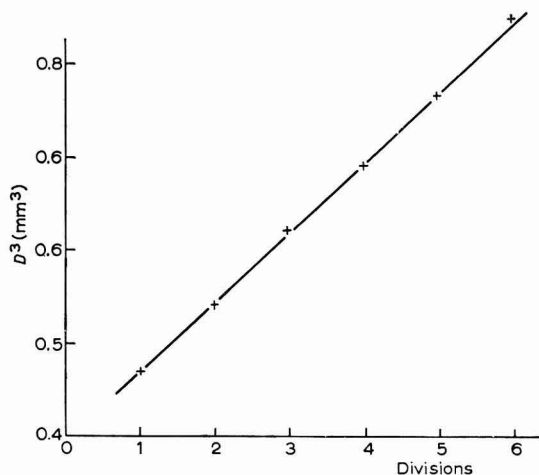
Fig. 16. Courbe $n = f(D)^3$.

En l'absence de bulle d'air dans le réservoir la reproductibilité de la taille des gouttes est de l'ordre de 1%. En raison de la faible compressibilité du mercure leur dimension doit être indépendante du potentiel auquel elles sont portées, malgré les variations de tension interfaciale mercure–solution. Nous avons vérifié expérimentalement ce fait en effectuant une série de mesures sur une goutte portée à des potentiels compris entre $+0.3$ et -1 V. Aucune variation de dimension n'a pu être décelée, la dispersion des résultats est celle de la méthode de mesure optique, de l'ordre de 1%.

II. CIRCUIT ELECTRIQUE

Le circuit électrique est un montage à trois électrodes ; la différence de potentiel variable est établie entre une électrode à potentiel fixe, ou électrode de référence et la goutte pendante de mercure. L'intensité qui traverse ce circuit est négligeable devant celle du circuit de la troisième électrode et de la goutte pendante, dans lequel est introduit le galvanomètre Sefram Graphirac dont l'échelle de plus grande sensibilité est 0.25 μA pour un déplacement du spot de 25 cm.

III. MONTAGE DES CELLULES D'ÉLECTROLYSE ET DES ÉLECTRODES

La cellule d'électrolyse d'un volume de 10 ml est à double paroi, pour permettre une régulation de température par circulation de fluide. L'agitation de la solution est réalisée au moyen d'un barreau magnétique entraîné par un moteur synchrone à arrêt instantané.

L'électrode de référence est constituée par le système Ag/AgCl en milieu KCl saturé. Pour supprimer toute diffusion des ions Cl^- on interpose entre l'électrode et la solution :

— un pont d'agar-agar contenant KCl (épaisseur : 1 cm)
— un verre fritté No. 3
— 10 ml d'une solution de nitrate de sodium 5–10 M
— un pont d'agar-agar contenant $NaNO_3$ (épaisseur : 6 cm)
— un verre fritté No. 3.

De même, la troisième électrode, constituée d'un fil de platine plongeant dans une solution de nitrate de sodium, est préservée de toute pollution de la part de la cellule par un verre fritté No. 3 et un pont d'agar-agar contenant $NaNO_3$, de 6 cm d'épaisseur.

RÉSUMÉ

Le dosage des halogénures est réalisé par redissolution d'un dépôt d'halogénure mercureux constitué par une électrolyse préalable.

Du point de vue analytique, la sensibilité est limitée au domaine de concentrations où les phénomènes sont interprétables et exploitables. Dans le cas de l'ion chlorure, la limite inférieure de ce domaine est voisine de 10^{-5} M ; elle est de 10^{-6} M pour le bromure et inférieure à 10^{-7} M pour l'iodure. Pour des concentrations inférieures, les lois simples susceptibles d'applications analytiques ne sont plus vérifiées. Cependant, le dédoublement du pic observé lors de la réduction de l'iodure mercureux déposé a été interprété en mettant en évidence les propriétés électrochimiques particulières de la couche monomoléculaire de Hg_2I_2 formée sur la goutte.

SUMMARY

Halides are determined by redissolving a deposit of mercurous halide previously deposited by electrolysis. Analytically, the use of the method is confined to a limited concentration range. In the case of chloride ion the lower limit of this range is 10^{-5} M ; it is 10^{-6} M for bromide and 10^{-7} M for iodide. For concentrations lower than these,

the relationship governing the analytical applications no longer hold. The doubling of the peak observed in the reduction of the mercurous iodide deposit has been interpreted as an electrochemical manifestation of the special properties of the monomolecular layer of mercurous iodide formed on the drop.

BIBLIOGRAPHIE

1 W. KEMULA, Z. KUBLIK ET J. TARASZEWSKA, *Proceedings International Symposium on Microchemical Techniques*, New York, 1961, p. 865.
2 I. HAVIGHURST, *J. Am. Chem. Soc.*, 49 (1927) 2113.
3 M. L. HUGGINS ET P. L. MAGILL, *J. Am. Chem. Soc.*, 49 (1927) 2357.
4 E. H. BOULT ET H. R. THIRSK, *Trans. Faraday Soc.*, 50 (1954) 404.
5 R. G. BALL, D. L. MANNING ET O. MENIS, *Anal. Chem.*, 32 (1960) 621.
6 T. BIEGLER, *J. Electroanal. Chem.*, 6 (1963) 357–380.
7 C. A. STREULI ET W. D. COOKE, *Anal. Chem.*, 26 (1954) 963.
8 T. BERZINS ET P. DELAHAY, *J. Am. Chem. Soc.*, 75 (1953) 555.
9 R. P. FRANKENTHAL ET I. SHAIN, *J. Am. Chem. Soc.*, 78 (1956) 2969.
10 J. W. ROSS, R. D. DE MARS ET I. SHAIN, *Anal. Chem.*, 28 (1956) 1768.

POTENTIAL-STEP ELECTROLYSIS FOLLOWED BY LINEAR-SWEEP VOLTAMMETRY

W. T. DE VRIES

Department of Chemistry, The Free University, De Lairessestraat 174, Amsterdam (The Netherlands)
(Received May 13th, 1966)

INTRODUCTION

The method of potential-step electrolysis followed by linear-sweep voltammetry has received attention recently[1,2]. YARNITSKY AND ARIEL[1] have introduced this method in the field of trace analysis by anodic stripping voltammetry. They found that, in some instances, this method gives better analytical results than the normal procedure of direct oxidation with a linear potential-sweep. SCHWARZ AND SHAIN[2]
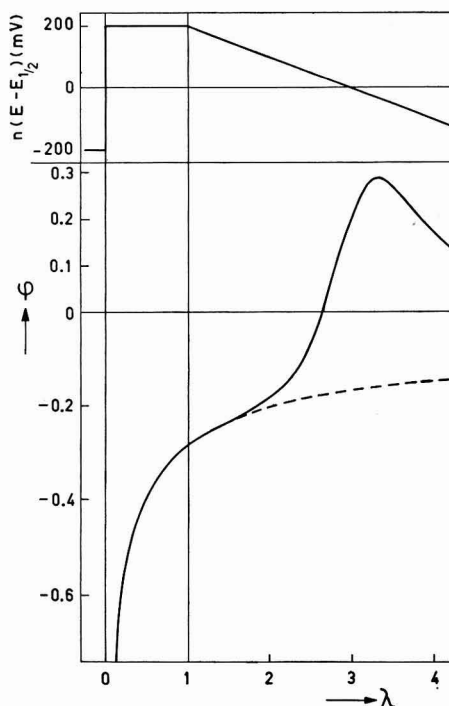
Fig. 1. Electrode potential and current as functions of time. λ and φ are defined by eqns. (15) and (16). The dashed line is a plot of eqn. (17) for $\lambda > 1$. The φ-curve was calculated for $K = \sigma\tau = 3.892\ n$.

have applied this method to the investigation of the benzidine rearrangement following reduction of azobenzene to hydrazobenzene.

The principle of the method is as follows. Consider a solution of R (which can be oxidized reversibly to O) with the electrode potential at such a negative value, E_1, that no current flows. At time $t=0$ the potential of the electrode is suddenly brought to a positive value, E_2, and an oxidation current inversely proportional to $\sqrt{t}$ will flow. Starting at time $t=\tau$, the potential of the electrode is linearly changed with time towards negative values: $E=E_2-v(t-\tau)$. The initially formed O is (partially) re-reduced to R, and a reduction current peak is recorded which resembles that in conventional linear-sweep voltammetry. These events are depicted in Fig. 1; in the upper part of this figure, the electrode potential is given as a function of time; the lower part gives the current, also as a function of time.

In this paper, oxidation of R and re-reduction is considered; adaptation of the results to reduction of O and re-oxidation is readily done by reversing potential signs and interchanging diffusion coefficients.

THEORY

It is assumed that the electrode reaction is reversible, without pre- or post-kinetics, and that conditions of semi-infinite planar diffusion for both O and R prevail. Thus, it is required to find the solution of

$$\frac{\partial}{\partial t} C_O(x, t) = D_O \cdot \frac{\partial^2}{\partial x^2} C_O(x, t) \ ; \tag{1}$$

$$\frac{\partial}{\partial t} C_R(x, t) = D_R \cdot \frac{\partial^2}{\partial x^2} C_R(x, t) \ , \tag{2}$$

with the following initial conditions:

$$C_R(x, 0) = C^0 \ ; \tag{3}$$

$$C_O(x, 0) = \theta_1 C^0 \quad (\theta_1 \ll 1), \text{ with} \tag{4}$$

$$\theta_1 = \sqrt{\frac{D_R}{D_O}} \exp\left[\frac{nF}{RT}(E_1-E_{\frac{1}{2}})\right] .$$

The boundary conditions are:

$$t<\tau: \quad C_O(0, t) = \theta_2 C_R(0, t) \quad (\theta_2 \gg 1), \text{ with} \tag{5}$$

$$\theta_2 = \sqrt{\frac{D_R}{D_O}} \exp\left[\frac{nF}{RT}(E_2-E_{\frac{1}{2}})\right] ;$$

$$t>\tau: \quad \frac{C_O(0, t)}{C_R(0, t)} = \theta_2 \exp[-\sigma(t-\tau)], \text{ with } \sigma = \frac{nF}{RT} \cdot v \ ; \tag{6}$$

$$-D_R \cdot \left(\frac{\partial C_R}{\partial x}\right)_{x=0} = D_O \cdot \left(\frac{\partial C_O}{\partial x}\right)_{x=0} = q(t) \ , \tag{7}$$

where $q(t)$, the flux of O and R at the electrode surface, is so defined as to have a

positive value for a reduction process;

$$\lim_{x \to \infty} C_R(x, t) = C^0 ; \quad \lim_{x \to \infty} C_O(x, t) = \theta_1 C^0 . \tag{8}$$

The symbols not defined above have their usual significance.

The differential equations (1) and (2), the initial conditions (3) and (4), and the boundary conditions (7) and (8) can be summarized in the following integral equations:

$$C_O(0, t) = \theta_1 C^0 - \frac{1}{\sqrt{\pi D_O}} \int_0^t \frac{q(\xi)}{\sqrt{t-\xi}} \, d\xi ; \tag{9}$$

$$C_R(0, t) = C^0 + \frac{1}{\sqrt{\pi D_R}} \int_0^t \frac{q(\xi)}{\sqrt{t-\xi}} \, d\xi , \tag{10}$$

which can easily be derived using the Laplace transformation technique.

Combination of these integral equations with boundary condition (5) gives an integral equation representation for the flux, $q(t)$, during the constant-potential electrolysis. This resulting integral equation can easily be solved by standard methods[3] and the result is:

$$q(t) = - \frac{C^0 \sqrt{D_R}}{\sqrt{\pi t}} \cdot \frac{\theta_2 - \theta_1}{\theta_2 + \sqrt{D_R/D_O}} . \tag{11}$$

The following dimensionless quantities are defined:

$$\gamma \quad = \sqrt{D_O/D_R} ; \tag{12}$$

$$Y \quad = (\theta_2 - \theta_1)/\sqrt{\pi}(\theta_2 + 1/\gamma) ; \tag{13}$$

$$K \quad = \sigma\tau ; \tag{14}$$

$$\lambda \quad = t/\tau ; \tag{15}$$

$$\varphi(\lambda) = \frac{q(t)\sqrt{\tau}}{C^0\sqrt{D_R K}} = \frac{q(t)}{C^0\sqrt{D_R\sigma}} , \tag{16}$$

and eqn.(11) is transformed into

$$\varphi(\lambda) = - \frac{Y}{\sqrt{K}} \cdot \frac{1}{\sqrt{\lambda}} . \tag{17}$$

The integral equation representation of the flux during the linear potential-sweep at $t > \tau$ can be found by combining boundary condition (6) with eqns. (9) and (10). After substitution of the appropriate dimensionless parameters into the resulting integral equation, the final result is:

$$\sqrt{\frac{\pi}{K}} \cdot \frac{\theta_1 - \theta_2 \exp[-K(\lambda-1)]}{1/\gamma + \theta_2 \exp[-K(\lambda-1)]} = \int_0^\lambda \frac{\varphi(\xi)}{\sqrt{\lambda-\xi}} \, d\xi . \tag{18}$$

The integral in eqn.(18) can be written as the sum of two integrals in the intervals $0 < \xi < 1$ and $1 < \xi < \lambda$. For $0 < \lambda < 1$, $\varphi(\lambda)$ is given by eqn.(17), and this can be sub-

stituted into the integral over the interval $0 < \xi < 1$. Working out the resulting definite integral results into:

$$\int_0^\lambda \frac{\varphi(\xi)}{\sqrt{\lambda-\xi}} \, d\xi = \frac{-Y}{\sqrt{K}} \arcsin\left(\frac{2}{\lambda} - 1\right) - \frac{\pi Y}{2\sqrt{K}} + \int_1^\lambda \frac{\varphi(\xi)}{\sqrt{\lambda-\xi}} \, d\xi . \tag{19}$$

Combination of eqns. (18) and (19) makes it possible to evaluate the current function, $\varphi(\lambda)$, obtained during the linear potential-sweep; standard numerical methods, e.g., the method of Huber[4], can be used for this purpose. However, the following will show that this is not necessary.

Let us define a new current function, $\Phi'(\lambda)$:

$$\Phi'(\lambda) = \varphi(\lambda) + \frac{Y}{\sqrt{K}} \cdot \frac{1}{\sqrt{\lambda}} , \tag{20}$$

which means that the current is measured not from the zero-current axis, but from a base-line formed by the $t^{-\frac{1}{2}}$-current during the constant-potential electrolysis. It is obvious that for $0 < \lambda < 1$, $\Phi'(\lambda) = 0$.

It is easily verified that substitution of eqn. (20) into the integral of eqn. (18) transforms this integral into:

$$\int_0^\lambda \frac{\varphi(\xi)}{\sqrt{\lambda-\xi}} \, d\xi = \int_1^\lambda \frac{\Phi'(\xi)}{\sqrt{\lambda-\xi}} \, d\xi - \frac{\pi Y}{\sqrt{K}} . \tag{21}$$

Because $\Phi'(\lambda) = 0$ for $0 < \lambda < 1$, the integration from $\xi = 0$ to $\xi = 1$ contributes nothing and can be omitted. By combination of eqns. (18) and (21), and introduction of a new current function, $\Phi(x) = \Phi'(\lambda)$, with $x = K(\lambda - 1) = \sigma(t - \tau)$, the following relationship is obtained:

$$\frac{1}{\sqrt{\pi}} \int_0^x \frac{\Phi(\xi)}{\sqrt{x-\xi}} \, d\xi = \frac{\theta_1 - \theta_2 e^{-x}}{1/\gamma + \theta_2 e^{-x}} + \frac{\theta_2 - \theta_1}{\theta_2 + 1/\gamma} . \tag{22}$$

In view of the definition of x, the current function, Φ, is a function of dimensionless potential, because

$$\sigma(t - \tau) = -(nF/Rt)(E - E_2).$$

Now we introduce the simplifying assumption that $\theta_1 = 0$ and $\gamma\theta_2 \gg 1$ (these assumptions are normal in electroanalytical theory). Putting $\theta_1 = 0$, the two fractions on the right-hand side of eqn. (22) can be combined into one fraction. This one fraction has the factor $\gamma\theta_2/(1 + \gamma\theta_2)$, which can be put equal to unity in view of the assumption that $\gamma\theta_2 \gg 1$, and eqn. (22) can be written as:

$$\frac{1}{\sqrt{\pi}} \int_0^x \frac{\Phi(\xi)}{\sqrt{x-\xi}} \, d\xi = \frac{1 - e^{-x}}{1 + \gamma\theta_2 e^{-x}} . \tag{23}$$

During the linear potential-sweep following the constant-potential electrolysis, the current, as measured from the extrapolated $t^{-\frac{1}{2}}$-current, is thus given by:

$$i = \frac{n^{\frac{3}{2}} F^{\frac{3}{2}}}{R^{\frac{1}{2}} T^{\frac{1}{2}}} AC^0 D_R^{\frac{1}{2}} v^{\frac{1}{2}} \Phi , \tag{24}$$

where Φ is a function of (dimensionless) potential only, and is independent of the parameters v and τ.

This behaviour can be compared to the direct reduction of O to R. Suppose O to be present in an initial concentration C^0 and R in an initial concentration C^0/θ_2, while, starting at time $t=0$, the potential of the electrode is linearly changed with time towards negative values: $E=E_2-vt$. Both the initial potential, E_2, and the sweep rate, v, are the same as in the case considered above. Let the flux, $q(t)$, of O and R at the electrode surface be again so defined as to be positive for the reduction process, and let the well-known Ševčik–Randles P-function[5] be defined by $P(x) = q(t)/C^0 D_0{}^{\frac{1}{2}}\sigma^{\frac{1}{2}}$, with $x=\sigma t = -(nF/RT)(E-E_2)$. Thus, Φ and P are both functions of the same independent variable, x. It is easily verified that the integral equation representation of $P(x)$ is given by:

$$\frac{1}{\sqrt{\pi}} \int_0^x \frac{P(\xi)}{\sqrt{x-\xi}}\, d\xi = \frac{1-e^{-x}}{1+\gamma\theta_2 e^{-x}} \; , \tag{25}$$

and the current is given by:

$$i = \frac{n^{\frac{3}{2}} F^{\frac{3}{2}}}{R^{\frac{1}{2}} T^{\frac{1}{2}}} A C^0 D_0{}^{\frac{1}{2}} v^{\frac{1}{2}} P \; , \tag{26}$$

where P is a function of potential only.

From eqns. (23) and (26) it follows that $\Phi(x)$ and $P(x)$ are the same functions. Thus, when measuring the current obtained during the linear-sweep re-reduction with respect to the extrapolated $t^{-\frac{1}{2}}$-current, the same peak (with respect to potential) is obtained as on reduction of a solution of O with the same concentration as the solution of R in the first case. In both cases, the peak potential, referred to $E_{\frac{1}{2}}$, is $-28.5/n$ mV (at 25°). The height of the first peak differs from that obtained in the latter case by a factor, $\sqrt{D_R/D_O}$.

When R is oxidized directly by an anodic potential sweep $(E = E_1 + vt)$, starting from the initial conditions (3) and (4), the same current peak is obtained as in the above cases, and the current is given by eqn. (24) In this case, Φ is a function of $(nF/RT)(E-E_1)$, and when it is assumed that $E_1=E_2$, the current is described by precisely the same current function, $\Phi(x)$ or $P(x)$, except for a sign reversal of the independent variable, x. The current peak is practically independent (with regard to shape and position relative to $E_{\frac{1}{2}}$) of the initial potential at which the sweep is initiated, provided this initial potential is sufficiently remote from $E_{\frac{1}{2}}$. Thus, direct linear-sweep oxidation of R to O, and the linear-sweep re-reduction of O formed by constant-potential oxidation of R, give the same current peaks, but in the latter case the peak potential is $57/n$ mV (at 25°) more cathodic.

ANALYTICAL IMPLICATIONS

The method described above can be a powerful tool for circumventing interferences when applied discriminatingly. For an excellent discussion of circumstances in which this method can be fruitfully applied, the reader is referred to the paper by YARNITSKY AND ARIEL[1], in which its application to anodic stripping voltammetry is discussed. It should be stressed, however, that this method has a wider scope than the field of anodic stripping voltammetry, and can also be applied to problems of *normal* linear potential-sweep voltammetry.

Another method of circumventing interferences caused by the presence of large amounts of foreign depolarizers consists of the recording of the di–dt curve[6-8], and this alternative possibility should also be borne in mind when coping with difficult problems of analysis.

Both methods (constant-potential electrolysis followed by potential-sweep, and derivative voltammetry) have one drawback in common, *viz.*, the difficulty in obtaining a representative base-line; for the method considered in this paper, this is discussed by YARNITSKY AND ARIEL[1], while PERONE *et al.*[6,7] treat this problem for derivative voltammetry.

CONCLUDING REMARKS

It seems that the connection between $\Phi(x)$ and $P(x)$ is valid only for the case of a reversible electrode reaction without kinetic complications. For kinetic systems it is obvious, from inspection of the various reaction schemes[9], that such a simple relationship will not exist between the corresponding Φ- and P-functions. It is equally obvious that, especially during the constant-potential electrolysis preceding the potential-sweep, convection can cause significant departures from the relationships derived above.

The theoretical calculations are valid only for semi-infinite planar diffusion. Thus, the effects of spherical diffusion at a hanging mercury-drop electrode are not taken into account. It is not yet known how spherical diffusion will affect the current–potential curve obtained during the linear potential-sweep following the constant-potential electrolysis, and this matter must await further investigation.

Another important aspect is the assumption of semi-infinite diffusion for O and R, and this assumption is probably not valid for the experiments described by YARNITSKY AND ARIEL. They used a conventional hanging mercury-drop electrode and oxidation times of 2–20 sec (at the longer oxidation times, convection can significantly influence the current–potential curves obtained during the linear potential-sweep.) Aside from the eventual influences of spherical diffusion, depletion of the mercury-drop probably plays a noticeable role in these experiments. When the mercury-drop becomes depleted of reduced metal (R) during the oxidation period, then the surface concentration of oxidized metal (O) will diminish by diffusion during the remainder of the oxidation period and during a certain period after initiation of the potential sweep. This effect will diminish the height of the subsequent reduction peak and will also affect the i_p *vs.* $v^{\frac{1}{2}}$ relationship. This aspect is under continued investigation.

SUMMARY

The method of potential-step electrolysis followed by linear potential-sweep voltammetry is considered theoretically. It is shown that, for a reversible electrode

reaction without kinetic complications, the current–potential curve obtained during the linear potential-sweep is closely connected with the Ševčik–Randles P-function of normal linear-sweep voltammetry. Analytical implications are pointed out, while the presence of kinetic complications and the effect of finite electrode volume are briefly discussed.

REFERENCES

1 CH. YARNITSKY AND M. ARIEL, *J. Electroanal. Chem.*, 10 (1965) 110.
2 W. M. SCHWARZ AND I. SHAIN, *J. Phys. Chem.*, 70 (1966) 845.
3 H. MARGENAU AND G. M. MURPHY, *The Mathematics of Physics and Chemistry*, D. van Nostrand, New York, 1956, 2nd ed. p. 525.
4 W. T. DE VRIES, *J. Electroanal. Chem.*, 9 (1965) 448.
5 P. DELAHAY, *New Instrumental Methods in Electrochemistry*, Interscience, New York, 1954, p. 118.
6 S. P. PERONE AND T. R. MUELLER, *Anal. Chem.*, 37 (1965) 2.
7 S. P. PERONE AND J. R. BIRK, *ibid.*, 37 (1965) 9.
8 S. P. PERONE AND C. V. EVINS, *ibid.*, 37 (1965) 1643.
9 R. S. NICHOLSON AND I. SHAIN, *ibid.*, 36 (1964) 711.

CURRENT–TIME CURVES AT THE DROPPING MERCURY ELECTRODE, CALCULATED FOR INTERACTIONS BETWEEN AN ADSORBED SPECIES AND THE REDUCED FORM OF THE DEPOLARIZER

LILIANA RAMPAZZO

Istituto di Chimica, Facoltà di Ingegneria, Roma (Italy)

A recent paper on polarographic current–time curves[1] reports the study of the effect of a specific interaction between the depolarizer (Ox), and an adsorbed species (A) present in a layer of finite thickness around the electrode. Species Ox and A are involved in the following processes: $Ox + ne \rightleftarrows Red$ at the electrode and $Ox + A \rightarrow OxA$ in the layer $0 < x < l$.

In the present work we deal with the case of an interaction, localized in layer, l, between the reduced form, Red, and the species, A, according to the electrode reaction: $Ox + ne \rightleftarrows Red$, and the reaction $Red + A \rightarrow B$ (where Ox is the oxidized, Red the reduced form of the depolarizer, and B the product). We suppose that B is not electrochemically active and not adsorbed at the potentials used.

The main features of this theoretical model is that the interaction is operating in a solution layer of finite thickness ($0 < x < l$) and that for $x > l$ no detectable interactions are present*. The concentration, C_A, of adsorbed species A, is assumed to be in excess with respect to the concentration of the reduced form, Red, and the diffusion coefficients of Ox and Red are assumed to have the same value in the whole solution.

The rate of the kinetic process described above is: $v = KC_{red}$ ($0 < x < l$) and $v = 0$ ($x > l$), where $K = K'C_A$. According to the plane and linear approximation, the conditions governing the concentration distributions $C(x,t)$, may be expressed by:

$$\frac{\partial C_{red}}{\partial t} = D \frac{\partial^2 C_{red}}{\partial x^2} - KC_{red} \qquad 0 < x < l \tag{1}$$

$$C_{red}(x,0) = 0 \tag{2}$$

$$C_{ox}(0,t) = rC_{red}(0,t) \qquad [r = \exp\{(nF/RT)(E-E_n)\}] \tag{3}$$

$$\frac{\partial C_{1red}}{\partial t} = D \frac{\partial^2 C_{1red}}{\partial x^2} \qquad x > l \tag{4}$$

$$C_{1red}(x,0) = 0 \tag{5}$$

$$\lim_{x \to \infty} C_{1red}(x,0) = 0 \tag{6}$$

---

* The layer l may be a multilayer, composed of several layers of adsorbed species, as for instance in the adsorption of polyelectrolytes at the dropping mercury electrode.

$$C_{red}(l,t) = C_{1red}(l,t) \tag{7}$$

$$\left(\frac{\partial C_{red}}{\partial x}\right)_{x=l} = \left(\frac{\partial C_{1red}}{\partial x}\right)_{x=l} \tag{8}$$

$$\frac{\partial C_{ox}}{\partial t} = D\frac{\partial^2 C_{ox}}{\partial x^2} \qquad x > 0 \tag{1'}$$

$$C_{ox}(x,0) = C_{ox}* \tag{2'}$$

$$\lim_{x\to\infty} C_{ox}(x,t) = C_{ox}* \tag{3'}$$

$$\left(\frac{\partial C_{ox}}{\partial x}\right)_{x=0} + \left(\frac{\partial C_{red}}{\partial x}\right)_{x=0} = 0 , \tag{4'}$$

where $C_{red}(x,t)$, $C_{1red}(x,t)$ are the concentration of the reduced species, Red, in $0 < x < l$ and in $x > l$, respectively, $C_{ox}(x,t)$ is the concentration of the oxidized form Ox, $C_{ox}*$ the concentration of the species Ox in the bulk of the solution, and D the diffusion coefficient of species Ox and Red.
By putting:

$$\varphi(t) = -D\left(\frac{\partial C_{red}}{\partial x}\right)_{x=0} ; \quad \mathscr{L}\{\varphi(t)\} = \bar{\varphi}(p)$$

($\mathscr{L}$ is the Laplace-transform operator), we get the expression★:

$$\varphi(p) = C_{ox}*\sqrt{D}\,\frac{1}{1+r\sqrt{p}}\,\frac{1}{\sqrt{p}} \times$$

$$\frac{\sqrt{p}\sqrt{p+K}\cosh\sqrt{\dfrac{p+K}{D}}\,l + p\sinh\sqrt{\dfrac{p+K}{D}}\,l + K\sinh\sqrt{\dfrac{p+K}{D}}\,l}{\sqrt{p}\sqrt{p+K}\cosh\sqrt{\dfrac{p+K}{D}}\,l + p\sinh\sqrt{\dfrac{p+K}{D}}\,l + \dfrac{K}{1+r}\sinh\sqrt{\dfrac{p+K}{D}}\,l} \tag{9}$$

If: $K \ll (r+1)p \qquad \vartheta = Kt$ \hfill (10)

★ In fact, the diffusion coefficients in the adsorbed layer and in the solution cannot be of the same value. The assumption of the equality of diffusion coefficients is a first approximation, for sake of simplicity and ease of calculation. The Laplace-transform of the flux is:

$$\bar{\varphi}(p) = \sqrt{D}C_{ox}*\frac{\sqrt{p+K}}{\sqrt{p}}\,\frac{\{\exp(q*l) - \varepsilon\exp(-q*l)\}\{a\exp(q'l) + b\exp(-q'l)\}}{\varepsilon[bc\exp\{(q'+q*)l\}ad\exp\{(q'-q)l\}] + ac\exp\{(q*+q')l\} - bd\exp\{(q*-q')l\}}$$

where: $a = \sqrt{p} + \gamma\sqrt{p+K}$; $b = \sqrt{p} - \gamma\sqrt{p+K}$; $c = r\sqrt{p} + f\sqrt{p+K}$; $d = r\sqrt{p} - f\sqrt{p+K}$;

$q* = \sqrt{p/D*}$; $q' = \sqrt{(p+K)/D}$;

D, D_1 are diffusion coefficients of Red in the layer l and solution, respectively; $D*$, D_1* are diffusion coefficients of Ox;

$$\gamma = \sqrt{D/D_1}; \gamma* = \sqrt{D*/D_1*}; f = \sqrt{D/D*}; \varepsilon = (1 - \gamma*)/(1 + \gamma*)$$

which is a very involved expression. If $D = D_1 = D* = D_1*$ we obtain eqn. (9).

$$(r>0) \qquad\qquad \lambda = \sqrt{K/D}\, l \tag{11}$$

$$g(\vartheta) = \frac{\varphi(\vartheta/K)(1+r)}{C^*\sqrt{KD}} \tag{12}$$

then

$$\bar{g}(p) = \frac{1}{\sqrt{p}} + \frac{1}{p}\frac{1}{\sqrt{p+1}}\frac{\mathrm{Sh}\,\lambda\sqrt{p+1}}{\mathrm{Ch}\,\lambda\sqrt{p+1} + \sqrt{p}\,\mathrm{Sh}\,\lambda\sqrt{p+1}}. \tag{13}$$

By adopting a method similar to that employed in ref. 1 (*cf.* appendix) for the calculations of the inverse transform of (13), we obtain:

$$g(\vartheta) = \frac{1}{\sqrt{\pi\vartheta}} - \frac{2}{\pi}\left\{\int_0^1 \frac{\mathrm{Sh}^2\lambda\sqrt{1-u^2}}{\mathrm{Ch}^2\lambda\sqrt{1-u^2} - u^2}\exp(-\vartheta u^2)\,\mathrm{d}u + \right.$$

$$\left. \int_1^\infty \frac{\sin^2\lambda\sqrt{u^2-1}}{u^2 - \cos^2\lambda\sqrt{u^2-1}}\exp(-\vartheta u^2)\,\mathrm{d}u\right\} + \mathrm{Th}\lambda \tag{14}$$

where $p = -u^2$. \tag{15}

The current $i(t)$ is derived by multiplying $\varphi(t)$ by the area of the drop, proportional to $t^{\frac{2}{3}}$. Thus, taking in account eqn. (12) we have:

$$i(t) = at^{\frac{2}{3}}\varphi(t) = at^{\frac{2}{3}}\frac{C_{\mathrm{ox}}^*}{1+r}\sqrt{KD}\,g(\vartheta) \tag{16}$$

(a = constant, depending on the characteristics of the capillary and units), with $g(\vartheta)$ given by eqn. (14).

Equation (16) can be put in the following way:

$$i = \frac{a\sqrt{D}C^*}{\sqrt{\pi}K^{\frac{1}{2}}(1+r)}g_1(\vartheta) \tag{17}$$

with

$$g_1(\vartheta) = \sqrt{\pi}\vartheta^{\frac{2}{3}}\,g(\vartheta) \tag{18}$$

Therefore from (14–18) it follows that:

$$g_1(\vartheta) = \vartheta^{\frac{1}{2}} + \sqrt{\pi}\vartheta^{\frac{2}{3}}\mathrm{Th}\lambda - \frac{2}{\sqrt{\pi}}\vartheta^{\frac{2}{3}}\left[\int_0^1 \frac{\mathrm{Sh}^2\lambda\sqrt{1-u^2}}{\mathrm{Ch}^2\lambda\sqrt{1-u^2} - u^2}\exp(-\vartheta u^2)\,\mathrm{d}u + \right.$$

$$\left. \int_1^{+\infty} \frac{\sin^2\lambda\sqrt{u^2-1}}{u^2 - \cos^2\lambda\sqrt{u^2-1}}\exp(-\vartheta u^2)\,\mathrm{d}u\right] \tag{19}$$

In Fig. 1, function $g_1(\vartheta)$ is plotted against ϑ (on semilogarithmic paper) for various values of the parameter, λ. This figure shows the change of current with time, on varying the thickness of the interaction layer, l; K and the remaining quantities being kept constant. For $\lambda = 0$, the curve gives the polarographic current in absence of interactions; on increasing the thickness of layer, l, the current is enhanced. An important feature of these graphs is that the percentage increase of the current grows faster when λ is small. Similarly, Fig. 2 shows the functions:

$$f(\tau) = \frac{\sqrt{\pi}\,(1+r)}{aC^* D^{\frac{1}{3}} l^{\frac{1}{3}}}\, i \qquad (20)$$

where $\tau = Dt/l^2$. Function $f(\tau)$ can easily be obtained noting that: $f(\tau) = \lambda^{-\frac{1}{3}} g_1(\lambda^2 \tau)$ hence:

$$f(\tau) = \tau^{\frac{1}{3}} \left\{ 1 + \sqrt{\pi\tau}\,\lambda\,\mathrm{Th}\lambda - 2\lambda\sqrt{\frac{\tau}{\pi}} \left[\int_0^1 \frac{\mathrm{Sh}^2\lambda\sqrt{1-u^2}}{\mathrm{Ch}^2\lambda\sqrt{1-u^2} - u^2} \exp(-\lambda^2\tau u^2)\,\mathrm{d}u \;+ \right. \right.$$

$$\left. \left. \int_1^\infty \frac{\sin^2\lambda\sqrt{u^2-1}}{u^2 - \cos^2\lambda\sqrt{u^2-1}} \exp(-\lambda^2\tau u^2)\,\mathrm{d}u \right] \right\} \qquad (21)$$
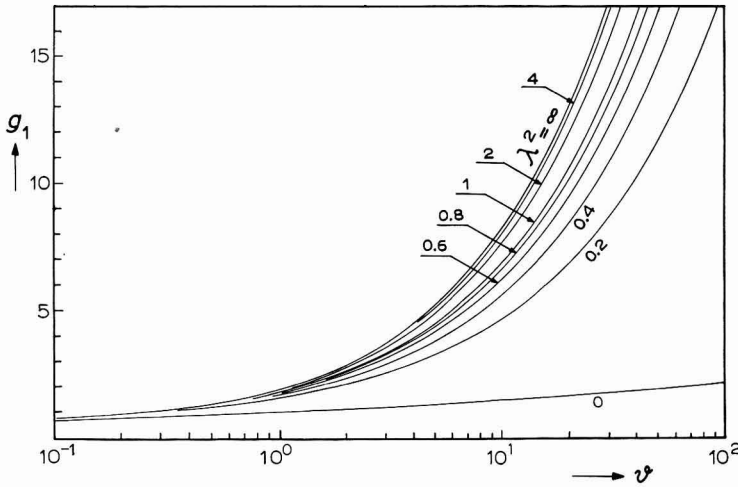
Fig. 1. The function $g_1(\vartheta)$ defined in eqn. (19). The numbers on the curves are values of $\lambda^2 = (K/D)l^2$.
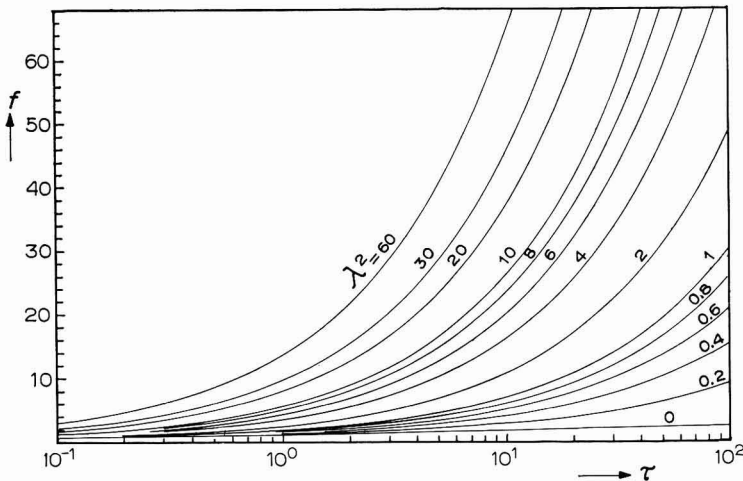
Fig. 2. The function $f(\tau)$ defined in eqn. (21). The numbers on the curves are values of $\lambda^2 = (K/D)l^2$.

The effect of an increase in constant K, can be clearly observed in Fig. 2). Numerical calculations in Figs. 1 and 2 have been performed by an Electronic Computer (FINAC) of "Istituto per le Applicazioni del Calcolo C.N.R. Roma".

DISCUSSION

From eqn. (17) or (20) it follows that the current is proportional to the analytical concentration of species Ox, and depends (through the constant a) on the characteristics of the capillary. For small values of ϑ the function $g_1(\vartheta)$ is expressed roughly by its first term, while for large values of ϑ, $g_1(\vartheta)$ can be approximated to $\vartheta^{\frac{1}{2}}/\mathrm{Ch}^2\lambda$ for small values of λ, and to $\sqrt{\pi}\vartheta^{\frac{3}{2}}$ for large values of λ.

The enhancement of current $i(t)$, promoted by interaction between the reduced form and a species present in excess at the interface, leads to a consequent increase of the current, with respect to that controlled by diffusion. Such an increase could take the shape of a maximum, if the thickness of layer l is potential-dependent in the range of the limiting current.

This theory suggests a simple way for treating experimental data, of the reduction of oxygen in the presence of substances (adsorbed on the electrode) that are known to interact with the reduced form of the depolarizer. Experiments in order to verify eqn. (19) are in progress in this laboratory*.

APPENDIX

In order to calculate the inverse transform of the function:

$$\bar{g}(p) = \frac{1}{\sqrt{p}} + \frac{1}{p}\frac{\mathrm{Sh}\,\lambda\sqrt{p+1}}{\sqrt{p+1}\,\mathrm{Ch}\,\lambda\sqrt{p+1} + \sqrt{p}\,\mathrm{Sh}\lambda\sqrt{p+1}} \tag{A1}$$

it is possible to write

$$\bar{h}(p) = \frac{1}{p}\frac{\mathrm{Sh}\,\lambda\sqrt{p+1}}{\sqrt{p+1}\,\mathrm{Ch}\,\lambda\sqrt{p+1} + \sqrt{p}\,\mathrm{Sh}\lambda\sqrt{p+1}} \tag{A2}$$

and since

$$\mathscr{L}^{-1}\{\bar{h}(p)\} = h(\vartheta) \tag{A3}$$

---

* The Laplace-transform of the flux $\varphi(t)$ (eqn. (9)) can be written:

$$\bar{\varphi}(p) = C_{\text{ox}}{}^{*}\sqrt{D}\cdot\frac{1}{\sqrt{p}}\frac{\sqrt{p+K}}{r\sqrt{p}\,\dfrac{\sqrt{p+K}+\sqrt{p}\,\mathrm{tgh}\sqrt{p+K/D}\cdot l}{\sqrt{p}+\sqrt{p+K}\,\mathrm{tgh}\sqrt{p+K/D'}\cdot l} + \sqrt{p+K}}$$

This for, $l \to \infty$, approaches:

$$\lim_{l\to\infty}\bar{\varphi}(p) = C_{\text{ox}}{}^{*}\sqrt{D}\,\frac{1}{\sqrt{p}}\frac{\sqrt{p+K}}{r\sqrt{p}+\sqrt{p+K}}$$

i.e., the same expression presented by KERN[2] for the case of a chemical reaction subsequent to the electron-transfer process.

$$g(\vartheta) = \mathscr{L}^{-1}\{\bar{g}(p)\} = \frac{1}{\sqrt{\pi\vartheta}} + \frac{1}{2\pi i}\int_L e^{p\vartheta}\bar{h}(p)\,dp \tag{A4}$$

where L is a straight line $R_e(p) = $ constant > 0.
For $\vartheta > 0$ and changing the integration part as in ref. 1 we have:

$$h(\vartheta) = \frac{1}{2\pi i}\int_{R^- + R^+} e^{p\vartheta}\bar{h}(p)\,dp + \text{Th}\lambda \tag{A5}$$

If we put

$$\alpha(p) = -\frac{\text{Sh}^2\lambda\sqrt{p+1}}{\text{Ch}^2\lambda\sqrt{p+1} + p} \tag{A6}$$

$$\beta(p) = \sqrt{p+1}\,\frac{\text{Ch}\,\lambda\sqrt{p+1}\,\text{Sh}\,\lambda\sqrt{p+1}}{\text{Ch}^2\lambda\sqrt{p+1} + p} \tag{A7}$$

we obtain:

$$h(\vartheta) = \frac{1}{\pi i}\int_{R^+} e^{p\vartheta}\frac{1}{\sqrt{p}}\alpha(p)\,dp + \text{Th}\lambda \tag{A8}$$

leading to

$$g(\vartheta) = \frac{1}{\sqrt{\pi\vartheta}} + \frac{1}{\pi i}\int_{R^+} e^{p\vartheta}\frac{1}{\sqrt{p}}\alpha(p)\,dp + \text{Th}\lambda \tag{A9}$$

and to (where $p = -u^2$)

$$g(\vartheta) = \frac{1}{\sqrt{\pi\vartheta}} + \text{Th}\lambda - \frac{2}{\pi}\left\{\int_0^1 \frac{\text{Sh}^2\lambda\sqrt{1-u^2}}{\text{Ch}^2\lambda\sqrt{1-u^2} - u^2}\exp(-\vartheta u^2)\,du + \right.$$

$$\left. \int_1^\infty \frac{\sin^2\lambda\sqrt{u^2-1}}{u^2 - \cos^2\lambda\sqrt{u^2-1}}\exp(-\vartheta u^2)\,du\right\} \tag{A10}$$

which is the (14) in the text.

SUMMARY

A quantitative theoretical approach is reported for the calculation of polarographic current–time curves. The case of a specific interaction between the reduced form of the electrically active species, and a substance present in excess at the electrode is considered. The main assumptions are: (1) the interaction is localized in a layer of finite thickness $(0 < x < l)$; (2) the product of the interaction is neither reducible nor adsorbed. The mathematical solution shows that the shape of the i–t curves depends on the values of the parameter, $\lambda = \sqrt{K/D}\,l$, the current being enhanced with respect to that controlled only by diffusion.

REFERENCES

1 P. SILVESTRONI AND L. RAMPAZZO, *J. Electroanal. Chem.*, 7 (1964) 73.
2 D. KERN, *J. Am. Chem. Soc.*, 76 (1954) 1011.

ELECTROANALYTICAL CHEMISTRY AND INTERFACIAL ELECTROCHEMISTRY
Elsevier Publishing Company, Amsterdam – Printed in The Netherlands

89

REVIEW

ELECTROCHEMISTRY IN DIMETHYL SULFOXIDE

JAMES N. BUTLER

Tyco Laboratories, Inc., Waltham, Mass. 02154 (U.S.A.)

(Received May 14th, 1966)

INTRODUCTION

Dimethyl sulfoxide (DMSO) is an excellent solvent for inorganic and organic materials; it is resistant to oxidation and reduction, and has a high dielectric constant. Although relatively few electrochemical investigations using this solvent have been made, it shows promise of being one of the most important electrochemical media. This paper is an attempt to compile a comprehensive, critical review of the literature on electrochemistry in DMSO available at the beginning of 1966.

In Table 1 are given values for a number of the physical properties of DMSO that are relevant to electrochemical investigations. Table 2 gives the solubilities of a number of salts in DMSO at room temperature. The most reliable work is that of KENTTÄMAA[26] and MELENDRES[30]. The solubility of most salts increases slightly with increasing temperature[1,26], but relatively little accurate solubility data is available. Hydrated salts are often quite soluble in DMSO[1], but they have not been included in Table 2 because their solubility is usually strongly dependent upon water concentration. For anhydrous salts, some qualitative rules of solubility are: perchlorates, nitrates, halides, and quaternary ammonium salts are soluble; fluorides, sulfates and carbonates are not. Of the alkali-metal salts, lithium salts are the most soluble, and potassium salts the least soluble. Covalent compounds, particularly mercuric halides, are highly soluble. Most univalent electrolytes in dilute solutions are completely dissociated[2], but DMSO acts as a Lewis base in forming co-ordination compounds with transition metals[1], and thus complex ions in solution are often quite stable.

The self-ionization of DMSO probably proceeds according to the reaction:

$$2\,(CH_3)_2\,SO \;\rightleftharpoons\; (CH_3)_2\,SOH^+ + CH_3SOCH_2^-$$
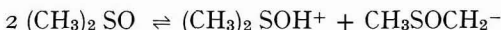
The equilibrium constant (ion product) for this reaction has been measured[23,31] to be $5 \cdot 10^{-18}$ at 25°. The conductivity of pure DMSO is consistent with this value and is probably between $2 \cdot 10^{-8}$ and $3 \cdot 10^{-8}$ $\Omega^{-1}cm^{-1}$ [2,19-21] although values over a hundred times larger have been reported[1,28,32].

The conjugate base of DMSO, methylsulfinyl carbanion, is formed[33] by reaction of DMSO with sodium hydride or amide at 65–70° under nitrogen:

$$NaH + CH_3\!\!-\!\!\overset{\displaystyle O}{\overset{\displaystyle \|}{S}}\!\!-\!\!CH_3 \rightarrow Na^+ + CH_3\!\!-\!\!\overset{\displaystyle O}{\underset{\displaystyle CH_2}{S}}{}^- + H_2$$
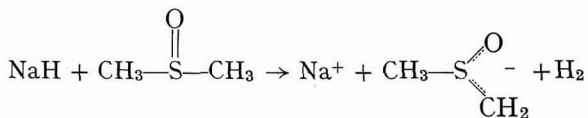
TABLE 1

PROPERTIES OF DIMETHYL SULFOXIDE

Property	Value	Temp.(°C)	Ref.
Molecular weight	78.13		
Boiling point at 760 mm	189°		1,2
Vapor pressure	0.417 mm	20	1,3
	0.600	25	
	1.66	40	
	5.0	60	
	14.3	80	
	23.6	100	
Heat of vaporization	12.64 kcal/mole	25	3
	10.3	189	
Melting point	18.55°		4,5,19
	18.5°		6
	18.42° (?)		3
	18.4° (?)		2,7,8
Heat of fusion	38.8 cal g^{-1}	18.5	9
	20 (?)	18.5	1
	42.7 (?)		10
Entropy of fusion	10.4 cal deg^{-1} $mole^{-1}$		9
	11.4		10
Cryoscopic constant	4.36° (molal)		9
	4.40°		4
	3.96° (M)		7
Heat of combustion	47.2 kcal $mole^{-1}$	25	1
	59.0	18	6
Heat of formation	$-$ 46.9 kcal $mole^{-1}$	25	1
	$-$ 49.99	25 (gas)	11
	$-$ 47.7	18 (liquid)	6
Free energy of formation	$-$ 27.65 kcal $mole^{-1}$	25 (gas)	11
Specific heat	0.47 $\pm$ 0.015 cal g^{-1} deg^{-1}	29.4	1
	0.48 $\pm$ 0.02	96.0	1
	0.52 $\pm$ 0.03	149	1
Specific gravity	1.1014	20	1
	1.098	20	12
	1.096	25	2
	1.100	25	14
	1.0956	25	13,82
	1.0946	25	12
	1.0721	50	12
Coefficient of expansion	$8.8 \cdot 10^{-4}$ deg^{-1}	25	1,19
	$9.90 \cdot 10^{-4}$	30–60	12
Refractive index	1.4783	20	1,19
	1.4773	25	15
	1.4765	25	82
	1.4768	25	13
	1.4742	30	19

TABLE 1 *(continued)*

Property	Value	Temp.(°C)	Ref.
Dielectric constant	48.9	20	1,19
	47.6 at 0.15 Mc	23	16
	46.4 at 8.0 Mc	23	16
	46.4	25	15
	46.6	25	2
	46.7	25	17
Dipole moment	3.9 ± 0.1 D		18
Conductivity	$3 \cdot 10^{-8}\ \Omega^{-1}cm^{-1}$	20	19
	$3 \cdot 10^{-8}$	25	2
	$2 \cdot 10^{-8}$	25	20,21
Viscosity	1.93 cP	25	5
	1.96	25	2
	1.98	25	1
	1.99	25	13
	2.003	25	82
	2.47	20	4
Surface tension	46.2 dyn/cm	20	4
	43.54	20	12
	42.85	25	1,12
	40.35	50	1
	40.05	50	12
	31.6	140	1

The reaction is complete in less than an hour, and solutions of the carbanion containing concentrations up to 3 M can be prepared[34]. The carbanion appears to be a stronger base than is suggested by the ion-product value given above[83].

PURIFICATION OF DMSO

DMSO of low conductivity ($3 \cdot 10^{-8}\ \Omega^{-1}cm^{-1}$) has been obtained by refluxing 99.9% material for several hours with CaO, and then fractionating repeatedly at 5-mm pressure[2]. A conductivity of $2 \cdot 10^{-8}\ \Omega^{-1}cm^{-1}$, with a water content (by Karl Fisher titration) of less than 100 p.p.m., was obtained by shaking DMSO overnight with freshly-heated and cooled chromatographic-grade alumina and repeatedly fractionating it at 2–3 mm pressure. CaO and BaO have been used as drying agents but are reported to cause decomposition of DMSO during distillation if not separated from the liquid before heating[21].

The removal of water from DMSO without distillation was attempted using CaO–MgO, or lithium powder[32]. Either treatment reduced the water content of commercial DMSO from approximately 100 p.p.m. to less than 15 p.p.m. (as determined by Karl Fisher titration). The conductivity did not change on dehydration but was considerably higher ($2 \cdot 10^{-6}\ \Omega^{-1}cm^{-1}$) than that of material purified by repeated fractionation. The results of this investigation are summarized in Table 3.

Treatment of DMSO with strongly basic reagents removes both water and dimethyl sulfide, an important impurity[91]. DMSO heated over NaOH for 2 h at 90° and then flash-distilled under vacuum had a water content of less than 0.01%, but no

J. N. BUTLER

TABLE 2

SOLUBILITY OF ANHYDROUS SALTS IN DIMETHYL SULFOXIDE AT 25°

Salt	Solubility	Ref.	Salt	Solubility	Ref.
$AlCl_3$	1.5 M (?)	22	$MgCl_2$	0.143 m	30
	0.05 m (decomp)	30	$Hg(COOCH_3)_2$	3.1 M	1
NH_4COOCH_3	>0.1 M	23	$HgBr_2$	2.5 M	1
NH_4Cl	<0.2 M	1	$Hg(CN)_2$	sol.	25
$(NH_4)_2CrO_4$	0.06 M	1	HgI_2	2.2 M	1
$(NH_4)_2Cr_2O_7$	2.0 M	1	$Ni(CN)_2$	insol.	25
NH_4PF_6	3 M	24	$KNi(CN)_3$	sol.	25
NH_4NO_3	10.0 M	1	$NiCl_2$	sol.	27
NH_4ClO_4	>0.1 M	23	NiF_2	insol.	27
NH_4SCN	3.9 M	1	KBr	0.50 m	26
$SbCl_3$	2.63 m	30	K_2CO_3	insol.	26
$BaCl_2$	0.287 m	30	KCl	0.27 m (?)	26
$Ba(NO_3)_2$	0.04 M	1		0.0225 m	30
$BiCl_3$	0.03 M	1		0.0280 M	81
$CdCl_2$	1.1 M	1	KCN	insol.	25
	2.81 m	30	KF	insol.	26
$Cd(CN)_2$	sol.	25	KPF_6	2.50 M	8
CdI_2	0.8 M	1	KOH	0.001 M (decomp.)	23
$CaCl_2$	1 M	23	KI	2.5 m	26
	4.87 m	30		1.2 M	1
	insol. (?)	1	KNO_3	1.0 m (decomp.)	26
$Ca(NO_3)_2$	1.13 m	30	KNO_2	0.23 M	1
$CeCl_3$	0.0713 M	41	$KClO_4$	2.5 m	26
$CeNH_4(NO_3)_5$	0.02 M	1	K_2SO_4	insol.	26
$CsCl$	0.0373 m	30	$KSCN$	2.0 M	1
$CrCl_3$	0.000447 m	30		17.0 M	28
$Co(CN)_2$	insol.	25	$RbCl$	0.0356 m	30
$KCo(CN)_3$	sol.	25	$KAg(CN)_2$	sol.	25
$CuBr_2$	0.045 M	1	$AgCl$	$8 \cdot 10^{-5}$ M	84
$CuCl_2$	0.206 M (?)	22	$AgBr$	$5 \cdot 10^{-5}$ M	84
	1.23 m	30	AgI	$2.4 \cdot 10^{-5}$ M	84
CuF_2	0.0049 M	22	$AgNO_3$	7.7 M	1
$CuCN$	insol.	25	$NaCOOCH_3$	0.0078 M	23
$KCu(CN)_2$	sol.	25	$NaCOOC_6H_5$	0.012 M	23
CuI	0.053 M	1	$NaHSO_4$	>0.1 M	23
$FeCl_3$	0.272 m	30	$NaBr$	0.55 m	26
$AuCl$	0.16 M	1	Na_2CO_3	insol.	26
$InBr_3$	0.210 m	30	$NaCl$	0.08 m	26
$InCl_3$	0.069 m	30		0.078 m	30
$In(NO_3)_3$	0.124 m	30		0.045 M	23
$PbCl_2$	0.36 M	1	$NaCN$	insol.	25
	0.547 m	30	NaF	insol.	26
$Pb(NO_3)_2$	0.6 M	1	$NaSbF_6$	1.5 M	24
$LiCOOCH_3$	0.0071 M	23	$NaPF_6$	1.36 M	20
$LiBr$	3.3 m	26	$NaOH$	0.0001 M (decomp.)	23
Li_2CO_3	insol.	26	NaI	1.0 m	26
$LiCl$	2.59 M	5		1.039 M	81
	2.13 m	30		2.0 M	1
	2.2 m	26	$NaOCH_3$	0.001 M	23
LiF	0.019 M	22	$NaNO_3$	2.4 M	1
LiI	2.8 m	26		4.6 m (decomp.)	26
	1.22 m	30	$NaNO_2$	0.15 M	1
$LiNO_3$	4.4 m (decomp.)	26	$NaClO_4$	1.8 m	26
	1.5 M	1	Na_2SO_4	0.001 M	23,26
$LiClO_4$	2.7 m	26	$NaSCN$	0.12 M	1
	2.65 m	30	$SrCl_2$	0.941 m	30
	2.35 M	22	Bu_4NI	>0.1 M	23
Li_2SO_4	insol.	26	Et_4NBr	<0.1 M	23

TABLE 2 (continued)

Salt	Solubility	Ref.	Salt	Solubility	Ref.
Et$_4$NClO$_4$	1 M	23	VCl$_3$	0.0133 m	30
Me$_4$NBr	<0.1 M	23	ZnCl$_2$	2.2 M	1
Me$_4$NI	>0.1 M	23		1.64 m	30
TlCl	0.0007 M	29	Zn(CN)$_2$	insol.	25
WCl$_6$	0.13 M	1	KZn(CN)$_3$	sol.	25
VCl$_2$	0.0147 m	30			

Note: Temp. dependence of solubility has been measured by KENTTÄMAA[26], and solubility in satd. LiCl solns. has been measured by MELENDRES[30]. See Table 8.

Bu = n-butyl, Et = ethyl, Me = methyl

TABLE 3

PURIFICATION OF DMSO WITHOUT DISTILLATION[32]

Solution	H$_2$O (p.p.m.)	Conductivity ($\Omega^{-1}cm^{-1} \cdot 10^6$)
DMSO (Crown-Zellerbach) as received	75	2.5
DMSO (Fisher) as received	150	1.7
DMSO (Fisher) treated with CaO–MgO	< 15	1.4
DMSO (Fisher) treated with Li powder (appeared yellow)	< 15	2.2

analysis for organic impurities was reported[50,91]. Calcium hydride has also been used to treat DMSO prior to fractional distillation, and is perhaps the most convenient reagent[33,34,37,91]. The sodium salt of methyl sulfinylcarbanion can also be used to remove acidic impurities prior to acid–base titrations[33,34,92].

A simple procedure recommended for purification was to pass the commercial reagent-grade material through a column of molecular sieve (Linde 5A), which reduces the water content to less than 0.02%[35,36]. However, DMSO dried over molecular sieve and vacuum distilled was reported to have a conductance of 3.4×10^{-7}, which is high[24].

The purification of DMSO by distillation has been studied, using gas chromatography for the analysis. From a column containing 10% Carbowax K1450 on No. 6-mesh Teflon powder, a well-shaped water peak was obtained. Two components besides DMSO, the second of which was water, were found under temperature programming. When the areas of the chromatogram peaks were used as a measure of the mixture composition by weight, the results shown in Table 4 were obtained. Little purification was obtained by fractional distillation[35].

The necessity of manipulating DMSO solutions in a dry, inert atmosphere was demonstrated by exposing a solution containing 0.46 M LiBr in dry, distilled DMSO to a water-saturated atmosphere. The results are shown in Table 5[36].

Except for water removal, purification of the best commercial grades of DMSO is not normally necessary for electrochemical studies. For example, the

TABLE 4

PURIFICATION OF DMSO BY DISTILLATION[35]

Vol. Distilled (ml)	Distillation pressure (mm)	Temp. (°C)	Reflux ratio	Peaks 1 and 2 (wt%)
As received	—	—	—	0.21
64	3–4	56–60	9:1	0.08
150	3–4	62	9:1	0.65
600	3	60–62	1:1	0.15
Dried with 5A molecular sieve	—	—	—	<0.002

TABLE 5

ABSORPTION OF WATER BY DMSO SOLUTIONS[36]

Pretreatment	Electrolyte	Water[a] (%)
None	None	0.018
Dried and distilled	0.46 M LiBr	0.064
Dried and distilled; exposed to water-satd. air for 24 h	0.46 M LiBr	1.7

[a] by Karl-Fisher titration

residual currents, observed in commercial C.P. grade DMSO were 20 times smaller than in acetonitrile of the best commercial purity that had been further purified by distillation from P_2O_5 and CaH_2[37].

CONDUCTANCE STUDIES

SEARS, LESTER AND DAWSON[2] measured the conductance of nineteen salts in dilute ($< 10^{-2} M$) DMSO solutions. The equivalent conductance values, Λ, were fitted to the Onsager equation:

$$\Lambda_0' = \frac{\Lambda + 35.7\sqrt{C}}{1 - 0.502\sqrt{C}} = \Lambda_0 + BC$$

Plots of Λ_0' vs. concentration, C, were linear in the range below $10^{-2} M$. The values of the constants, Λ_0 and B, obtained are given in Table 6. The Kohlrausch law of independent migration was verified by combining the values of Λ_0 for various salts. This, together with the excellent fit to the Onsager equation, indicated that all the salts listed in Table 6 are completely dissociated in DMSO at concentrations below $10^{-2} M$. The temperature dependence of conductance in dilute solutions has been measured for three salts, and the values of Λ_0 obtained are listed[19] in Table 6.

Ionic mobility values (Table 7) were calculated taking the limiting conductances of the two largest ions (n-octadecyltrimethylammonium, and n-octadecyl sulfate) to be equal. Included in Table 7 is also a value for the mobility of solvated hydrogen ion in DMSO, obtained from a polarographic diffusion coefficient[21]. The large variation in cation mobility compared to anion mobility indicates that anions are only slightly solvated in DMSO, if at all. The measurements of Λ in KCl[19] may be in

TABLE 6

LIMITING EQUIVALENT CONDUCTANCES AND ONSAGER SLOPES IN DMSO

Measurements at 25°			Temp. dependence[c]		
Salt	Λ_0	B	Salt	Temp. (°C)	Λ_0
LiCl[a]	35.3	—	KCl	20	49.2
LiBr[a]	35.2	—	(see text)	40	68.0
NaCl[a]	37.3	—		60	91.6
NaBr	38.0	60		80	119.0
NaI	37.6	100	KPi	20	31.3
NaSCN	43.0	65		40	43.6
NaNO$_3$	40.8	−95		60	57.7
NaClO$_4$	38.3	145		80	72.2
NaPi	31.1	55	Bu$_4$NPi	20	25.3
NaSO$_3$Ph	30.6	8		40	37.7
KBr	38.5	90		60	55.5
KI	38.2	90		80	63.1
KSCN	43.5	100			
KNO$_3$	41.5	−80			
KClO$_4$	39.1	115			
KPi	31.7	90			
KOctdSO$_4$	24.5	110			
Bu$_4$NI	35.0	80			
Me$_3$PhNI	37.9	50			
Me$_3$PhNSO$_3$Ph	30.9	8			
Me$_3$OctdNNO$_3$	37.0	90			
Me$_3$OctdNI	33.8	150			
HCl[b]	42.2 (?)	—			

[a] Ref. 5. [b] Ref. 23, 30°. [c] Ref. 19. All other data from Ref. 2. Pi = picrate, Ph = phenyl, Octd = n-octadecyl, Bu = n-butyl, Me = methyl.

TABLE 7

IONIC MOBILITIES IN DMSO AT 25°

Cation	Λ_0^+	Anion	Λ_0^-
H$^+$[a]	18.3 (?)	SCN$^-$	29.2
H$^+$[b]	17	NO$_3^-$	27.0
K$^+$	14.4	ClO$_4^-$	24.6
Me$_3$PhN$^+$	14.1	Br$^-$	24.2
Na$^+$	13.8	Cl$^-$	23.9
Li$^+$[c]	11.4	I$^-$	23.8
Bu$_4$N$^+$	11.2	Pi$^-$	17.3
Me$_3$OctdN$^+$	10.0	PhSO$_3^-$	16.8
		OctdSO$_4^-$	10.0

[a] Ref. 23, 30° [b] Ref. 21, 30°. [c] Ref. 5. All other data from ref. 2.

error, since the concentration dependence does not fit the Onsager equation, and the experimental value of Λ_0 is nearly 50, compared to a value of 38.3 calculated from the mobilities in Table 7.

The limiting conductances of the salts listed in Table 6 parallel the values observed in dimethyl formamide[38,39] and pyridine[40]: the values in DMF are approximately 2.14 times as large as in DMSO, while the values in pyridine are approximately

2.03 times as large. These gross differences are probably due, primarily, to the higher viscosity of DMSO.

The conductance values of LiCl[5,22], LiClO$_4$[22], NaPF$_6$[20], KPF$_6$[8], and KCNS[28] have been measured in relatively concentrated solutions; the results are summarized in Fig. 1. The conductance of all these salts goes through a maximum value at
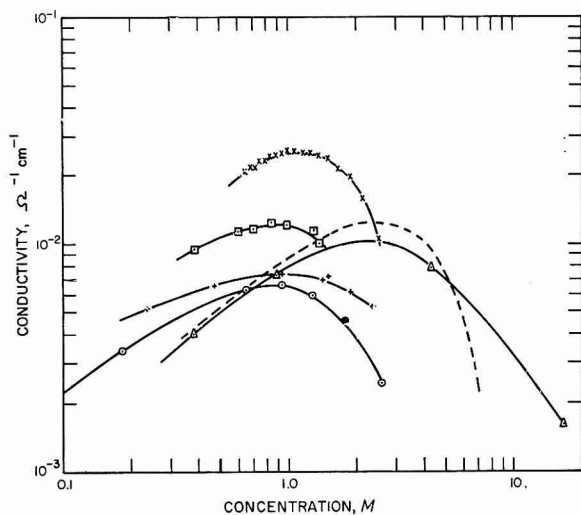
Fig. 1. Conductance of several electrolytes in DMSO at high concns: ($\times$), KPF$_6$[8]; ($\square$), NaPF$_6$[20]; ($\triangle$), KCNS[28]; (---), KCNS[36]; ($+$), LiClO$_4$[22]; ($\odot$), LiCl[5]; ($\bullet$), LiCl[22].
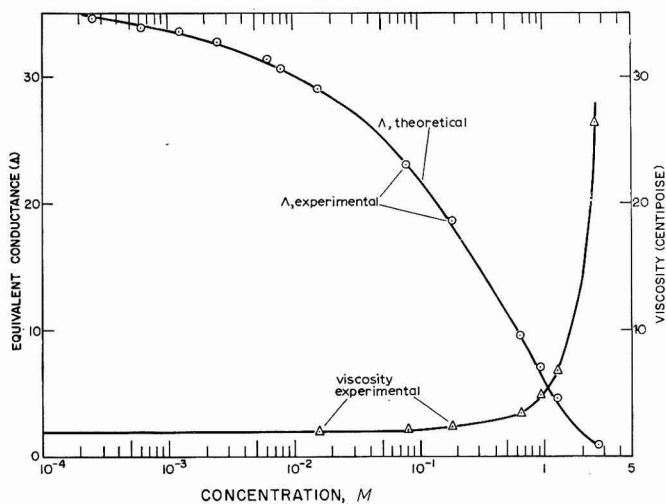
Fig. 2. Equiv. conductance and viscosity of LiCl solns. in DMSO[5].

approximately $1\ M$ concentration, which may result either from ion-pairing or from the large increase in viscosity of DMSO solutions containing high concentrations of salts.

Conductance measurements have been made over the entire accessible range

TABLE 8

CONDUCTANCE VALUES FOR MISCELLANEOUS SALT SOLUTIONS IN DMSO

Solns. are satd. except where noted

Salt	Concn.	Temp. (°C)	Conductance ($\Omega^{-1}cm^{-1}$)	Ref.
LiF		24	$5 \cdot 10^{-6}$	27
LiF	0.0193 M	25	$3.5 \cdot 10^{-6}$	22
NaF		24	$3 \cdot 10^{-6}$	27
KF		24	$3.9 \cdot 10^{-4}$	27
RbF		24	$4.8 \cdot 10^{-4}$	27
RbF + LiF		24	$4.15 \cdot 10^{-4}$	27
NH$_4$F		24	$2.88 \cdot 10^{-4}$	27
MgF$_2$		24	$7 \cdot 10^{-6}$	27
BaF$_2$		24	$8 \cdot 10^{-6}$	27
CuF$_2$	$4.9 \cdot 10^{-3} M$	25	$1.35 \cdot 10^{-5}$	27
ZnF$_2$		24	$8.5 \cdot 10^{-4}$	22
ZnF$_2$ + LiF		24	$4.15 \cdot 10^{-4}$	27
PbF$_2$		24	$8 \cdot 10^{-6}$	27
AlF$_3$		24	$1.8 \cdot 10^{-5}$	27
LiCl	2.13 m	25	$2.92 \cdot 10^{-3}$	30
NaCl	0.078 m	25	$1.79 \cdot 10^{-3}$	30
KCl	0.0225 m	25	$7.33 \cdot 10^{-4}$	30
RbCl	0.0356 m	25	$1.085 \cdot 10^{-3}$	30
CsCl	0.0373 m	25	$1.133 \cdot 10^{-3}$	30
MgCl$_2$	0.1435 m	25	$5.095 \cdot 10^{-3}$	30
CaCl$_2$	4.87 m	25	$3.52 \cdot 10^{-3}$	30
SrCl$_2$	0.941 m	25	$2.98 \cdot 10^{-3}$	30
BaCl$_2$	0.287 m	25	$4.93 \cdot 10^{-3}$	30
PbCl$_2$	0.547 m	25	$8.85 \cdot 10^{-4}$	30
ZnCl$_2$	1.641 m	25	$2.664 \cdot 10^{-3}$	30
CdCl$_2$	2.807 m	25	$1.729 \cdot 10^{-3}$	30
VCl$_2$	0.0147 m	25	$4.875 \cdot 10^{-4}$	30
CuCl$_2$	0.206 M	25	$1.06 \cdot 10^{-3}$ (?)	22
	1.23 m	25	$8.328 \cdot 10^{-4}$	30
AlCl$_3$	1.5 M	25	$3.73 \cdot 10^{-4}$ (?)	22
	0.05 m	25	$4.9 \cdot 10^{-5}$	30
CeCl$_3$	0.0713 M	25	$2.90 \cdot 10^{-3}$	41
CrCl$_3$	$4.47 \cdot 10^{-4} m$	25	$1.133 \cdot 10^{-4}$	30
FeCl$_3$	0.272 m	25	$3.058 \cdot 10^{-3}$	30
InCl$_3$	0.069 m	25	$1.64 \cdot 10^{-4}$	30
SbCl$_3$	2.63 m	25	$5.395 \cdot 10^{-4}$	30
VCl$_3$	0.0133 m	25	$7.73 \cdot 10^{-4}$	30
LiI	1.219 m	25	$7.88 \cdot 10^{-3}$	30
LiClO$_4$	2.65 m	25	$6.32 \cdot 10^{-3}$	30
InBr$_3$	0.2096 m	25	$1.657 \cdot 10^{-3}$	30
Ca(NO$_3$)$_2$	1.127 m	25	$1.832 \cdot 10^{-3}$	30
In(NO$_3$)$_2$	0.124 m	25	$2.533 \cdot 10^{-3}$	30
NH$_4$PF$_6$	~ 3 m	-12	$7.7 \cdot 10^{-3}$	24
	(H$_2$O 484 p.p.m.)	23.2	$1.17 \cdot 10^{-2}$	24
		35.2	$1.52 \cdot 10^{-2}$	24
NH$_4$PF$_6$	Satd. diluted 1:1	-12	$9.85 \cdot 10^{-3}$	24
	(~ 1.5 m)	23.2	$1.37 \cdot 10^{-2}$	24
		35.2	$1.58 \cdot 10^{-2}$	24
NH$_4$PF$_6$	Satd. diluted 1:9	27.2	$4.62 \cdot 10^{-3}$	24
	(~ 0.24 m)			
KPF$_6$	Satd. at temp. indicated	-12	$7.92 \cdot 10^{-3}$	24
	(2.50 M at 25°)	23.2	$1.14 \cdot 10^{-2}$	24
		35.2	$1.34 \cdot 10^{-2}$	24
NaSbF$_6$	~ 1.5 m	-7	$7.20 \cdot 10^{-3}$	24
	(H$_2$O 530 p.p.m.)	23.2	$9.78 \cdot 10^{-3}$	24
		32.7	$1.28 \cdot 10^{-2}$	24

TABLE 8 *(continued)*

Salt	Concn.	Temp. (°C)	Conductance ($\Omega^{-1}cm^{-1}$)	Ref.
Me_4NPF_6	Satd. ($< 20\%$)	23.2	$7.92 \cdot 10^{-3}$	24
	(H_2O, 856 p.p.m.)	35.2	$8.94 \cdot 10^{-3}$	24
Me_4NBF_4	Satd. ($< 20\%$)	27.2	$7.20 \cdot 10^{-3}$	24
	(H_2O, 520 p.p.m.)			
Me_3PhNPF_6	Satd. ($< 50\%$)	-7	$6.86 \cdot 10^{-3}$	24
	(H_2O 480 p.p.m.)	27.2	$1.05 \cdot 10^{-2}$	24
	Satd. diluted 9:1 ($< 45\%$)	27.2	$1.09 \cdot 10^{-2}$	24
	Satd. diluted 4.5:1 ($< 41\%$)	27.2	$1.14 \cdot 10^{-2}$	24
	Satd. diluted 3:1 ($< 38\%$)	27.2	$1.14 \cdot 10^{-2}$	24
	Satd. diluted 1.6:1 ($< 31\%$)	27.2	$1.06 \cdot 10^{-2}$	24

Solns. satd. with LiCl and another salt at 25° [30]

Salt	Concn. of salt	Concn. of LiCl	Conductance ($\Omega^{-1}cm^{-1} \cdot 10^3$)
KCl	$0.00715\ m$	$1.77\ m$	3.93
RbCl	$0.0242\ m$	$1.83\ m$	3.66
CsCl	$0.0186\ m$	$1.85\ m$	3.66
$CuCl_2$	$0.580\ m$	$3.34\ m$	1.23
$SrCl_2$	$0.756\ m$	$0.926\ m$	4.83
$ZnCl_2$	$1.57\ m$	$2.38\ m$	1.275
VCl_2	$0.00742\ m$	$3.96\ m$	2.365
VCl_3	$0.00451\ m$	$2.34\ m$	2.235
$CrCl_3$	$0.000454\ m$	$2.00\ m$	6.04
$FeCl_3$	$0.891\ m$	$2.18\ m$	3.17

of concentration for LiCl[5]. The equivalent conductance decreases from 35.3 (at infinite dilution) to 0.93 at 2.59 M, as shown in Fig. 2. The viscosity (Fig. 2) increases sharply in the region above, approximately, 0.8 M. In spite of the wide variation in equivalent conductance, it was not necessary to invoke ion-pairing to obtain a theoretical curve to fit the data. The solid line in Fig. 2 was calculated from an extended Onsager-type equation, using 3 Å as the distance of closest approach.

Table 8 lists a number of conductance measurements in miscellaneous solutions, many of them saturated solutions of the salt. In only a few cases were analyses made for water, and in these cases the water content was below 0.1%. The addition of as much as 10% water to solutions of KPF_6 in DMSO did not change the measured conductivity by more than 2%[8]; thus, small traces of water probably have little effect. An independent compilation of conductance values has been made[30] which encompasses some of these data.

A brief study of ternary $LiClO_4$–DMSO–SO_2 mixtures has been made[22] (Table 9). Increasing the pressure of inert gas over a 1 M solution of LiCl in DMSO changes the conductance only slightly, but replacing the argon atmosphere with SO_2 causes a substantial increase in conductance. The conductance appears to go through a maximum at approximately 1.5 moles of dissolved SO_2/mole of DMSO. These data must be evaluated with caution, however, since the expected change in conductance

TABLE 9

CONDUCTANCE OF 1.0 M LiClO$_4$–SO$_2$ SOLUTIONS IN DMSO[22]

Pressure (atm)	Temp. (°C)	Conductivity ($\Omega^{-1}cm^{-1} \cdot 10^3$)	moles SO$_2$/ moles DMSO[a]
1 (Argon)	25	7.3	
7.8 (Argon)	21	10.1	
9.2 (Argon)	22.5	9.0	
1.7 (SO$_2$)	24	11.6	0.32
1.8 (SO$_2$)	24.5	15.5	0.83
2.1 (SO$_2$)	25.5	17.6	1.2
3.5 (SO$_2$)	25	12.6	~ 2

[a] At 1 atm SO$_2$ above pure DMSO, this ratio is 1.52[1].

for a pressure change of 10 atm is approximately 0.5% by analogy with dimethyl formamide[42], and the changes of 20–30% with argon pressure given in Table 9 probably reflect the experimental error of the measurements.

POLAROGRAPHY OF CATIONS AND ANIONS

GUTMANN AND SCHÖBER[43] were the first to study the polarography of a number of inorganic ions in DMSO, using 0.1 M tetraethylammonium nitrate or perchlorate as supporting electrolyte. Tetraethylammonium iodide showed a decomposition potential approximately 0.1 V more negative than either the nitrate or perchlorate. However, the dropping mercury electrode was unstable in even highly purified solutions of the iodide, and a high residual current was observed[44]. Tetra-n-butylammonium perchlorate appears to have a slightly more negative decomposition potential than tetraethylammonium perchlorate[45].

The half-wave potentials observed by various investigators are listed in Table 10, referred to a saturated aqueous calomel electrode (SCE). The liquid junction between the aqueous KCl and the DMSO electrolyte appeared to be stable to ±3 mV and was the same for 0.1 M Et$_4$NClO$_4$ and 0.1 M Et$_4$NNO$_3$. In general, the order of the half-wave potentials in DMSO is similar to that in aqueous solutions[46,80], and the DMSO–H$_2$O liquid junction potential has been estimated to be approximately 120 mV by equating the redox potentials of large ions in the two media[46]. One study[80] used a Zn(Hg)/Zn^{2+} reference electrode in DMSO; their data have been converted to the SCE-scale by assuming that their reference electrode is −1.08 V vs. SCE.

Diffusion coefficients calculated from the Ilkovič equation using measured polarographic diffusion currents are listed in Table 11. The increase of diffusion coefficient with increasing temperature is due primarily to the decrease in viscosity of DMSO. Similarly, the lower values of D in 1.0 M KClO$_4$ probably result primarily from its higher viscosity[45].

Many polarographic reductions appear to be irreversible in DMSO according to the shape observed for the waves[44,45,80], but no further studies of the kinetics have been made except for the lithium electrode[29], discussed in a later section.

The determination of the alkali metals by polarography appears to be quite feasible in DMSO solutions. Lithium can be determined in the presence of either Na

TABLE 10

HALF-WAVE POTENTIALS IN DMSO *vs.* A SATURATED AQUEOUS CALOMEL ELECTRODE

Ion	Dissolved as	Temp. (°C)	$E_{\frac{1}{2}}$ (V)	Ref.
Bu_4N^+	Bu_4NClO_4	25	-3.00[a]	45
Et_4N^+	0.1 M Et_4NClO_4	25	-2.80[a]	21,80
	Et_4NNO_3	21	-2.75[a]	43
Li^+	$LiCl$	21	-2.45	43
	$LiClO_4$	25	-2.53[f]	80
Ca^{2+}	$Ca(NO_3)_2$	21	-2.30	43
Mg^{2+}	$Mg(ClO_4)_2$	21	-2.28	43
La^{3+}	$LaCl_3$	21	-2.26	88
Ce^{3+}	$CeCl_3$	21	-2.24	88
N_2O		21	-2.22	87
Pr^{3+}	$PrCl_3$	21	-2.20	88
Nd^{3+}	$NdCl_3$	21	-2.20	88
Tb^{3+}	$TbCl_3$	21	-2.19	88
Gd^{3+}	$GdCl_3$	21	-2.16	88
NH_4^+	NH_4NO_3	21	-2.13	43
	NH_4ClO_4	25	-2.11[f]	80
K^+	$KClO_4$	21	-2.11	43
			-2.10[f]	80
Sr^{2+}	$Sr(NO_3)_2$	21	-2.10	43
	$Sr(ClO_4)_2$	25	-2.30[f]	80
Ba^{2+}	$Ba(NO_3)_2$	21	-2.09	43
		25	-2.07[f]	80
Ho^{3+}	$HoCl_3$	21	-2.09	88
Er^{3+}	$ErCl_3$	21	-2.09	88
Dy^{3+}	$DyCl_3$	21	-2.08	88
Na^+	$NaClO_4$	21	-2.07	43
		25	-2.07	21
		25	-2.08[f]	80
Rb^+	$RbCl$	21	-2.06	43
Cs^+	$CsCl$	21	-2.03	43
Sm^{3+}	$SmCl_3$	21	-2.02[c]	88
			-2.12[d]	88
Mn^{2+}	$Mn(ClO_4)_2$	25	-1.68	45
Th^{4+}	$ThCl_4$	21	-1.57[c]	89
			-1.72 to -1.95[d]	89
Yb^{3+}	$YbCl_3$	21	-2.07[e]	89
			-1.48[c]	88
			-2.21[d]	88
Co^{2+}	$Co(ClO_4)_2$	25	-1.39[b]	21
	(see text)	25	-1.32	45
NO		21	-1.44	87
Ti^{4+}	Et_2TiCl_2	21	-1.21	43
N_2O_3		21	-1.18	87
Zn^{2+}	$Zn(ClO_4)_2$	25	-1.10	45
	$Zn(NO_3)_2$	25	-1.06[f]	80
U^{4+}	UCl_4	21	-1.09[c]	90
			-1.56[d]	90
Hf^{4+}	$HfCl_4$	21	-1.07[c]	43
			-1.17[d]	43
Ni^{2+}	$Ni(ClO_4)_2$	25	-1.08[b]	21
	$Ni(NO_3)_2$		-1.14	45
			-1.05[f]	80
H^+	HCl	30	-1.08	21
H^+	$HClO_4$, H_2SO_4	30	-1.06	21
NO_2		21	-1.06[c]	87
			-1.53[d]	87
Zr^{4+}	$ZrCl_4$	21	-1.04	43
Nb^{5+}	$NbCl_5$	21	-0.92	43

TABLE 10 (continued)

Ion	Dissolved as	Temp. (°C)	$E_{\frac{1}{2}}(V)$	Ref.
O_2	(see text)	25	-0.85	48
			-0.77	45,49
			-0.73^f	80
			-0.73	50
			-0.72	21
Duroquinone	(see text)	25	-0.73^c	21
			-1.53^d	21
Fe^{3+}	$Fe(ClO_4)_3$	25	-0.73^c	45
			-1.41^d	45
Cd^{2+}	$Cd(ClO_4)_2$	25	-0.70	45
	$Cd(NO_3)_2$	25	-0.70^f	80
Cr^{3+}	$CrPO_4$, $Cr(NO_3)_3$	21	-0.67^c	51
	$Cr(ClO_4)_3$		-1.05^d	51
			-0.82^c	45
			-1.56^d	45
	$CrCl_3$	21	-1.41^c	51
	(see text)		-1.81^d	51
Tl^+	$TlNO_3$	25	-0.54^f	80
Pb^{2+}	$Pb(ClO_4)_2$	25	-0.53	45
	$Pb(NO_3)_2$	25	-0.55^f	80
UO_2^{2+}	$UO_2(ClO_4)_2$	21	-0.53	90
Quinone	(see text)	25	-0.40^c	21,52
			-1.24^d	21,52
Si^{4+}	$SiCl_4$, SiF_4	21	-0.52^c	43,47
	RCl_3Si		-1.09^d	43,47
			-2.70^e	
Sb^{3+}	SbI_3	21	-0.36^c	43
			-0.52^d	43
			-1.13^e	43
	$Sb(NO_3)_3$	25	-0.29^f	80
Cu^{2+}	$Cu(ClO_4)_2$	25	-0.06	45
	$Cu(NO_3)_2$		$-0.004^{c,f}$	80
			$-0.12^{d,f}$	80
Tetrachloroquinone	(see text)	25	$+0.08^c$	21
			-0.73^d	21
Hg electrode	Et_4NClO_4	25	$+0.25$	21,80
	(anodic limit)		$+0.30^b$	21
			$+0.35$	45
I^- (anodic)	(see text)	25	$+0.48^{c,\ g}$	53
			$+0.70^{d,\ g}$	53
Cl^- (anodic)	KCl	25	$+0.5^g$	52
Pt electrode	$Et_4N(ClO_4)$	25	$+0.7$	21
	(anodic limit)		$+1.0$	52

[a] Decomposition potential of supporting electrolyte. [b] Rotating mercury pool electrode. All others at the dropping mercury electrode. [c] First wave. [d] Second wave. [e] Third wave. [f] All half-wave potential values from ref. 80 were measured vs. a satd. Zn amalgam–satd. $Zn(ClO_4)_2$ electrode in DMSO. This electrode was assumed to have a potential of -1.08 V vs. SCE for comparison with the data of other investigators. [g] Platinum electrode.

or K; but the separation of Na, K, Rb, or Cs, from one another requires derivative polarography. NH_4^+ gives an ill-formed wave, with irregular dropping at the mercury electrode[43].

Of particular interest is the observation that many silicon compounds (including $SiCl_4$, SiF_4, and compounds of the form RCl_3Si) can be determined polarographically in DMSO solutions[47]. The polarographic waves occur at approximately the

TABLE 11

Species	Supporting electrolyte	$D \cdot 10^6$ (cm^2/sec)		Ref.
		$25°$	$35°$	
O_2	0.1 M Et$_4$NClO$_4$	28 ± 5		48
CO_2	0.03 M Et$_4$NClO$_4$	1.5		37
H^+	0.01 M Et$_4$NClO$_4$	4.3 ± 0.7		48
H^+	0.1 M NaClO$_4$		4.4[a]	21
K^+	0.1 M Bu$_4$NClO$_4$	6.7		45
Cd^{2+}	0.1 M Bu$_4$NClO$_4$	4.9	6.8	45
	0.1 M KClO$_4$	4.4		
	1.0 M KClO$_4$	1.7	2.5	
Co^{2+}	1.0 M KClO$_4$	0.7	1.1	45
Cr^{3+}	0.1 M KClO$_4$	0.94		45
Cr^{2+}	0.1 M KClO$_4$	0.81		
Cu^{2+}	0.1 M Bu$_4$NClO$_4$	4.8		45
	0.1 M KClO$_4$	7.1		
	1.0 M KClO$_4$	1.7	2.5	
Fe^{3+}	0.1 M KClO$_4$	1.63		45
Fe^{2+}	0.1 M KClO$_4$	0.80		
Mn^{2+}	1.0 M KClO$_4$	2.9	3.7	45
Ni^{2+}	0.1 M Bu$_4$NClO$_4$	5.9	7.7	45
	0.1 M KClO$_4$	3.9	5.7	
	1.0 M KClO$_4$	0.85	2.1	
Pb^{2+}	0.1 M KClO$_4$	2.3	2.6	45
	1.0 M KClO$_4$	1.6	2.2	
Zn^{2+}	0.1 M Bu$_4$NClO$_4$	3.4	3.6	45
	0.1 M KClO$_4$	5.4		
	1.0 M KClO$_4$	2.3	3.2	

[a] $30°$

same potential for all these compounds, and may be due to the reduction of HF produced by reaction with traces of water in the solvent[83].

The reduction of water has been observed, and its polarographic determination in DMSO has been suggested[44]. The reduction of water has recently been confirmed in NaPF$_6$ and KPF$_6$ electrolytes[8].

The effect of supporting electrolyte concentration on the half-wave potentials and diffusion currents for Pb^{2+}, Co^{2+}, and Cd^{2+} has been studied in KClO$_4$ solutions. The half-wave potential of Pb^{2+} shifts more positive by about 0.04 V as the concentration of KClO$_4$ is increased from 10^{-3} to 1.0 M. The half-wave potential of Cd^{2+} goes through a maximum negative value at approximately 0.1 M KClO$_4$. Both these effects have been attributed to the irreversibility of the reduction. The half-wave potential of cobalt, on the other hand, exhibits a smooth trend from -1.22 to -1.46 V as the KClO$_4$ concentration is increased from 10^{-3} to 1.0 M. This has been interpreted as evidence for the formation of complexes such as $Co(ClO_4)^+$, but no formation constants have been calculated[45].

The addition of up to 1 M water to an 0.1 M KClO$_4$–DMSO supporting electrolyte shifts the half-wave potential of cadmium more negative by approximately 0.03 V, which may be interpreted as evidence for the formation of weak cadmium complexes with water. The equilibrium constants for the stepwise formation of the complex with one water molecule and two water molecules have been calculated to be 0.048

and 0.82, respectively[45]. It is well to remember, however, that all these shifts of half-wave potential may be due, at least in part, to changes in the potential of the aqueous KCl–DMSO junction at the reference electrode.

A ten-fold increase of chloride concentration in an 0.1 M KClO$_4$ supporting electrolyte shifts the half-wave potential of Cd^{2+} as much as 0.2 V more negative. From this dependence, the formation constants for the cadmium chloride complexes have been calculated[45]. The logarithms of the stepwise formation constants are as follows: K_1 3.40, K_2 3.16, K_3 2.32, K_4 2.03, K_5 1.87, K_6 2.18, where the subscript indicates the number of chloride ligands bound to the cadmium ion in the product of the stepwise reaction. Similarly, a ten-fold increase of chloride concentration shifts the half-wave potential of lead by approximately 0.05 V more negative. The logarithms of the stepwise formation constants of the lead chloride complexes calculated from these data are[45] K_1 3.88, K_2 2.45.

Electroless deposition of Pb on Pb or Cu substrates has been observed in DMSO solutions containing Pb(NO$_3$)$_2$ with thiourea as a reducing and complexing agent[86].

Although Cu^{2+} has been reported[45] to be reduced in a single step, recent data[80] have shown that two one-electron steps are involved, with half-wave potentials separated by 0.12 V.

The half-wave potentials for chromium reduction are the same in phosphate, nitrate, and perchlorate media[51], but both waves are approximately 0.8 V more negative in chloride medium (Table 10). SCHÖBER AND REHAK[54] identified the two waves in the non-complexing media with the reductions Cr^{3+} → Cr^{2+} and Cr^{2+} → Cr; whereas in the chloride medium, the two waves were identified with the reduction of the CrCl$_2$(DMSO)$_4^+$ and CrCl$_4^-$ ions, to Cr(II). The reduction of CrCl$_4^-$ was found to be reversible[54], but the reduction of CrCl$_2$(DMSO)$_4^+$ is less reversible.

Aluminum chloride and aluminum acetylacetonate are reduced in DMSO and give well-formed waves[55,56]. The half-wave potentials were measured with respect to a mercury pool; for this reason they are not listed in Table 10. For AlCl$_3$, $E_{\frac{1}{2}} = -1.5$ V, and for the acetylacetonate, $E_{\frac{1}{2}} = -2.2$ V in 0.1 M Et$_4$NClO$_4$ supporting electrolyte. When chloride is added to the acetylacetonate, the half-wave potential shifts to -1.0 V. Beryllium has also been determined by polarography of the acetylacetonate in a medium consisting of 90% DMSO, 10% acetylacetone, 0.03% gelatin, which is 0.1 M in Et$_4$NClO$_4$[57].

The reduction of nitrate ion is influenced by the presence of polyvalent cations such as the alkaline earths, Ce^{3+}, or La^{3+} in the same way as in aqueous solutions. The half-wave potential was reported as -1.83 V $vs.$ a mercury pool[58], which implies that the anodic limit of -0.2 V $vs.$ SCE reported for Et$_4$NNO$_3$ supporting electrolyte[43] is not the reduction of nitrate ion and may in fact be a typographical error since all other workers (Table 10) report an anodic limit of $+0.2$ to $+0.3$ V $vs.$ SCE.

The oxidation of iodide ion at a platinum electrode in DMSO is similar to the reaction in acetonitrile, occurring as a two-step process:

$$6 \text{ I}^- \rightleftharpoons 2 \text{ I}_3^- + 4 e \qquad E_{\frac{1}{2}} = 0.48 \text{ V } vs. \text{ SCE}$$
$$2 \text{ I}_3^- \rightleftharpoons 3 \text{ I}_2 + 2 e \qquad E_{\frac{1}{2}} = 0.70 \text{ V } vs. \text{ SCE}$$

The potentials were obtained in the course of the mechanism study from chronopotentiograms in 0.1 M NaClO$_4$ supporting electrolyte[53].

The oxidation of chloride ion can be observed at a platinum electrode at a potential of approximately $+0.5$ V *vs.* SCE in a perchlorate supporting electrolyte[52].

POLAROGRAPHY OF GASES

The reduction of oxygen at the dropping mercury electrode in DMSO was noted in the early studies[44,21] to be irreversible and strongly dependent on the medium. When two waves were obtained, the second wave was only about 75% of the height of the first. MARICLE AND HODGSON[50] showed by cyclic voltammetry at a platinum electrode and by electron-spin resonance studies that the first step in the reduction of oxygen in DMSO is the formation of the superoxide ion, O_2^-. This reaction is reversible at platinum and mercury electrodes and has a half-wave potential in the range near -0.73 V *vs.* SCE. The addition of phenol (a proton source) shifted $E_{\frac{1}{2}}$ anodically and increased the diffusion current, which showed that the superoxide ion is easily protonated.

Similar observations were made by PEOVER AND WHITE[49] who also showed that the reduction of oxygen in anhydrous DMSO leads to O_2^-, with a half-wave potential at approximately -0.77 V *vs.* SCE. The addition of acids changed the one-electron wave to a 2-electron wave and shifted it anodically; they interpreted this as indicating the reduction of a protonated O_2 molecule. SLOUGH[59] confirmed the production of O_2^- by electron-spin resonance and ultraviolet spectra in pyridine and dimethyl formamide.

JOHNSON, POOL AND HAMM[48] studied the effect of acids and cations on the polarographic reduction of oxygen. The second wave, which they interpreted as resulting from the reactions

$$O_2^- + e + 2\,H^+ = H_2O_2$$
$$O_2^- + e + 2\,M^+ = M_2O_2$$
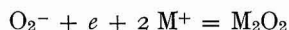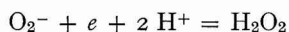
depends strongly on the supporting electrolyte. In 0.1 M Et_4NClO_4, oxygen gave two waves with $E_{\frac{1}{2}}$-values of -0.85 and -2.20 V *vs.* SCE. In 1.5 mMKO$_2$ solutions, an anodic wave with a half-wave potential of -0.85 V was observed, as well as a cathodic wave at -2.20 V; this confirms that the first step in the reaction results from the reversible formation of O_2^-. In the presence of HCl, the first wave shifted to -0.54 V and the second wave decreased in height, reaching zero when 4 equivalents of HCl had been added/mole of dissolved O_2. Under these conditions, the first wave corresponded to a 2-electron reduction of O_2. The addition of $NaClO_4$ and $KClO_4$ shifted the second wave more positive, with Na^+ giving a limiting value of -1.14 V, which agrees with the second wave (-1.13 V) observed for oxygen reduction in 0.1 M $NaClO_4$ supporting electrolyte[21]. The addition of K^+ gave a limiting half-wave potential of -1.55 V; Li^+, -0.75 V; and Ca^{2+}, Sr^{2+}, and Mg^{2+}, -0.6 V *vs.* SCE[48].

The reduction of CO_2 at the dropping mercury electrode in 0.1 M Et_4NClO_4–DMSO supporting electrolyte shows a half-wave potential of -2.24 V *vs.* a mercury pool. The addition of up to 20% H_2O has little effect on the half-wave potential. The reaction was assumed to proceed to oxalate ion[60]. More detailed studies have been made using linear-scan voltammetry. Analytically useful reduction waves, which were shown to be diffusion controlled, could be obtained at gold or amalgamated platinum electrodes, but the amalgamated platinum electrode gave more reproducible

results and lower residual currents. Chronopotentiometric studies led to the postulation of a one-electron reduction on gold electrodes, and a two-electron reduction on an amalgamated platinum electrode. Chronopotentiometric studies with current-reversal provided evidence for the formate ion being the primary product of reduction[37].

Other gases besides oxygen and carbon dioxide have been shown to give diffusion-controlled polarographic waves, with a height proportional to the concentration of the gas. At a dropping mercury electrode in Et_4NClO_4–DMSO supporting electrolyte, SO_2, HCl, H_2S, and $POCl_3$ were reduced. Small amounts of water did not interfere, and simultaneous determination of CO_2 and SO_2 was shown to be possible[61,62]. The nitrogen oxides NO_2, N_2O_3, NO, and N_2O give polarographic waves in DMSO[87].

THE REACTIONS OF QUINONES

The reactions of quinones in DMSO are similar to the reactions in acetonitrile and dimethylformamide. Two polarographic waves are obtained for benzoquinone in 0.1 M Et_4NClO_4, at -0.4 and -1.24 V $vs.$ SCE, the first corresponding to the one-electron reversible step

$$Q + e \rightleftharpoons Q^-$$
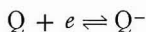
The second wave appears to be irreversible, with a height somewhat less than the first wave. Similar results were obtained with duroquinone. With tetrachloroquinone, both waves appeared to be irreversible[21].

Linear sweep and chronopotentiometric measurements showed that both waves for benzoquinone are reversible. The first wave cannot be observed clearly in chloride supporting electrolytes because it is obscured by the anodic oxidation of chloride at both platinum and mercury electrodes. The presence of the semiquinone radical (Q^-) has been verified by its electron-spin resonance spectrum[52].

In the presence of acids such as HCl, acetic acid, or water, the second wave shifts to more positive potentials until at sufficiently high acid concentrations only a single wave is observed. This single wave has a height equal to the sum of the original two, and a half-wave potential approximately that of the original first[21,52]. Reversal of the current during chronopotentiometry in the presence of acid showed the presence of hydroquinone[52]. These effects can be explained by the secondary reactions:

$$Q^- + HA = HQ + A^-$$
$$HQ + e = HQ^-$$
$$HQ^- + HA = H_2Q + A^-$$
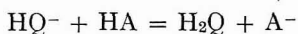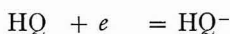
The protonated quinone radical (HQ) is always reduced more easily than the quinone itself, so that only a single wave is seen. In the absence of acids, the second wave observed results from the further reversible reduction of the quinone radical ion:

$$Q^- + e = Q^{2-}$$
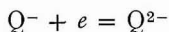
The doubly-charged quinone is very reactive and on diffusing into the solution may

react with traces of acidic impurities, with benzoquinone or with the solvent, resulting in apparent irreversibility and a diffusion current less than that of the first wave[21].

If Li+ is added, the second wave decreases in height and eventually disappears, but the first wave is unaffected. This occurs at both platinum and mercury electrodes. Chronopotentiometry showed that the reaction that occurs at -1.1 V in benzoquinone alone changes to a reaction occurring at approximately -0.9 V in the presence of Li+. The reversibility of the first step and the potential at which it occurs were unaffected by the presence of Li+. The reactions

$$Q^- + Li^- = Li^+Q^-$$
$$Q^{2-} + Q = 2 Q^-$$
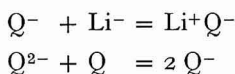
would explain both the effect of Li+ and the apparent irreversibility of the second step, but a disproportionation reaction such as the one above would be unlikely to have a great effect unless the diffusion coefficient of Q^{2-} were much greater than that of Q^-. A constant-potential electrolysis experiment, however, showed that the disproportionation reaction does indeed take place[52].

The quinone–hydroquinone redox couple, which is a satisfactory pH electrode in solvents that are good proton donors, does not operate reversibly in dimethyl sulfoxide and other aprotic solvents. No anodic wave for hydroquinone oxidation could be observed at the dropping mercury electrode[21], but at a platinum electrode in perchlorate supporting electrolyte, an anodic wave has been observed at approximately $+0.7$ V. However, oxidation of the supporting electrolyte does not occur appreciably below $+1.0$ V at a platinum electrode. Both polarography and chronopotentiometry indicate a single-step oxidation, and reversal of the current during chronopotentiometry shows a cathodic reaction of the oxidation product at approximately -0.3 V. This indicates that the hydroquinone is *not* oxidized to the semiquinone radical anion or to the quinone itself. This is probably because no strong base is present to remove the proton from the hydroquinone, which appears to be the rate-determining step in water and other protic solvents. The system is still not completely understood, however. The mechanism presented implies that the first step in the quinone reduction would occur at the same potential in the presence or absence of acid. Although this appears to be approximately the case, chronopotentiometric studies indicate that in the presence of acid the first step occurs at slightly more positive potentials. This implies an interaction of the proton with the reduction of the quinone which has not been included in the mechanism outlined above[52].

THE LITHIUM ELECTRODE

The alkali metals differ greatly in their reactivity towards DMSO. At room temperature potassium reacts violently and sodium rapidly[63], with the formation of sodium methanesulfenate, methylsulfinyl carbanion, methane and dimethyl sulfide[64]. On the other hand, lithium has been reported on numerous occasions to be unreactive towards DMSO, and several electrochemical studies have been made using lithium electrodes.

Deposition of lithium from LiCl solutions in DMSO on a tungsten-foil base electrode was easily accomplished, as was anodic dissolution of the deposited metal. Little polarization was observed, and deposition-dissolution efficiencies were 60–70%,

although no stringent efforts were made to remove residual water from the electrolyte[52].

DMSO has been used as a solvent for the carboxymethyl cellulose binder in pasting experimental lithium battery electrodes. The electrodes were dried in vacuum at 90–100° to remove the DMSO without apparent damage or deterioration. There was no apparent reaction of lithium with DMSO solutions of LiCl, RbF, or ZnF_2[27].

On the basis of conductance and decomposition potential studies, DMSO electrolytes containing $Al_2(SO_4)_3$ + LiCl or NaI + $NaCOOCCl_3$ + SO_2 have been suggested for use in constructing batteries with energy density greater than 200 W-hours/pound of electrode material[14].

A lithium electrode prepared by compressing Li foil between nickel or copper Exmet screens was shown to have an open-circuit potential constant within 0.1 V for more than 3 days in a LiBr–DMSO electrolyte. This was in contradiction to earlier screening tests which showed poor stability of lithium in this electrolyte[65].

Lithium could be electrodeposited from LiBr solutions on Pt or Ni substrates and reoxidized with about 60% efficiency. The failure to achieve 100% efficiency was attributed to the formation of a Pt–Li alloy, the reaction of Li with solvent, or the formation of LiOH or Li_2O. No attempt was made to determine which reaction was actually occurring[36]. The electrolysis of $LiClO_4$–DMSO solutions at platinum electrodes gives very irreproducible current–potential data. The cathodic reaction is probably lithium deposition, but the anodic reaction is not known[22,79].

A lithium–silver oxide battery, using a LiBr–DMSO electrolyte, has been reported to achieve 400 W-hours/pound of electrode material at a discharge rate of 10 mA/cm² [66].

The rate of gas evolution when a lithium ribbon was placed in a cell containing $LiClO_4$ in DMSO at 30° was measured and found to be negligible over a period of 16 h[67].

Vigorous reaction and gas evolution were observed, on the other hand, in DMSO solutions of NH_4PF_6, $NaPF_6$, and $NaSbF_6$. The solution turned yellow; a gas smelling of sulfide was evolved; and in 12–14 days the 1-g sample of lithium had completely dissolved in 20 ml of solution[24]. Strong attack of Li by $CuCl_2$ in DMSO was observed over a period of 2–24 h; $LiClO_4$ solutions showed moderate attack on Li after 24 h; and pure DMSO, LiCl, LiF, of CuF_2 solutions showed slight or no attack on Li after 168 h[22]. Lithium wire did not react with pure DMSO at temperatures up to 80°[64]. These varied reports probably reflect corrosion by water or acids that are introduced along with the solutes.

TABLE 12

ANODIC POLARIZATION OF Li ELECTRODES IN 0.64 M LiBr[36]

Current density	Potential of Li vs. Ag/AgBr reference (V)	Potential of Li–AgO cell	Potential of Li(Hg) electrode vs. Li(Hg) reference[a]
Open circuit	−2.86	3.14	0
2 mA/cm²	−2.76	2.79	0.15
10 mA/cm²	−2.71	2.34	0.40

[a] 2 mole-% Li amalgam in 0.5 M LiCl[29].

The polarization of a lithium electrode (with respect to an AgBr/Ag reference electrode) was measured in 0.64 M LiBr, with the results shown in Table 12[36]. An experimental battery using a silver oxide cathode was also measured; the polarization data obtained are indicated in Table 12[36]. The much higher polarization of the battery can probably be attributed to the cathode reaction, not to the internal resistance of the cell. Other experimental batteries have been constructed using a lithium anode and MnO_2 cathode with a $LiClO_4$–DMSO electrolyte[79].

Polarization of a cell consisting of two identical lithium amalgam electrodes (2 mole-% Li) showed that the Tafel equation

$$\eta = \frac{RT}{\alpha F} \ln (i/i_0)$$

(where η is overvoltage, R the gas constant, T the absolute temperature, α the transfer coefficient, F the faraday constant, i the current, and i_0 the exchange current) was obeyed within experimental error over the current range from 10^{-7}–$5 \cdot 10^{-3}$ A/cm², with $\alpha = 0.5$ and $i_0 = 5 \cdot 10^{-4}$ A/cm² [29]. For comparison with the polarization data on solid lithium electrodes, some of these data have been included in Table 12. Although the polarization at a given current density appears to be higher for the amalgam than for solid lithium, the true surface area of the solid metal is almost certainly much higher than its geometric area, and the polarization curves may in fact be similar when based on the true area.

THE ELECTRICAL DOUBLE LAYER

The only measurements in DMSO relating to the structure of the electrical double layer at the electrode–electrolyte interface are a few electrocapillary curves obtained by measuring the natural drop lifetime at a dropping mercury electrode.

TABLE 13

ELECTROCAPILLARY MAXIMUM POTENTIAL FOR MERCURY IN DMSO

Electrolyte	E.C.M. potential (V)[a]		Ref.
	vs. SCE	vs. Hg pool in same electrolyte	
0.1 M NaClO$_4$	−0.30		21
1 M KClO$_4$	−0.28		45
0.1 M NaNO$_3$ or Et$_4$NClO$_4$	−0.39[b]		80
0.1 M KClO$_4$		−0.22	45
0.1 M KClO$_4$ + 0.1 M H$_2$O		−0.16	
0.1 M Bu$_4$NClO$_4$		−0.058	
0.1 M KI		−0.08	
0.1 M KI + 0.1 M H$_2$O		−0.15	
0.1 M Bu$_4$NI		−0.10	
0.1 M Bu$_4$NClO$_4$ + 0.6% Triton X-100		−0.70	

[a] Potential of maximum drop lifetime at a dropping mercury electrode.
[b] Reference electrode used was Zn(Hg)/Zn²⁺ in DMSO. Its potential was assumed to be −1.08 V vs. SCE for comparison with the other data.

Typical parabolic curves are observed, and the potentials of the electrocapillary maximum obtained by this method are listed in Table 13.

It appears that a polarized mercury pool in an unreactive electrolyte attains a potential approximately -0.2 V $vs.$ the ECM, and $+0.08$ V $vs.$ the saturated aqueous calomel electrode. However, the extreme sensitivity of the mercury pool potential to traces of reducible or oxidizable impurities makes it a poor reference electrode, although stable potentials have been reported[45].

With the reservation that the potential of a mercury pool may change as much as the potential of the ECM when the electrolyte composition is changed, we may tentatively conclude that the adsorption of ions on mercury from DMSO solutions is similar to that from aqueous solutions: tetra-alkylammonium cations are adsorbed at negative potentials, tending to make the ECM potential more positive, and iodide ions are adsorbed at positive potentials, tending to make the ECM more negative. The effect of water and the surface-active agent Triton X-100 are not easy to discern from the presently available data.

REFERENCE ELECTRODES

For most of the polarographic studies discussed above, a saturated aqueous calomel electrode has been used for a reference electrode. The working solutions were usually protected from contamination by water by placing the reference electrode (a commercial unit with built-in aqueous KCl salt bridge) in a compartment separated from the working electrode by a glass frit[44], sometimes inhibiting diffusion of water by using an agar plug in addition to the glass frit[21]. A calomel electrode in which the saturated aqueous KCl has been replaced with saturated methanolic KCl has also been used[68,69].

Although the Ag/Ag$^+$ electrode is reversible in DMSO[70,84], Ag/AgCl reference electrodes are troublesome to use because of the high solubility of AgCl in excess chloride, which presumably results from the formation of complexes such as $AgCl_2^-$[23,29,70,84].

AgBr and AgI, similarly, are soluble in excess anion[70,71,84]. A silver–silver chloride electrode has been used for studies in DMSO by saturating the solution with respect to both NaCl and AgCl and connecting the reference compartment to the test solution through a glass-frit liquid junction. The potential difference between two such electrodes connected by a saturated $NaClO_4$ salt bridge was less than 0.8 mV[23]. An AgBr/Ag reference electrode in 0.64 M LiBr is reported to have a potential of -0.44 V $vs.$ SCE[36].

Analogues of the calomel electrode, using Hg_2Cl_2, Hg_2Br_2, or Hg_2I_2 in DMSO are unsuitable because of the rapid disproportionation of the mercurous salts. After a short time in contact with DMSO, metallic mercury is visible on the salts; this reaction is enhanced by the high solubility of the mercuric halides in DMSO[71].

The thallium amalgam–thallous chloride electrode appears to be the most stable reference electrode yet discovered for use in DMSO solutions. In a dry argon atmosphere, electrodes made by placing a layer of crystalline thallous chloride over a pool of 1% thallium amalgam showed potential differences less than 0.03 mV in RbCl, $MgCl_2$, and $InCl_3$ and less than 0.01 mV in LiCl[71].

The polarization behavior of a 40% thallium amalgam–thallous chloride

electrode in LiCl–DMSO solutions has been studied, and the exchange current found to be $7 \cdot 10^{-4}$ A/cm², which is adequate for virtually all potentiometric measurements. Within a few minutes after cathodic or anodic polarization by as much as 10^{-4} A/cm², the equilibrium potential difference between two identical electrodes was re-established to within 0.01 mV[29].

The lithium amalgam–lithium ion electrode has been shown to be reversible in DMSO, with an exchange current of $5 \cdot 10^{-4}$ A/cm² for a 2 mole-% amalgam in 0.5 M LiCl. The potential of two identical electrodes differed by less than 0.02 mV, even after cathodic or anodic polarization at 10^{-4} A/cm². Some slight decomposition of the electrolyte was noted after several weeks[29].

A zinc amalgam in a saturated solution of $Zn(ClO_4)_2 \cdot 4$ DMSO has been used as a reference electrode for polarographic studies. Its potential is -1.08 V $vs.$ SCE, and it appears to be stable over long periods of time[80].

Attempts to use a platinized-platinum hydrogen electrode in DMSO were unsuccessful. No stable readings could be attained, and decomposition of the electrolyte occurred, probably with the formation of sulfides. A glass electrode, which was stored in water when not in use, gave reproducible potentiometric measurements in DMSO solutions, but equilibration times as long as 90 min were required to obtain steady readings. The Nernst relation was approximately obeyed for a glass electrode–AgCl/Ag cell[23,31].

POTENTIOMETRIC STUDIES

Concentration cells using silver electrodes in $AgNO_3$–DMSO solutions obey the Nernst relation over a concentration range from 0.001–0.1 M when a 1.5-M NH_4NO_3 or $KClO_4$ salt bridge was used to eliminate the liquid junction potential. No effect of water was observed[72]. Solubility products and complex formation constants of the silver halides in DMSO have been determined by potentiometric titration of $AgClO_4$ with halide in Et_4NClO_4 to maintain constant ionic strength, as well as by voltammetry at a rotating platinum electrode[84]. The results are summarized in Table 14.

The solubility product and complex formation constants for the thallous chloride system have been determined by titration of Tl^+ solutions with Cl^-, using a thallium amalgam electrode. The solubility product was found to be $K_{so} = (5.5 \pm 0.5)$

TABLE 14

SOLUBILITY PRODUCTS AND COMPLEX FORMATION CONSTANTS FOR SILVER HALIDES IN DMSO[84]

Log of equilibrium constant, in 0.100 M Et_4NClO_4 at 23°[a]

	K_{so}	β_2[b]	β_2[c]
AgCl	-10.4	11.9	12.1
AgBr	-10.6	11.7	12.3
AgI	-12.0	13.1	13.2

[a] K_{so} is the solubility product of AgX, and β_2 is the overall formation constant of the complex AgX_2^-.
[b] From potentiometric titration data.
[c] From the shift of the polarographic wave obtained at a rotating platinum electrode.

$\times$ 10^{-7}, and the overall formation constants for the complexes TlCl and TlCl$_2$ were estimated to be $\beta_1 = (5 \pm 1) \times 10^2$ and $\beta_2 = (9 \pm 2) \times 10^3$, respectively[29].

From measurements of the EMF of the cell

Li(Hg)/LiCl in DMSO/TlCl(s)/Tl(Hg)

with varying concentrations of LiCl in the electrolyte, the Nernst relation was verified from 0.01–1.0 M within the accuracy of the known activity coefficients of LiCl in DMSO. The difference in standard potentials between the Li/Li$^+$ and Tl/Tl$^+$ electrodes was calculated to be 2.641 $\pm$ 0.003 V, which may be compared to the value of 2.694 Volts for aqueous solutions[29].

The potential of a solid Li electrode has been measured to be -2.86 V $vs.$ an Ag/AgBr electrode in 0.64 M LiBr, which corresponds to -3.30 V $vs.$ SCE[30]. This is 0.3 V more negative than the decomposition potential of Bu$_4$N$^+$ at a mercury electrode, and 0.85 V more negative than the polarographic half-wave potential for Li$^+$. This large difference results from the very low activity of Li in mercury[73].

The stability of the Fe(III) chloride complexes has been studied potentiometrically, and FeCl$_3$ has been found to be essentially completely dissociated in DMSO[74]. The homogeneous exchange reaction between Fe(II) and Fe(III) has been studied by isotopic techniques and found to be first order in each ion[75]. These results imply that the Fe^{2+}–Fe^{3+} redox couple should be simple and reversible in DMSO.

Potentiometric titrations of the halides and nitrates of NH$_4^+$, Cd^{2+}, Zn^{2+}, Mn^{2+}, Pb^{2+}, Sn^{2+} with NaOCH$_3$ in DMSO are possible using an antimony indicator electrode and an aqueous calomel reference electrode[85].

Although most acid–base studies that have been carried out in DMSO have used spectrophotometric measurements on indicators[23,31,76,77], some potentiometric studies have also been made using glass electrodes[23].

A potentiometric pH-scale was set up in DMSO solutions using a glass electrode with a silver chloride reference electrode, and standardizing with an 0.0441 M HCl solution. The pH was then assumed to be given by the equation:

$$\text{pH} = \frac{E - E^\circ}{0.0591}$$

in spite of the fact that the slope of the Nernst plot had given a change of about 70 mV/decade change in HCl concentration. The value of E° for the system used was -0.392 V, but this value presumably depends on the particular glass electrode under study[23].

With this system, the pH of an 0.01 M picric acid solution was measured and found to be 1.88, in agreement with the observation from conductance measurements that picric acid is completely dissociated in DMSO. A number of buffer solutions were measured, and the good agreement obtained between the potentiometric dissociation constants and those obtained spectrophotometrically is shown in Table 15.

From measurements of the conductance of Bu$_2$NH solutions, the ionization constant of this base was determined to be approximately $1 \cdot 10^{-7}$. From the potentiometric studies with a glass electrode summarized in Table 15, the ionization constant of the acid Bu$_2$NH$_2^+$ was determined to be $5 \cdot 10^{-11}$. These two values taken together give a value of $5 \cdot 10^{-18}$ for the autoprotolysis constant (ion product) of

TABLE 15

POTENTIOMETRIC ACID–BASE STUDIES IN DMSO USING THE GLASS ELECTRODE[23]

Buffer composition[a]	EMF[b] (V)	Potentiometric		Spectro. pKa
		pH	pKa	
0.0441 M HCl (standard)	−0.312	(1.35)	—	—
0.01019 M HPi	−0.281	1.88	—	—
0.0527 M HSal + 0.0506 M NaSal	+0.015	6.90	6.92	6.86
0.0111 M HBz + 0.0110 M NaBz	+0.193	9.92	9.92	9.95
4.98 × 10⁻⁴ M Na₂SO₄ + 4.95 × 10⁻⁴ NaHSO₄	+0.124	8.8	8.8	9.1
0.0482 M Bu₂NH + 0.0482 M Bu₂NH₂Cl + 0.01 to 0.1 M Et₄NClO₄	+0.213	10.3	10.3 uncertain due to	
0.0482 M Bu₄NH + 0.0482 M Bu₂NH₂Cl + 0.1 M NaClO₄	+0.158	9.3	effect of Na⁺	
0.111 M NH₄Cl	−0.045	5.87	10.8 (?)	
9.75 × 10⁻⁴ M Et₄NOH + 0.1% H₂O	+0.605	16.9	—	
0.0975 M Et₄NOH + 10% H₂O	+0.764	19.6	—	

[a] Pi = picrate, Sal = salicylate, Bz = benzoate, Bu = n-butyl.
[b] Glass electrode vs. Ag electrode in DMSO satd. with AgCl and NaCl. No correction for liquid junction potential.

DMSO. Using this value together with the measured pH of NH₄Cl, the ionization constant of NH_4^+ listed in Table 15 was obtained[23,31].

Tetraethylammonium hydroxide could not be prepared in an anhydrous solution in DMSO, but measurements with up to 10% water indicated that it was indeed a strong base and that pH-values as high as 20 can be attained. A titration of Et₄NOH with HCl shows two distinct end-points, the first corresponding to the titration of OH⁻ and the second, to the titration of some weaker base produced by the reaction of OH⁻ with DMSO. However, this other base is probably not the carbanion of DMSO[23]. Potentiometric titrations of quaternary ammonium ions have carried out using a glass indicator electrode and Bu₄NOH, NaOMe, or KOMe as titrant. No evidence of decomposition in the presence of these strong bases was observed[68]. Sulfinic and sulfonic acids in DMSO have been titrated using 0.1 N Bu₄NOH and Bu₄NOMe in benzene–methanol, with a glass indicator electrode[69].

ACTIVITY COEFFICIENTS OF ELECTROLYTES

Although DMSO has a convenient melting point (18.55°) and a reasonable cryoscopic constant (4.36°, molal scale), only two studies have been made of activity coefficients of electrolyte solutions in DMSO by the freezing-point depression method. The results of the first study[7], in which activity coefficients of LiClO₄, KI, KClO₄, KNO₃, NH₄NO₃, and AgNO₃ were determined, are probably incorrect[5] because no attempt was made to exclude water and an erroneous value (3.96) was used for the cryoscopic constant[10]. Unfortunately, no numerical data were given from which the results might be recalculated.

The only other study of this type was made recently by DUNNETT AND GASSER[5], who used carefully purified solvent with the highest freezing point (18.55°) yet reported, and obtained the activity coefficient values for LiCl shown in Figure 3.

The experimental data were lower than the values calculated using the extended Debye–Hückel equation with the constants for aqueous LiCl. This result was tentatively interpreted as evidence for ion-pairing, with an ion-pair dissociation constant of 0.19. The fact that no evidence was found for ion-pairs in the conductance studies
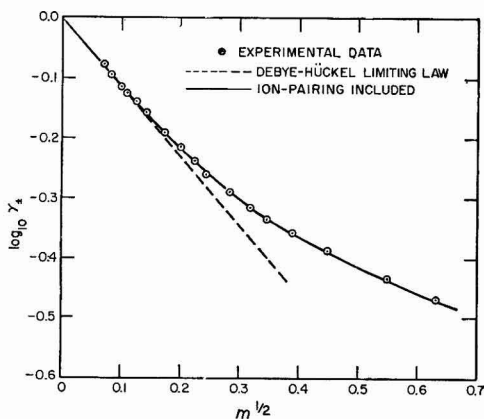
Fig. 3. Activity coefficients of LiCl in DMSO[5].

of LiCl–DMSO solutions does not contradict this result, because the large viscosity changes in the concentrated solutions could mask a small ion-pairing effect.

No measurements of activity coefficients by the potentiometric method have been published, but two such studies are in progress[29,71].

SAFETY CONSIDERATIONS

Although DMSO itself is of low toxicity, it is transported through the skin and incorporated into the bloodstream with incredible speed. Minutes after touching a drop of DMSO to the palm of the hand, its sweetish taste can be detected in the mouth. Thus, the primary safety precaution to be observed with DMSO is that solutions of toxic materials, particularly thallium, mercury, and other heavy-metal salts, must be scrupulously kept from contacting the skin. The use of polyethylene gloves, spill trays, and extremely careful waste disposal practices cannot be emphasized too strongly in experiments with solutions of any toxic material in DMSO[78].

SUMMARY

The literature on electrochemistry in dimethyl sulfoxide available at the beginning of 1966 is reviewed. Tables of physical properties, solubilities, conductance and polarographic and potentiometric data are given. The purification of DMSO; conductance studies; polarography of cations, anions, and gases; the reactions of quinones; the lithium electrode; the electrical double layer; reference electrodes; potentiometric studies; and the activity coefficients of electrolytes in DMSO are discussed.

REFERENCES*

1 *Dimethyl Sulfoxide, Technical Bulletin (ca. 1962)*, Crown Zellerbach Corp., Chemical Products Division, Camas, Wash.
2 P. G. SEARS, G. R. LESTER AND L. R. DAWSON, *J. Phys. Chem.*, 60 (1956) 1433–6.
3 T. B. DOUGLAS, *J. Am. Chem. Soc.*, 70 (1948) 2001–2.
4 W. H. SMYRL, *Solvent Properties of Dimethyl Sulfoxide*, U.S. Naval Ordnance Laboratory Symposium on Ammonia Batteries, 6 (1964) 30–33, AD 433 973.
5 J. S. DUNNETT AND R. P. H. GASSER, *Trans. Faraday Soc.*, 61 (1965) 922–7.
6 T. B. DOUGLAS, *J. Phys. Chem.*, 68 (1946) 1072–76.
7 T. SKERLAK, B. NIKOV AND V. SISLOV, *Glasnik Drustva Hemicara Tehnol. NR Bosne Hercegovine*, 11 (1962) 39–42; *C.A.*, 61 (1964) 3749f.
8 A. LYALL, H. N. SEIGER AND R. C. SHAIR, unpublished data, 1966.
9 J. J. LINDBERG, J. KENTTÄMAA AND A. NISSEMA, *Suomen Kemistilehti*, 34B (1961) 98–100.
10 T. SKERLAK AND B. NIKOV, *Glasnik Drustva Hemicara Tehnol. NR Bosne Hercegovine*, 11 (1962) 43–7; *C.A.*, 61 (1964) 2496d.
11 H. MACKLE AND P. A. G. O'HARE, *Trans. Faraday Soc.*, 58 (1962) 1912–15.
12 H. L. CLEVER AND C. C. SNEAD, *J. Phys. Chem.*, 67 (1963) 918–20.
13 R. G. LeBEL AND D. A. I. GORING, *J. Chem. Eng. Data*, 7 (1962) 100–1.
14 W. F. MEYERS, *Development of High Energy Density Primary Batteries*, Third Quarterly Report, Contract NAS 3-2775 (March 1964), NASA N64-18441.
15 J. J. LINDBERG, J. KENTTÄMAA AND A. NISSEMA, *Suomen Kemistilehti*, 34B (1961) 156–60.
16 Y. DOUCET, F. CALMES-PERRAULT AND M. T. DURAND, *Compt. Rend.*, 260 (1965) 1878–81.
17 R. A. HOVERMALE AND P. G. SEARS, *J. Phys. Chem.*, 60 (1956) 1579–80.
18 F. A. COTTON AND R. FRANCIS, *J. Am. Chem. Soc.*, 82 (1960) 2986.
19 H. L. SCHLÄFER AND W. SCHAFFERNICHT, *Angew. Chem.*, 72 (1960) 618–26.
20 H. F. BAUMAN, *Limited Cycle Secondary Battery Using Lithium Anode*, Technical Documentary Report APL-TDR-64-59 (May 1964), AD 601128.
21 I. M. KOLTHOFF AND T. B. REDDY, *J. Electrochem. Soc.*, 108 (1961) 980–5.
22 W. F. MEYERS AND S. G. ABENS, *Development of High Energy Density Primary Batteries*, Second Quarterly Report, Contract NAS 3-6004 (Dec. 1964), NASA CR 54307.
23 T. B. REDDY, *Electrochemical and Acid–Base Studies in Dimethyl Sulfoxide*, Ph.D. Thesis, University of Minnesota, 1960, University Microfilms No. 60–5606.
24 H. F. BAUMAN, J. E. CHILTON AND R. MAURI, *Lithium Anode Limited Cycle Battery Investigation*, Technical Report AFAPL-TR-66-35 (April 1966).
25 R. E. DODD AND R. P. H. GASSER, *Proc. Chem. Soc.*, (1964) 415.
26 J. KENTTÄMAA, *Suomen Kemistilehti*, 33B (1960) 179–82.
27 A. LYALL, H. N. SEIGER AND R. C. SHAIR, *Lithium–Nickel Halide Secondary Battery Investigation*, Technical Report AFAPL-TR-65-11 (Jan. 1965), AD 612 492.
28 J. FARRAR, R. KELLER AND M. M. NICHOLSON, *High Energy Battery System Study*, First Quarterly Report, Contract DA-36-039-AMC-03201(E) (Sept. 1963), AD 429 290.
29 D. R. COGLEY AND J. N. BUTLER, *J. Electrochem. Soc.*, 113 (1966) 1074–8.
30 C. A. MELENDRES, M.S. Thesis, University of California, 1965. U.S. Atomic Energy Comm. Report UCRL 16330.
31 I. M. KOLTHOFF AND T. B. REDDY, *Inorg. Chem.*, 1 (1962) 189–94.
32 W. F. MEYERS AND S. G. ABENS, *Development of High Energy Density Primary Batteries*, Third Quarterly Report, Contract NAS 3-6004 (March 1965), NASA CR 54659.

* All reports listed in this bibliography are available from the U.S. Department of Commerce, Clearinghouse for Federal, Scientific and Technical Information, Springfield, Virginia 22151.

33 E. J. COREY AND M. CHAYKOVSKY, *J. Am. Chem. Soc.*, 84 (1962) 866–7.
34 E. J. COREY AND M. CHAYKOVSKY, *J. Am. Chem. Soc.*, 87 (1965) 1345–53.
35 R. G. SELIM, K. R. HILL AND M. B. RAO, *Research and Development of a High-Capacity Non-aqueous Secondary Battery*, Fourth Quarterly Report, Contract NAS 3-6017 (Nov. 1965), NASA CR 54874.
36 J. FARRAR, R. KELLER AND M. M. NICHOLSON, *High Energy Battery System Study*, Final Report, Contract DA-36-039-AMC-03201(E) (June 1965), AD 622 818.
37 J. L. ROBERTS AND D. T. SAWYER, *J. Electroanal. Chem.*, 9 (1965) 1–7.
38 D. P. AMES AND P. G. SEARS, *J. Phys. Chem.*, 59 (1955) 16–19.
39 P. G. SEARS, R. K. WOLFORD AND L. R. DAWSON, *J. Electrochem. Soc.*, 103 (1956) 633–6.
40 W. F. LUDER AND C. A. KRAUS, *J. Am. Chem. Soc.*, 69 (1947) 2481.
41 J. A. PORTER, U. S. Atomic Energy Comm. Report DP-389 (1959).
42 S. B. BRUMMER, *J. Chem. Phys.*, 42 (1965) 1636–46.
43 V. GUTMANN AND G. SCHÖBER, *Z. Anal. Chem.*, 171 (1959) 339–43.
44 G. SCHÖBER AND V. GUTMANN, *Advances in Polarography: Proceedings 2nd International Congress, Cambridge, 1959*, 3, 940-7, Pergamon Press, London, 1960.
45 R. T. BURRUS, *Polarographic Studies in Dimethyl Sulfoxide*, Ph.D. Thesis, University of Tennessee, 1962, University Microfilms No. 63-4101.
46 G. SCHÖBER AND V. GUTMANN, *Monatsh.*, 90 (1959) 897–902.
47 V. GUTMANN, P. HEILMAYER AND G. SCHÖBER, *Monatsh.*, 92 (1961) 240–5.
48 E. L. JOHNSON, K. H. POOL AND R. E. HAMM, *Anal. Chem.*, 38 (1966) 183–5.
49 M. E. PEOVER AND B. S. WHITE, *Chem. Commun.*, (1965) 183–4.
50 D. L. MARICLE AND W. G. HODGSON, *Anal. Chem.*, 37 (1965) 1562–5.
51 V. GUTMANN AND G. SCHÖBER, *Monatsh.*, 93 (1962) 212–18.
52 R. A. OSTERYOUNG, R. L. MCKISSON, P. H. DUTCH, G. LAUER AND E. B. LUCHSINGER, *Development of a Light-weight Secondary Battery System*, Final Report, Contract DA-36-039 SC-88925 (1962), AD 290 326.
53 R. IWAMOTO, *Anal. Chem.*, 31 (1959) 955.
54 G. SCHÖBER AND G. REHAK, *Monatsh.*, 93 (1962) 445–52.
55 H. DEHN, V. GUTMANN AND G. SCHÖBER, *Monatsh.*, 93 (1962) 453–4.
56 H. DEHN, V. GUTMANN AND G. SCHÖBER, *Mikrochim. Acta*, (1962), 959–62.
57 H. DEHN, V. GUTMANN AND G. SCHÖBER, *Monatsh.*, 93 (1962) 877–80.
58 H. DEHN AND G. SCHÖBER, *Monatsh.*, 93 (1962) 1448–9.
59 W. SLOUGH, *Chem. Commun.*, (1965) 184–5.
60 G. SCHÖBER, *Abhandl. Deut. Akad. Wiss. Berlin, Kl. Chem. Geol. Biol.*, (1964) 496–7.
61 H. DEHN, V. GUTMANN, H. KIRCH AND G. SCHÖBER, *Monatsh.*, 93 (1962) 1348–52.
62 V. GUTMANN, *Polarographic Studies in Non-aqueous Systems*, U.S. Dept. Comm. (1964), AD 433 694.
63 A. LEDWITH AND N. MCFARLANE, *Proc. Chem. Soc.*, (1964) 108.
64 D. E. O'CONNOR AND W. I. LYNESS, *J. Org. Chem.*, 30 (1965) 1620–3.
65 J. FARRAR, R. KELLER AND M. M. NICHOLSON, *High Energy Battery System Study*, Fourth Quarterly Report, Contract DA-36-039-AMC-03201(E) (June 1964), AD 450 559.
66 J. FARRAR, R. KELLER AND C. J. MAZAC, *Procedings Power Sources Conference*, 18 (1964) 92–94.
67 D. P. BODEN, H. R. BUHNER AND V. J. SPERA, *High Energy Battery System–Organic Electrolyte*, First Quarterly Report, Contract DA 28-043-AMC-0134(E) (Oct. 1965).
68 K. K. BARNES AND C. K. MANN, *Anal. Chem.*, 36 (1964) 2502–3.
69 D. L. WETZEL AND C. E. MELOAN, *Anal. Chem.*, 36 (1964) 2474–7.
70 T. SKERLAK AND V. MILICEVIC, *Glasnik Drustva Hemicara Tehnol. NR Bosne Hercegovine*, 11 (1962) 49–52; *C.A.*, 61 (1964) 2461c.
71 W. H. SMYRL AND C. W. TOBIAS, *J. Electrochem. Soc.*, 113 (1966) 754–5.
72 T. SKERLAK, B. SKUNDRIC AND P. DUTINA, *Glasnik Drustva Hemicara Tehnol. NR Bosne Hercegovine*, 11 (1962) 53–7; *C.A.*, 61 (1964) 2724b.
73 M. O. DAVIES et al., *The Physical and Chemical Properties of Dilute Alkali Metal Amalgams*, Technical Report No. 7, Contract Nonr 581(00) (1957), AD 138 849.
74 V. GUTMANN AND G. HAMPEL, *Monatsh.*, 94 (1963) 830–7.
75 J. MENASHI, W. L. REYNOLDS AND G. VAN AUKEN, *Inorg. Chem.*, 4 (1965) 299–304.
76 E. C. STEINER AND J. M. GILBERT, *J. Am. Chem. Soc.*, 85 (1963) 3054–5.
77 E. C. STEINER AND J. M. GILBERT, *J. Am. Chem. Soc.*, 87 (1965) 382–4.
78 A. BUCKLEY, *J. Chem. Educ.*, 42 (1965) 674.
79 S. G. ABENS, T. X. MAHY, W. MERZ AND W. F. MEYERS, *High Energy Density Primary Batteries*, Final Report, Contract NAS 3-6004 (March 1966), NASA CR-54803.
80 D. L. MCMASTERS, R. B. DUNLAP, L. W. KREIDER, T. R. SHEARER AND J. R. KÜMPEL, *Anal. Chem.*, in press, 1966.
81 W. L. REYNOLDS AND H. S. SILESKY, *J. Chem. Eng. Data*, 5 (1960) 250.

82 J. M. G. COWIE AND P. M. TOPOROWSKI, *Can. J. Chem.*, 39 (1961) 2240–3.
83 T. B. REDDY AND D. L. MARICLE, unpublished results, 1966.
84 D. C. LUEHRS, R. T. IWAMOTO AND J. KLEINBERG, *Inorg. Chem.*, 5 (1966) 201–4.
85 T. JASINSKI AND K. STEFANIUK, *Chem. Anal. (Warsaw)*, 10 (1965) 983–87.
86 B. G. SLAY AND B. G. CARBAJAL, *J. Electrochem. Soc.*, 113 (1966) 306.
87 G. GRITZNER, V. GUTMANN AND G. SCHÖBER, *Mikrochim. Acta*, (1964) 193–195.
88 G. GRITZNER, V. GUTMANN AND G. SCHÖBER, *Monatsh.*, 96 (1965) 1056–64.
89 G. GRITZNER, V. GUTMANN AND M. MICHLMAYR, *Z. Anal. Chem.*, in press.
90 M. MICHLMAYR, G. GRITZNER AND V. GUTMANN, in press.
91 T. B. REDDY, *Purification of Dimethyl Sulfoxide for Electrochemical Experimentation*, Report to the Sub-commission on Non-Aqueous Solvents, IUPAC, 1965.
92 G. G. PRICE AND M. C. WHITING, *Chem. and Ind. London*, (1963) 775.

NOTE ADDED IN PROOF (OCT. 1966)

The following references appeared too late to be included in the review, but are presented here because of their importance.

93 E. M. ARNETT AND D. R. McKELVEY, Enthalpies of transfer from water to DMSO for some ions and molecules, *J. Am. Chem. Soc.*, 88 (1966) 2598–9.
94 J. I. BRAUMAN AND N. J. NELSON, Rates of proton exchange between DMSO and its conjugate base, *J. Am. Chem. Soc.*, 88 (1966) 2332–4.
95 B. W. CLARE, D. COOK, E. C. F. KO, Y. C. MAC AND A. J. PARKER, Solvation of ions. IX. The effect of anion solvation on acid dissociation constants in methanol, water, dimethylformamide, and DMSO, *J. Am. Chem. Soc.*, 88 (1966) 1911–16.
96 R. S. GEORGE AND R. K. ROHWER, Cryoscopic molecular weight determinations using DMSO as solvent, *Anal. Chem.*, 38 (1966) 1285.
97 M. C. GIORDANO, J. C. BAZAN AND A. J. ARVIA, The electrolysis of DMSO solutions of NaCl and NaI, *Electrochim. Acta*, 11 (1966) 741–8.
98 M. R. LINDBECK, Controlled potential coulometry in non-aqueous solvents, *Thesis*, Oregon State University, 1966. University Microfilms No. 66-3931.
99 R. PAYNE, The electrical double layer in DMSO solutions, *J. Am. Chem. Soc.*, (1967) in press.
100 M. E. PEOVER AND B. S. WHITE, Electrolytic reduction of oxygen in aprotic solvents: The superoxide ion, *Electrochim. Acta*, 11 (1966) 1061–7.
101 D. T. SAWYER AND J. L. ROBERTS, Electrochemistry of oxygen and superoxide ion in DMSO at Pt, Au and Hg electrodes, *J. Electroanal. Chem.*, 12 (1966) 90–101.

SHORT COMMUNICATIONS

A note on the theory of catalytic currents in linear-sweep polarography. A reversible chemical reaction (pseudo-first order) parallel to the electron-transfer process

The problem of catalytic currents in voltammetry with linearly changing potential has been treated from a theoretical point of view by many authors[1-5]; in the present work, a solution of the same problem is attempted for a chemical reaction, parallel to the electron-transfer process, and reversible. The differential system was solved by the Laplace transform method. A solution is achieved where the i–t expression in the absence of a catalytic process is that given by SevČik[6].

Let us assume that the electron-transfer process is reversible, and then the Nernst equation can be applied. The kinetic process is:

$$R + Z \underset{K_2'}{\overset{K_1'}{\rightleftharpoons}} Ox + Y \tag{1}$$

where K_1' and K_2' are the rate constants. In the case of an excess of Z and Y we can write: $K_1 = K_1'Z$ and $K_2 = K_2'Y$ (Z and Y are not reducible in the potential range used).

The rate expression of this process is:

$$v = K_1 C_{red} - K_2 C_{ox} \tag{2}$$

where $C_{ox}(x,t)$, $C_{red}(x,t)$ are the instantaneous concentrations of the oxidized and reduced forms, respectively.

The potential of the electrode varies as:

$$E = E_1 - vt \tag{3}$$

(E_1 = potential at $t = 0$; v = rate of potential sweep).

At the electrode ($x = 0$), the Nernst equation holds:

$$C_{ox}(0,t) = C_{red}(0,t) \exp(nF/RT)(E - E_n) \tag{4}$$

where E_n is the formal electrode potential and n the number of electrons.

At $t = 0$, the forms Ox and Red are at equilibrium:

$$C_{red}^*/C_{ox}^* = K_2/K_1 = r \tag{5}$$

C_{ox}^*, C_{red}^* are the bulk concentrations of Ox and Red. The diffusion coefficients of Ox and Red are assumed to be equal (D). Adsorption or migration phenomena and double-layer effects are neglected. The diffusion is planar and semi-infinite and the electrode surface (q) may be considered as constant. These assumptions are justified under the experimental conditions[1].

If the proper differential system with the Laplace transformation are used the following expressions for the electrode concentrations can be obtained (details of calculations will be published elsewhere):

$$C_{ox}(0,t) = \frac{(1+r)C_{ox}{}^*}{1+\alpha \exp(v^*t)} \tag{6}$$

$$C_{red}(0,t) = \frac{(1+r)C_{ox}{}^* \exp(v^*t)}{1+\alpha \exp(v^*t)} \tag{7}$$

Here $\alpha = \exp(nF/RT)(E_n - E_i)$, $v^* = (nF/RT)v$.

The instantaneous current is given by:

$$i(t) = \frac{n^{\frac{3}{2}}F^{\frac{3}{2}}q\sqrt{D}\,C_{ox}{}^*(1+r)\sqrt{v}}{\sqrt{RT}} \cdot \frac{1}{2}\int_0^{\tau} \frac{1}{2\cosh^2\frac{1}{2}(\eta - \tau_{\frac{1}{2}})} \times$$

$$\left[\frac{e^{-\lambda(\tau-\eta)}}{\sqrt{\pi(\tau-\eta)}} + \sqrt{\lambda}\,\mathrm{erf}\sqrt{\lambda(\tau-\eta)}\right]d\eta \tag{8}$$

where $\lambda = (K_1 + K_2)/v^* = l/v^*$; $\tau = v^*t$, and $t_{\frac{1}{2}} =$ the instant when $C_{ox}(0,t) = C_{red}(0,t)$.

For $\lambda = 0$ we have that the current is diffusion controlled (SEVĆIK's equation[6]).

For $t \to \infty$ $(\tau \to \infty)$ the current approaches:

$$\lim_{t\to\infty} i(t) = nFq\sqrt{D}\,C_{ox}{}^*\sqrt{K_1 + K_2} \tag{9}$$

Therefore we find the asymptotic value of the current in the form reported by the above mentioned authors[1], with the difference that, in our case, the asymptotic current is proportional to: $\sqrt{K_1 + K_2}$.

For $\lambda \gg 1$ $(l \gg v^*)$:

$$i(t) = nFq\sqrt{D}\,C_{ox}{}^*\sqrt{l}\,\frac{(1+r)\,\mathrm{tgh}\dfrac{v^*}{2}(t-t_{\frac{1}{2}}) + (1-r)}{2} \tag{10}$$

Equation (9) shows that the set of curves obtained for various values of v, presents a common asymptote parallel to the t-axis. Hence, if the remaining quantities are known it is possible to calculate $l = K_1 + K_2$.

The general behaviour of the curves, given by (8), is easily obtainable from the numerical evaluation of the integral. The current is always proportional to $\sqrt{v}$; for $l < (nF/RT)v$ the curves present a peak which disappears for $l > (nF/RT)v$.

Istituto di Chimica,   L. Rampazzo
Facolta' di Ingegneria,
Rome (Italy)

1 J. M. Savéant and E. Vianello, *Advances in Polarography*, Pergamon Press, London, 1960, p. 367.
2 R. S. Nicholson and J. Shain, *Anal. Chem.*, 36 (1964) 706.
3 J. M. Savéant and E. Vianello, *Electrochim. Acta*, 10 (1965) 905.
4 J. Weber, *Collection Czech. Chem. Commun.*, 24 (1959) 1770.
5 H. Kao, T. S. Chang and W. B. Chang, *Sci. Sinica (Peking)*, 13 (1964) 1411.
6 A. Sevćik, *Collection Czech. Chem. Commun.*, 13 (1948) 349.

The reduction of N,N-dimethyl-p-nitrosoaniline

The quantitative usage of cyclic techniques in electrode mechanism studies has been given a great impetus by recent theoretical developments. In particular, the studies by BARD AND HERMAN in cyclic chronopotentiometry[1] and by NICHOLSON AND SHAIN in cyclic voltammetry[2] have been very valuable. Despite the advances in both theory and technique, the successful elucidation of organic electrode processes *at solid electrodes* is fraught with many problems. Specifically, it is difficult to generalize from one system to the next with regard to how important a role the electrode surface will play in the overall process. In this connection we believe it is very worthwhile to establish several test or model systems for various types of electrode processes. A test system is one that adheres to the diagnostic criteria of at least several electroanalytical methods and has product or intermediate identification by independent techniques. More complex situations or cases where electrode surface interactions cause anomalies in the experimental data can be compared and evaluated with respect to the test systems.

Test systems for a simple follow-up chemical reaction (EC) process[3] and a two-stage oxidation with and without chemical complications on the second step have been described[4]. This short communication describes a test system for an ECE process (electron transfer–chemical reaction–electron transfer). This is the reduction of N,N-dimethyl-p-nitrosoaniline. While the overall process is to be expected from previous studies of nitroso compounds, it is the adherence of the experimental data to theoretical predictions that is of interest in the sense of a test system.

Experimental

A carbon-paste electrode (CPE) of geometrical area 0.238 cm^2, as described previously, was used[3]. The N,N-dimethyl-p-nitrosoaniline was Eastman White Label and was recrystallized from benzene, m.p. 87–88°. N,N-dimethyl-p-phenylenediamine hydrochloride was also Eastman White Label and was used without further purification. Solutions were prepared immediately before use by dissolving a weighed amount of the sample in de-aerated buffer solutions. Triply-distilled water was used in the preparation of Britton and Robinson (B & R) buffers. All electrochemical measurements were made in a thermostatted water bath at $25.0 \pm 0.1°$ and all potentials are reported *vs.* S.C.E.

The instrumentation for cyclic voltammetry and chronopotentiometry was conventional. EPR-measurements were made at room temperature on a Varian V-4500 X-band spectrometer with 100-kc field modulation.

Figure 1 shows a cyclic polarogram of N,N-dimethyl-p-nitrosoaniline (DMNA) at the CPE in pH 2.3 buffer. On the first cathodic scan initiated at $+0.6$ V, one wave is observed with $E_{p/2} = +0.063$ V corresponding to the reduction of DMNA. On reversal of the potential scan at *ca.* -0.15 V, no reverse current is indicated for the oxidation of the reduction product. Instead, a new redox couple is observed with an anodic $E_{p/2} = +0.392$ V on the second and all subsequent scans. As was originally suggested, but not verified, by HOLLECK AND SCHINDLER[5] the new couple may be readily identified as belonging to N,N-dimethyl-p-phenylenediamine (DPPD).

The reduction of aromatic nitroso compounds, in particular p-nitrosophenol, has been shown to proceed by an ECE mechanism[6], *i.e.*, an electrode reaction followed
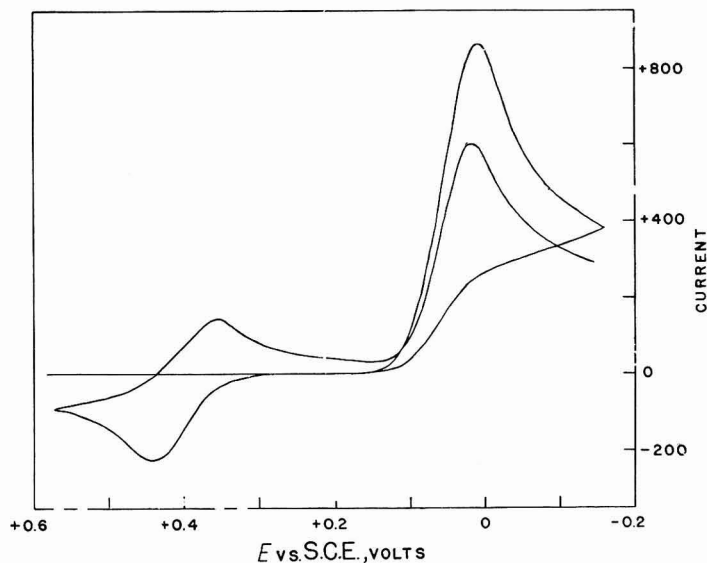
Fig. 1. Cyclic voltammetry of DMNA. 2.37×10^{-3} M N,N-dimethyl-p-nitrosoaniline in pH 2.3 Britton and Robinson buffer at 25.0°. CPE area, 0.238 cm²; scan rate, 10.00 V/min.

by a chemical reaction (or series of chemical reactions) to produce a product which is also electrolyzed at the potential in question. A similar mechanism may also be written for the reduction of DMNA:
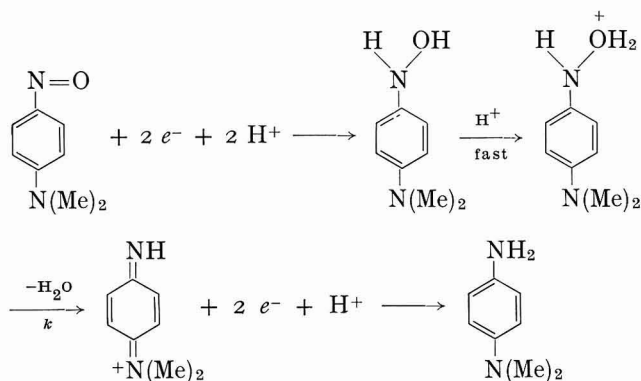
Cyclic chronopotentiometry combined with current program techniques was used to verify this mechanism. Chronopotentiometric reduction of DMNA according to the above scheme involves a total of four electrons. The reoxidation of the product, N,N-dimethyl-p-phenylenediamine (DPPD), is a two-electron process. Therefore, if the current for the oxidation process is programmed such that $i_{anodic} = -0.207$ $i_{cathodic}$ (*i.e.*, $i_{anodic}/n_{anodic} = -0.414$ $i_{cathodic}/n_{cathodic}$, where n represents the number of electrons involved in each step) a 1:1 ratio of the anodic transition time to the cathodic reduction time, $t_c \leq \tau_c$, should result. Furthermore, if the current is again

reversed so that the product of the oxidation process is reduced and $i_{cathodic}' = -0.414$ $i_{anodic} = 0.086$ $i_{cathodic}$, a cathodic transition time should be observed, the ratio of which to the previous anodic transition time should be $1:1$. Therefore, for the total cyclic process, $t_c:\tau_a:\tau_c = 1:1:1$ if the above mechanism is correct. Figure 2 shows a cyclic chronopotentiogram obtained from the reduction of DMNA and the cyclic oxidation and reduction processes. Initially, the potential drops to $ca.$ $+0.08$ V where DMNA is reduced, in an overall process of four electrons, to DPPD. Upon current reversal, the potential increases rapidly to $ca.$ $+0.4$ V where DPPD is oxidized. As
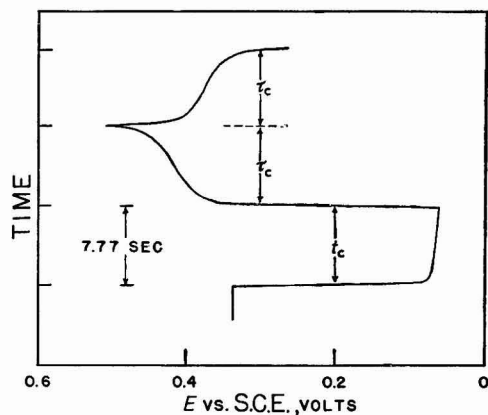
Fig. 2. Cyclic chronopotentiogram of DMNA. 2.75×10^{-3} M N,N-dimethyl-p-nitrosoaniline in pH 2.3 Britton and Robinson buffer at 25.0°. CPE area, 0.238 cm²; $i_c = 139$ μA; $i_a = -28.8$ μA; $i_c' = 11.95$ μA.

was observed in the cyclic voltammetry, no oxidation wave is observed at potentials corresponding to the oxidation of the initial reduction product, $i.e.$, the oxidation of p-N,N-dimethylaminophenylhydroxylamine to DMNA. On current reversal at the anodic transition time, the wave for the reduction of N,N-dimethyl-p-phenylenedi-imine is observed. As was predicted by the above mechanism, the observed ratios of the forward time, t_c, to the anodic and cathodic transition times, τ_a and τ_c, respectively, is $1:1:1$.

Electrolysis coupled with EPR spectroscopy further substantiated that DPPD is the product of the reduction of DMNA. The following experiment was performed. An approximately 10^{-3} M solution of DMNA in pH 2.3 buffer was exhaustively electrolyzed at -0.1 V. After electrolysis the potential was switched to $ca.$ $+0.5$ V and the product of the reduction was reoxidized. This solution was then flowed under nitrogen into the cavity of the EPR spectrometer. An EPR spectrum was recorded which was identical with one obtained from the oxidation of an authentic sample of N,N-dimethyl-p-phenylenediamine. This EPR spectrum is that of the so-called Wurster's Red cation radical; as this is an unsymmetrical radical ion, the EPR spectrum is complex and its complete, unequivocal interpretation was unsuccessful in our hands. Others have had difficulty with a complete interpretation of this spectrum but it is not a particularly important system. The absolute identity of the EPR spectra from the electrolysis mixture and an authentic sample of N,N-dimethyl-p-phenylenediamine is sufficient for the present arguments.

Although the rate of dehydration of p-N,N-dimethylphenylhydroxylamine was very fast, as indicated by the CV and cyclic chronopotentiometry, an estimate of the pseudo-first-order rate constant in pH 2.3 buffer was obtained from the empirical relationship

$$\frac{k}{V} = \frac{nF}{RT}\left[\frac{0.4 - (i_k/i_d)\,(0.396)}{(i_k/i_d)\,(0.469) - 1}\right]$$

as given by NICHOLSON AND SHAIN[6]. The i_k-values are peak currents obtained from linear sweep polarograms at various sweep rates; i_d is the peak current that would have been observed in the absence of a chemical reaction, V is the scan rate in V sec^{-1}, n is the number of electrons in the first electron-transfer reaction and the other terms have their usual significance. Values of i_d were calculated from the known electrode area and diffusion coefficient value of 1.13×10^{-5} cm^2 sec^{-1} as determined by chronopotentiometric and Cottrell measurements. Voltage sweep rates from 1.25 to 25.00 V/min were employed. A plot of k/V against $1/V$ yielded a straight line the slope of which gave a value of 0.9 sec^{-1} for the rate constant. This value is consistent with that observed in the p-nitrosophenol system and is in the direction one would expect from elementary substituent effects.

The adherence of the reduction of DMNA to the recent theoretical treatment of NICHOLSON AND SHAIN[2] was also briefly investigated. However, there was difficulty in correlating experimental peak polarograms with those constructed from theory, due to the apparent irreversibility of the initial electron-transfer process. As was expected, a pH-dependence on the peak potential of 60 mV/pH was observed, corresponding to the two-proton dependence of the initial reduction of DMNA to p-N,N-dimethylaminohydroxylamine. For a reversible two-electron process, $E_{p/2} - E_p$ should equal 28.5 mV. A value of 56 mV was obtained in this study from which αn_a was calculated to be 0.856. Theoretical peak polarograms constructed from the data given by NICHOLSON AND SHAIN for an irreversible charge transfer followed by an irreversible chemical reaction and another charge-transfer process, agreed well within 5% of the experimentally observed polarogram over the complete polarographic wave.

Department of Chemistry,   DONALD W. LEEDY
University of Kansas,   RALPH N. ADAMS
Lawrence, Kansas 66044 (U.S.A.)

1 A. J. BARD AND H. B. HERMAN, *Polarography 1964, Proc. 3rd Intern. Congr. Polarogr., Southampton, 1964*, edited by G. J. HILLS, Macmillan, London, 1966, p. 373, and references therein.
2 R. S. NICHOLSON AND I. SHAIN, *Anal. Chem.*, 36 (1964) 706; 37 (1965) 178.
3 D. HAWLEY AND R. N. ADAMS, *J. Electroanal. Chem.*, 8 (1964) 163.
4 R. F. NELSON, D. W. LEEDY, E. T. SEO AND R. N. ADAMS, *Z. Elektrochem.*, in press.
5 L. HOLLECK AND R. SCHINDLER, *Z. Elektrochem.*, 60 (1956) 1138.
6 R. S. NICHOLSON AND I. SHAIN, *Anal. Chem.*, 37 (1965) 190.

The electrometric estimation of citral present in lemon grass oil

During the course of an investigation of the electroreduction of lemon grass oil, it was necessary to estimate the content of citral which is a very important constituent of lemon grass oil. It is usually estimated by the hydroxylamine hydrochloride method[1] in which the colour change at the end-point using indicators such as bromophenol blue or methyl orange is difficult to see. It was considered that a more precise determination of the hydrochloric acid released during oxime formation could be obtained using an electrometric method.

Experimental

Lemon grass oil. The indigenously available oil was purified by distillation under reduced pressure. The portion boiling in the range 125–135° at a pressure of 85 mm of mercury was collected and used for the estimation. In some experiments, the oil was used without purification.

Isolation of pure citral. Pure citral for calibration experiments was isolated from the lemon grass oil by the sodium bisulphite method[2].

Procedure. 5 ml of lemon grass oil was made up to 100 ml with pure alcohol. Exactly 35 ml of 0.5 N alcoholic hydroxylamine hydrochloride was added to 10 ml of the solution in a 250-ml conical flask. The solution was left for an hour with frequent shaking to complete oxime formation. After completion of the reaction, the hydrochloric acid released during oximation was estimated by titration with standard 0.5 N sodium hydroxide by the following methods. A blank was carried out under identical conditions, for each experiment.

(i) Redoxokinetic method. The technique employed has already been described[3]. Quinhydrone was added after oximation and the solution was titrated with 0.1 N sodium hydroxide. The curves were obtained by plotting the volume of titrant against galvanometer deflection and a typical result is given in Fig. 1(a). Inset in the graph is the corresponding derivative curve near the end-point. This indicates the sensitivity of this method.

(ii) Visual method. The method employed was the same as that given in ref. 1. The direct titration of the liberated acid with sodium hydroxide was not adopted since the colour change of the indicator at the end-point is not sharp. Excess of sodium hydroxide was added and the excess titrated with standard hydrochloric acid using methyl orange as indicator.

(iii) Potentiometric and conductometric methods. The released hydrochloric acid was titrated potentiometrically (quinhydrone–calomel electrodes); the curve is shown in Fig. 1(b). The titration was also carried out using a glass–calomel electrode system and a Beckmann pH meter. The results obtained in the conductometric titration using a Philips conductivity bridge are shown in Fig. 1(c).

(iv) Polarographic method[4]. Current–voltage curves were obtained with a manual polarograph (Southern Analytical Ltd., A 1650) in conjunction with a Pye spot-galvanometer, having a sensitivity corresponding to 0.86 μA/100 mm. The temperature was kept at 30° ± 2°. A saturated calomel electrode was used as a reference electrode. The capillary characteristics were: $m = 1.56$ mg/sec; $t = 3.05$ sec/dsec (open circuit); $h = 40$ cm of mercury. All the solutions were prepared from analytical-grade reagents. An H-type polarographic cell was used. All solutions were degassed by a
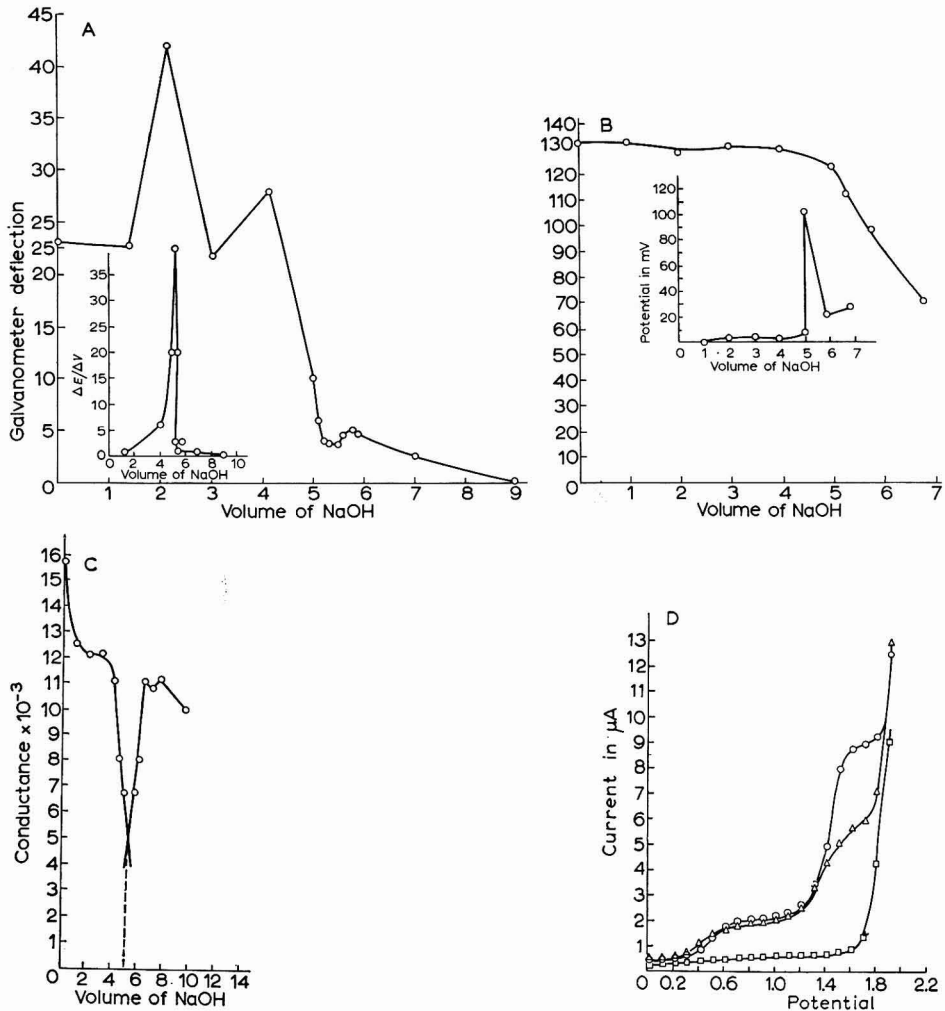
Fig. 1. (a) Redoxokinetic titration. (b) Potentiometric titration (quinhydrcne–calomel). (c) Conductometric titration. (d) Polarograms of citral in lemon grass oil.

stream of electrolytically-prepared oxygen-free hydrogen. The glass electrode was used for pH measurements. Representative polarograms for the reduction of citral are presented in Fig. 1(d).

Calibration procedure. A calibration curve for pure citral isolated from lemon grass oil was prepared by pipetting a suitable aliquot of a standard stock solution (0.2 g of pure citral diluted to 100 ml with pure ethanol) into a 100-ml volumetric flask. Citral solutions of 7 different concentrations were prepared and polarograms taken for each using a borate buffer as supporting electrolyte. A plot of citral concentration (C) *vs*. diffusion current (i_d) is linear for a citral concentration range of 0.5–5.00 mm. The extrapolated curve passes through the origin and the average relative standard deviation of the diffusion current quotient (i_d/C) is 2.8%. The

proportionality between diffusion current and citral concentration is shown in Table 1.

Results

The results obtained by various methods for the estimation of citral (see Table 2) show that electrometric methods are more accurate than the direct visual titration using indicators. Among the electroanalytical methods, the polarographic method has been found to be especially advantageous as it is very quick and accurate.

TABLE 1

PROPORTIONALITY BETWEEN i_d AND CITRAL CONCENTRATION

Citral concn. (mM)	i_d	i_d/c
0.1	1.19	2.38
1.0	2.28	2.28
1.5	3.56	2.37
2.0	4.80	2.40
2.5	5.60	2.24
	Av.	2.34

TABLE 2

ESTIMATION OF CITRAL IN LEMON GRASS OIL BY DIFFERENT METHODS

0.3801 g of citral is taken for each estimation

Method employed	W. of citral estimated (g)	Error (%)
1. Direct volumetric using indicators	0.4050	6.55
2. Potentiometric:		
(i) Quinhydrone–calomel	0.3896	1.97
(ii) Glass–calomel	0.3723	2.05
3. Conductivity	0.3723	2.05
4. Redoxokinetic	0.3876	1.84
5. Polarographic	0.3780	0.50

Central Electrochemical   A. P. Shakunthala
Research Institute,   M. S. V. Pathy
Karaikudi-3 (India)

1 J. Mitchell, *Organic Analysis*, Vol. I, Interscience Publishers, New York-London, 1953, p. 260,
2 A. Russel and R. L. Kenyon, *Organic Synthesis*, Vol. 23, John Wiley & Sons, New York, 1943. p. 78.
3 S. Krishnan, M. S. V. Pathy and H. V. K. Udupa, *J. Electroanal. Chem.*, 11 (1966) 68.
4 I. M. Kolthoff and J. J. Lingane, *Polarography*, Vol. II, Interscience Publishers, New York-London, 2nd edn., 1955, p. 660.

Identifikation der Anodic-Stripping-Peaks von Pb/Au-Legierungen

Bei früheren chronoamperometrischen Anodic-Stripping-Versuchen[1] an extrem dünnen Bleiniederschlägen auf Goldelektroden wurde das Auftreten einer Serie von fünf anodischen Strommaxima festgestellt, von denen zwei (in Tab. 1 mit IIIa und IIIb bezeichnet) aller Wahrscheinlichkeit nach der Auflösung definierter intermetallischer Pb/Au-Verbindungen zuzuschreiben sind. Eine röntgenographische Identifikation der vorliegenden Legierungen nach dem Rückstrahlverfahren scheiterte jedoch an experimentellen Schwierigkeiten, ebensowenig führten Zuordnungsversuche durch Vergleich der gemessenen Peakpotentiale mit den Ruhepotentialen thermisch hergestellter Pb/Au-Legierungen[2] zum Ziel.

Nach Angaben von WEAVER UND BROWN[3] lässt sich aber die Legierungsbildung in kombinierten Blei/Gold-Aufdampfschichten optisch und diffraktographisch gut verfolgen; es lag daher nahe zu prüfen, ob sich möglicherweise aus dem Anodic-Stripping-Verhalten von Pb/Au-Belägen dieser Art, deren Phasenzusammensetzung röntgenographisch offenbar leicht überprüft werden kann, irgendwelche Schlüsse hinsichtlich der Natur der chronoamperometrischen Ablösepeaks IIIa und IIIb herleiten lassen. Dazu wurde eine geeignete inerte Trägerfolie (Polyesterfolien Mylar (du Pont) bzw. Melinex (ICI), Stärke 0.127 mm) in einer Hochvakuumaufdampfanlage (Balzers Typ BA 350 E, Restdruck ca. 10^{-5} mm Hg) nacheinander (ohne Vakuumunterbruch) mit einem Goldüberzug von ca. 150 Atomlagen und einer Bleischicht von ca. 500 Atomlagen versehen.

Die erhaltenen Zweifachbeläge wurden bei Zimmertemperatur im Vakuum 0 bis 48 Stunden lang gealtert und anschliessend in PbCl$_2$–KCl-Lösung ($5 \cdot 10^{-4}$ M Pb^{2+}, 0.25 M KCl) mit linear ansteigender Spannung anodisch abgelöst (single-sweep-Chronoamperometrie; Potentialvorschubrate $v = 0.57$ mV/sec; Polarisation mittels eines potentiostatisierten Gleichspannungspolarographen, Steuerelektrode SCE).

Typische Beispiele der erhaltenen Chronoamperogramme zeigt Fig. 1. Man erhält bei nicht allzu hohen Alterungszeiten drei Strippingpeaks, die ihrer Potentiallage gegenüber dem Ruhepotential kompakter Bleielektroden nach* den früher gefundenen Maxima Nr. II, IIIa und IIIb entsprechen**. Ein vierter, sehr viel positiverer und in die Fig. 1 nicht eingetragener Peak ist eindeutig auf die Ablösung der Au-Unterlage zurückzuführen. Die beobachtete anodische Verschiebung der Spitzenpotentiale im Vergleich zu den Angaben der Tab. 1 ist durch die grössere Pb-Depotmenge bedingt, da die Depoterschöpfung bei anodischer Belastung und der damit verbundene Stromabfall um so später bzw. (konstante Spannungsvorschubrate vorausgesetzt) bei um so positiverem Potential einsetzt, je mehr Depolarisator zur anodischen Ablösung zur Verfügung steht. Bei Extrapolation auf die Depolarisatormenge Null streben die Peakpotentiale den in Tab. 1 genannten Werten zu (vgl. den Potentialgang der Maxima in den Kurven A bis C der Fig. 1).

Der der Ablösung von reinem Blei ($a_{Pb} = 1$) zuzuordnende Hauptpeak (Nr. II) besitzt den höchsten relativen Wert seines Stromintegrals unmittelbar nach der Herstellung der Schichten und verliert mit zunehmender Alterungszeit zugunsten

---

* Unter dem Ruhepotential $_{Pb}E_r$ wird die Summe $_{Pb}E_r = {}_{Pb}E_0 + (RT/2F)\ln m_{Pb}$ verstanden.
** Die Monoschichtspeaks Ia und Ib liegen bei der gewählten Strommempfindlichkeit unterhalb der Nachweisgrenze.

der beiden folgenden Peaks (Nr. IIIa und IIIb) immer mehr an Flächenausdehnung. Der relative Flächeninhalt des mittleren Peaks (Nr. IIIb) geht durch ein Maximum,
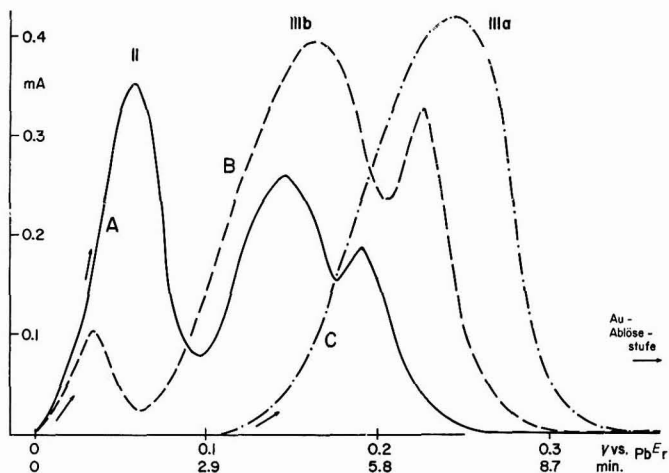
Fig. 1: Chronoamperometrische Ablösestufen von Pb/Au-Aufdampfschichten in Abhängigkeit von ihrer Alterungszeit.
(II), Anodische Bleihauptstufe; (IIIa,b), Legierungsstufen. →, Richtung des Potentialvorschubes. Alterungszeit: (A), $\frac{1}{4}$ Stunde; (B), 5 Stunden; (C), 20 Stunden. Ruhepotential, $_{Pb}E_r = -0.50$ V vs. SCE; Elektrodenflächen, 0.25–0.3 cm^2; Durchlaufgeschwindigkeit, $v = 0.57$ mV sec^{-1}.

TABELLE 1

CHRONOAMPEROMETRISCHE ABLÖSEPEAKS VON Pb-NIEDERSCHLÄGEN AUF Au-ELEKTRODEN

Peak Nr.	Peakpotential gegenüber dem Ruhepotential $_{Pb}E_r$ in KCl-Leitlösungen	Deutung
Ia	385 ± 10 mV ⎫	
Ib	205 ± 5 mV ⎬	Ablösung der Pb-Monoschicht
II	0 ± 5 mV	Ablösung der gesättigten Pb-Schicht (Hauptpeak, $a_{Pb} = 1$)
IIIa	175 ± 5 mV ⎫	
IIIb	105 ± 5 mV ⎬	Ablösung einer Pb-Legierung

das bei den vorliegenden Schichtdicken nach ca. 4 bis 5 Stunden erreicht wird und bei etwa 70% der Gesamtfläche aller Peaks liegt. Die Fläche des elektropositivsten Peaks (Nr. IIIa) nimmt kontinuierlich zu und ist nach einer Alterungszeit von rund 20 Stunden praktisch der Gesamtmenge des vorhandenen Bleis aequivalent.

   In den Röntgenbeugungsdiagrammen der Schichten (Guinier-Kamera nach DE WOLFF, Bauart Nonius, Cu-Kα-Strahlung: 20 mA, 40 kV, Belichtungszeit 3 Stunden, Eichsubstanz KCl) treten bis ins Gebiet von $4\theta \approx 160°$ insgesamt 57 Reflexe auf, die (mit Ausnahme weniger sehr schwacher Linien) mit den Reflexen von Au, Pb und den intermetallischen Phasen[4] AuPb$_2$ und[5] AuPb$_3$ übereinstimmen (Tab. 2)*. An Schichten mit drei Ablösepeaks sind die Linien sämtlicher drei Blei-

TABELLE 2

GEGENÜBERSTELLUNG DER GEFUNDENEN RÖNTGENREFLEXE MIT DEN REFLEXEN VON Au, AuPb$_2$, AuPb$_3$ UND Pb

Nr. des Reflexes	d-Werte der Reflexe in Å				
	Gefundene Reflexe und ihre visuelle Intensität	Reflexe nach ASTM			
		Au	AuPb$_2$	AuPb$_3$	Pb
1	5.188 (50)	—	5.18 (—)ᵃ	—	—
2	2.900 (80)	—	—	2.890 (80)	—
3	2.855 (100)	—	—	—	2.855 (100)
4	2.833 (100)	—	2.84 (100)	—	—
5	2.824 (100)	—	—	2.822 (100)	—
6	2.790 (40)	—	—	2.781 (50)	—
7	2.680 (40)	—	—	2.672 (30)	—
8	2.675 (10)	—	—	?	—
9	2.605 (100)	—	—	2.597 (100)	—
10	2.597 (10)	—	2.59 (30)	—	—
11	2.479 (50)	—	2.477 (50)	—	—
12	2.476 (50)	—	—	—	2.475 (50)
13	2.424 (50)	—	—	2.418 (80)	—
14	2.354 (100)	2.355 (100)	—	—	—
15	2.330 (50)	—	—	2.338 (50)	—
16	2.316 (80)	—	2.310 (80)	2.314 (50)	—
17	2.239 (60)	—	2.236 (50)	—	—
18	2.220 (20)	—	—	2.227 (20)	—
19	2.104 (10)	—	—	2.098 (10)	—
20	2.079 (20)	—	—	2.075 (20)	—
21	2.039 (80)	2.039 (52)	—	—	—
22	1.907 (5)	—	1.901 (—)ᵃ	—	—
23	1.888 (5)	—	—	?	—
24	1.866 (20)	—	—	1.863 (50)	—
25	1.751 (50)	—	—	—	1.750 (31)
26	1.722 (5)	—	1.727 (5)	—	—
27	1.697 (50)	—	1.693 (70)	—	—
28	1.691 (50)	—	—	1.691 (80)	—
29	1.657 (20)	—	—	1.651 (30)	—
30	1.638 (50)	—	1.632 (80)	1.628 (80)	—
31	1.589 (20)	—	—	1.584 (30)	—
32	1.576 (10)	—	—	1.574 (20)	—
33	1.541 (30)	—	1.535 (70)	1.533 (20)	—
34	1.526 (10)	—	—	1.519 (20)	—
35	1.492 (50)	—	—	—	1.493 (32)
36	1.485 (5)	Zuordnung unsicher			
37	1.474 (50)	—	1.470 (80)	—	—
38	1.471 (50)	—	—	1.470 (80)	—
39	1.443 (50)	1.442 (32)	und	1.438 (50)	—
40	1.428 (10)	—	—	—	1.429 (9)
41	1.416 (10)	—	1.414 (30)	—	—
42	1.394 (10)	—	—	1.388 (30)	—
43	1.366 (10)	—	—	1.361 (30)	—
44	1.338 (10)	—	—	1.335 (20)	—
45	1.326 (50)	—	1.322 (80)	—	—
46	1.312 (5)	Zuordnung unsicher			
47	1.306 (10)	—	—	1.307 (30)	—
48	1.295 (40)	—	1.294 (70)	1.293 (50)	—
49	1.284 (20)	—	1.280 (50)	—	—
50	1.269 (5)	—	—	1.265 (20)	—

TABELLE 2 (Fortsetzung)

Nr. des Reflexes	d-Werte der Reflexe in Å							
	Gefundene Reflexe und ihre visuelle Intensität		Reflexe nach ASTM					
			Au		AuPb₂		AuPb₃	Pb
51	1.264	(5)	Zuordnung unsicher					
52	1.257	(30)	—		1.257	(50)	—	—
53	1.254	(5)	—		—		1.249 (10)	—
54	1.241	(10)	—		1.238	(30)	1.240 (20)	—
55	1.230	(50)	1.230	(36)	—		—	—
56	1.224	(50)	—		1.219	(70)	—	—
57	1.207	(10)	—		1.205	(80),	1.205 (30)	—

[a] Diese Linien kommen in der ASTM-Kartei nicht vor, lassen sich jedoch einfach indizierten Netzebenen von AuPb₂ zuordnen (vgl. auch Lit. 4)

phasen nachzuweisen, die der Kurve C in Fig. 1 entsprechenden ausgealterten Ueberzüge zeigen nur die Linien von AuPb₂ (Tab. 3).

Auf Grund des Vergleichs der Peakstruktur der Ablösekurven mit den zugehörigen Röntgendaten darf als gesichert gelten, dass der Peak Nr. IIIb der Ablösung von AuPb₃, der Peak Nr. IIIa der Ablösung von AuPb₂ zuzuordnen ist und dass die Reaktion zwischen der Goldunterlage und der Bleischicht sowohl in Aufdampf- wie auch elektrolytisch erzeugten Belägen über AuPb₃ als Zwischenstufe zum Endprodukt AuPb₂ führt:

$$Au, Pb \rightarrow AuPb_3 \rightarrow AuPb_2$$

was mit der von WEAVER UND BROWN[3] postulierten einseitigen Diffusion von Au in die Pb-Phase sowie mit den eigenen chronoamperometrischen Beobachtungen[1] übereinstimmt.

Versuche, die Legierungsschichten durch kathodisches Belasten im Potentialgebiet der Legierungspeaks aufzubauen bzw. weiterwachsen zu lassen, sind ohne positives Ergebnis geblieben; damit scheint sich der frühere Befund[1] zu bestätigen, dass die Legierungsbildung nur durch Reaktion zwischen Phasenblei ($a_{Pb} = 1$) und -gold ($a_{Au} = 1$), nicht aber durch direkte Entladung von Pb^{2+} an der Legierungsphase und unmittelbaren Gittereinbau zustande kommt.

Infolge des Ausbleibens kathodischer Ströme im Legierungsgebiet sind sichere chronoamperometrische Ruhepotentialmessungen nicht möglich, und die Frage nach den Beziehungen zwischen den Potentialwerten der Legierungspeaks und den zugehörigen Gleichgewichtspotentialen der Verbindungen AuPb₂ bzw. AuPb₃ respektive den ΔG-Werten der Reaktionen

$$Au + 2 Pb \rightarrow AuPb_2$$

und

$$Au + 3 Pb \rightarrow AuPb_3$$
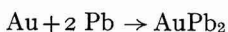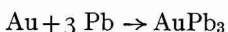
bleibt daher vorerst offen.

---

* Die Existenz der Verbindung AuPb₃, die in dem von HANSEN UND ANDERKO[6] angegebenen Zustandsdiagramm Pb/Au nicht vorkommt, wurde von FUJIKI, SUGANUMA UND YOSHIDA[5] röntgenographisch nachgewiesen.

TABELLE 3

AUFTRETEN DER VERSCHIEDENEN Pb/Au-PHASEN IN DEN AUFDAMPFSCHICHTEN IN ABHÄNGIGKEIT
VON DER ALTERUNGSZEIT

Nr. des Reflexes	Zuordnung der Reflexe nach Tabelle 2	Auftreten der Reflexe in verschiedenen lang gealterten Pb/Au-Aufdampfschichten (entsprechend den Ablösekurven nach Fig. 1)		
		Kurve A	Kurve B	Kurve C
1	$AuPb_2$	+	+ +	+ + +
2	$AuPb_3$	+ +	+ + +	—
3	Pb	+ + +	—	—
4	$AuPb_2$	+	+ +	+ + +
5	$AuPb_3$	+ +	+ + +	=
6	$AuPb_3$	+ +	+ + +	—
7	$AuPb_3$	+ +	+ + +	—
8	$(AuPb_3)$	+ +	+ + +	—
9	$AuPb_3$	+ +	+ + +	—
10	$AuPb_2$	+	+ +	+ + +
11	$AuPb_2$	+	+ +	+ + +
12	Pb	+ + +	—	—
13	$AuPb_3$	+ +	+ + +	—
14	Au	+ + +	+ +	+
15	$AuPb_3$	+ +	+ + +	—
16	$AuPb_2, AuPb_3$	+ +	+ + +	+ + +
17	$AuPb_2$	+	+ +	+ + +
18	$AuPb_3$	+ +	+ + +	—
19	$AuPb_3$	+ +	+ + +	—
20	$AuPb_3$	+ +	+ + +	—
21	Au	+ + +	+ +	+
22	$AuPb_2$	+	+ +	+ + +
23	$(AuPb_3)$	+ +	+ + +	—
24	$AuPb_3$	+ +	+ + +	—
25	Pb	+ + +	—	—
26	$AuPb_2$	+	+ +	+ + +
27	$AuPb_2$	+	+ +	+ + +
28	$AuPb_3$	+ +	+ + +	—
29	$AuPb_3$	+ +	+ + +	—
30	$AuPb_2, AuPb_3$	+ +	+ + +	+ + +
31	$AuPb_3$	+ +	+ + +	—
32	$AuPb_3$	+ +	+ + +	—
33	$AuPb_2, AuPb_3$	+ +	+ + +	+ + +
34	$AuPb_3$	+ +	+ + +	—
35	Pb	+ + +	—	—
36	Zuordnung unsicher			
37	$AuPb_2$	+	+ +	+ + +
38	$AuPb_3$	+ +	+ + +	—
39	$Au, AuPb_3$	+ + +	+ + +	+
40	Pb	+ + +	—	—
41	$AuPb_2$	+	+ +	+ + +
42	$AuPb_3$	+ +	+ + +	—
43	$AuPb_3$	+ +	+ + +	—
44	$AuPb_3$	+ +	+ + +	—
45	$AuPb_2$	+	+ +	+ + +
46	Zuordnung unsicher			
47	$AuPb_3$	+ +	+ + +	—
48	$AuPb_2, AuPb_3$	+ +	+ + +	+ + +
49	$AuPb_2$	+	+ +	+ + +
50	$AuPb_3$	+ +	+ + +	—

TABELLE 3 (Fortsetzung)

Nr. des Reflexes	Zuordnung der Reflexe nach Tabelle 2	Auftreten der Reflexe in verschiedenen lang gealterten Pb/Au-Aufdampfschichten (entsprechend den Ablösekurven nach Fig. 1)		
		Kurve A	Kurve B	Kurve C
51	Zuordnung unsicher			
52	$AuPb_2$	+	+ +	+ + +
53	$AuPb_3$	+ +	+ + +	−
54	$AuPb_2$, $AuPb_3$	+ +	+ + +	+ + +
55	Au	+ + +	+ +	+
56	$AuPb_2$	+	+ +	+ + +
57	$AuPb_2$, $AuPb_3$	+ +	+ + +	+ + +

Bedeutung der Symbole: −, Reflex fehlt; +, Reflex schwach ausgeprägt; + +, Reflex mittelstark ausgeprägt; + + +, Reflex stark ausgeprägt.

Bei den vorliegenden Versuchen wurden, ähnlich wie bei den von WEAVER UND BROWN[3] beschriebenen Experimenten, keinerlei Anzeichen für ein Auftreten der Phase Au_2Pb (vgl. PERLITZ[7]) festgestellt, die nach Angaben von KLEPPA UND CLIFTON[8] bei niedrigen Temperaturen nicht beständig zu sein scheint.

Institut für anorganische, analytische und   E. SCHMIDT
physikalische Chemie der Universität Bern   H. R. GYGAX

1 E. SCHMIDT UND H. R. GYGAX, *J. Electroanal. Chem.*, 13 (1967) 378.
2 F. GRIENGL UND R. BAUM, *Monatsh.*, 57 (1931) 165.
3 C. WEAVER UND L. C. BROWN, *Phil. Mag.*, 8 (1963) 1379.
4 H. WALLBAUM, *Z. Metallk.*, 35 (1943) 218 (ASTM-Kartei Nr. 8-419).
5 Y. FUJIKI, R. SUGANUMA UND T. YOSHIDA, *J. Phys. Soc. Japan*, 13 (1958) 965 (ASTM-Kartei 11-573).
6 M. HANSEN UND K. ANDERKO, *Constitution of Binary Alloys*, McGraw-Hill, New York, 1958, S. 222.
7 H. PERLITZ, *Acta Comment. Univ. Dorpatensis*, Series A, 27 (1934) 115.
8 O. J. KLEPPA UND D. F. CLIFTON, *Acta Cryst.*, 4 (1951) 74.

BOOK REVIEWS

Zone Melting, by WILLIAM G. PFANN, 2nd ed., John Wiley & Sons, Inc., New York, London and Sydney, 1966, xi + 310 pages, 89s.

The author is the inventor of the technique of zone refining and he writes an authoritative account of its theory and practice. The theory of normal freezing and of zone refining given in Chapters 2 and 3, together with 20 figures summarising theoretical solute distributions in an ingot as a function of number of zone passes and

distribution coefficient, is of considerable value in delineating the capabilities of the technique. Chapters on the practical aspects and applications provide basic information to a reader wanting to design equipment for a particular purpose. The author presents some interesting ideas for methods of continuous zone refining, a process likely to become increasingly important in the manufacture of pure chemicals. The last part of the book is concerned with zone levelling, problems arising with volatile materials, methods of perturbing the concentration, temperature gradient zone melting and other miscellaneous phenomena. It deals with these almost exclusively from the point of view of semiconductor technology. Many of the principles are, however, of general application.

The author states that his main aims are to provide complete coverage of the theory and practice of zone melting. He has succeeded completely in the first, and largely in the second. The slight qualification is due to the comparatively small space devoted to chemical compounds. He does, however, give a valuable list of references to the latter. The book is strongly recommended to the physicist, metallurgist or chemist concerned with the preparation and technology of ultra-pure metals or semiconductors. It will also be of value to chemists concerned with the preparation or analysis of pure chemicals, as a guide to the capabilities of the techniques and the literature.

C. A. PARKER, Admiralty Materials Laboratory, Poole, Dorset

Les Piles à Combustible, Editions Technip, Paris, 1965, pages xv + 530, 125.00NF.

This is the sixth volume in a series under the general title *Science et Technique du Pétrole* published by the Institut Français du Pétrole. It is a collection of 27 papers by 42 authors and is divided into four sections. The first and longest (190 pages) section covers the general scientific background, especially the subject of electrochemical mechanisms. Thus it includes reviews of thermodynamics of cells, statistical mechanics of liquids, kinetics of electrode reactions and the methods used for studying them, the properties of porous electrodes, etc. Such a section is the most difficult to write because it covers a wide range of phenomena, and in a collective work it is practically impossible to achieve a real synthesis. Section II (150 pages) on technological problems is more like a collection of papers presented to a conference in that each author presents essentially his own results rather than a general view. Sections III and IV (each 90 pages) describe practical examples of fuel cells and their future prospects, respectively. The "sales-talk" of the latter section is, of course, an essential part of any book on fuel cells and there are also a number of pictures of practical fuel cells, but it is a pleasure to note the absence of pictures of tractors or fork-lift trucks.

There is a large amount of practical information in this well-produced book which will make it required reading for those active in fuel-cell research. The price seems high, but not perhaps in relation to the expenditure on fuel cell research as a whole.

ROGER PARSONS, University of Bristol

CONTENTS

DIFFRACTION OF X-RAYS BY CHAIN MOLECULES

by B. K. VAINSHTEIN

Foreword by M. F. PERUTZ

6 x 9", xiii + 414 pages, 3 tables, 258 illus., 256 lit.refs., Dfl. 65.00, £6.10.0, $23.50

Contents: 1. Principles of the theory of X-ray diffraction. 2. Structures of chain molecules and assemblies. 3. Diffraction by an isolated chain molecule. 4. Scattering intensity and structure of object. 5. Properties of the distribution and interference functions. 6. Diffraction by assemblies of parallel chain molecules. 7. Diffraction by assemblies with nonparallel packing of chain molecules and by amorphous polymers. Subject index.

INFRA RED INSTRUMENTATION AND TECHNIQUES

by A. E. MARTIN

$5\frac{1}{2}$ x $8\frac{1}{2}$", x + 180 pages, 13 tables, 94 illus., 86 lit.refs., 1966, Dfl. 32.50, 65s., $12.00

Contents: 1. Historical. 2. Modern infra-red spectrometers. 3. Miscellaneous instruments. 4. Interferometric spectrometers. 5. Accessories. 6. Experimental methods and techniques. Index.

ENERGY TRANSFER IN RADIATION PROCESSES

Chemical, Physical and Biological Aspects

Proceedings of the International Symposium held in Cardiff, 1965

edited by G. O. PHILLIPS

$5\frac{1}{2}$ x $8\frac{1}{2}$", xvi + 182 pages, 10 tables, 81 illus., 273 lit.refs., 1966, Dfl. 32.50, 65s., $12.00

Contents: Introductions to the sections by F. S. Dainton, G. F. J. Garlick and Tikvah Alper. Invited papers by E. J. Bowen, Jett C. Arthur, N. Riehl, R. Mason. Contributed papers.

MASS SPECTROMETRIC ANALYSIS OF SOLIDS

edited by A. J. AHEARN

$5\frac{1}{2}$ x $8\frac{1}{2}$", viii + 167 pages, 13 tables, 46 illus., 242 lit.refs., 1966, Dfl. 30.00, 60s., $10.75

Contents: 1. Introductory survey. 2. The production of ions from solids. 3. Photographic emulsions as ion detectors in quantitative mass spectrography. 4. Analysis of special samples. 5. Mass spectrographic microprobe analysis. Subject index.

RADIOCHEMICAL SURVEY OF THE ELEMENTS

Principal characteristics and applications of the elements and their isotopes

by M. HAISSINSKY
and
J.-P. ADLOFF

6 x 9", ix + 177 pages, 1965, Dfl. 32.50, 65s., $12.00

Contents: Introduction. The elements in alphabetical order. Element 102. Element 104.

1 9 ศ.ย. 2510